UiT
–
THE ARCTIC
UNIVERSITY
OF NORWAY

Faculty of Health Sciences
Department of Clinical Medicine

Development and evaluation of gonadotropin releasing hormone antagonists as SPECT radiotracers

Richard Fjellaksel

A dissertation for the degree of Philosophiae Doctor – May 2018

Development and evaluation of gonadotropin releasing hormone antagonists as SPECT radiotracers

Faculty of Health Sciences, Department of Clinical Medicine

Richard Fjellaksel

A dissertation for the degree of Philosophiae Doctor – May 2018

iii

ABSTRACT

The overall aim of the thesis was to evaluate the potential of gonadotropin releasing hormone receptor (GnRH-R) antagonists as radiotracers for the early detection and understanding of Alzheimer`s disease (AD). The molecular imaging field is a symbiosis between organic chemistry, radiochemistry, *in vitro* biology, as well as preclinical- and clinical trials, therefore an evaluation should involve all respective subfields. In light of this, the development of a new radiotracer is often a time- consuming and laborious process. Consequently, this thesis represents a highly collaborative project involving various subfields and their interplay in the field of molecular imaging.

Initially a series of GnRH-R antagonists were synthesized and evaluated for affinity for the GnRH-receptor. A competitive binding study was performed and the synthesized GnRH-R antagonists were compared to control compounds. By the use of a copper mediated late-stage iodination, radiolabeling was further investigated. In addition, an acylation Finkelstein approach was examined by a thorough mechanistic analysis using both experimental and computational methods. The *in vitro* analyses of two promising GnRH-R antagonists were performed, where human and rat serum stability, a competitive inhibition assay, a metabolic profile (phase 1) and autoradiography evaluated the potential these compounds exhibit as radiotracers. Furthermore, preclinical evaluation of a α-halogenated compound was performed on the basis of literature findings and serum stability analysis.

In summary, the project has resulted in several potential GnRH-R antagonist radiotracers. Although more analyses need to be performed, one compound has already been evaluated in preclinical trials and excluded from further investigation. Two more compounds have been radiolabeled and assessed thoroughly *in vitro*. The compounds showed good affinity for the GnRH-R. Serum stability analysis and the metabolic profiling showed stable compounds for imaging. In addition, several metabolites were identified and the metabolic rate was quantified. Furthermore, autoradiography in rat brain showed binding, which was in compliance with binding affinities for the compound. These new GnRH-R antagonists possess high potential as GnRH- antagonistic radiotracers for the pathophysiologic examination of AD and warrant further preclinical evaluation.

ACKNOWLEDGEMENTS

Tromsø, March 2018

Richard Fjellaksel

LIST OF PUBLICATIONS

PAPER I

Richard Fjellaksel, Marc Boomgaren, Rune Sundset, Ira H. Haraldsen, Jørn H. Hansen and Patrick J. Riss. Small molecule piperazinyl-benzimidazole antagonists of the gonadotropin-releasing hormone (GnRH) receptor. *MedChemComm* **2017**, *8* (10), 1965-1969.

PAPER II

Richard Fjellaksel, Rune Sundset, Jørn H. Hansen, Patrick J. Riss. Copper-mediated late-stage iodination and ^{123}I-labelling of triazole-benzimidazole bioactives. *Synlett* **2018**. Accepted 16 March

PAPER III

Richard Fjellaksel, Damir Dugalic, Taye B. Demissie, Patrick J. Riss, Ole-Kristian Hjelstuen, Rune Sundset, and Jørn H. Hansen. An Acylation-Finkelstein Approach to Radioiodination of Bioactives: The role of amide group anchimeric assistance. *Journal of Physical Organic Chemistry* **2018**, e3835-n/a. DOI: 10.1002/poc.3835

PAPER IV

Richard Fjellaksel, Angel Moldes-Anaya, Ana Oteiza, Montserrat Martin-Armas, Terje Vasskog, Patrick J. Riss, Ole K. Hjelstuen, Jørn H. Hansen and Rune Sundset. *In vitro* evaluation of two promising bioactive triazole-benzimidazole GnRH Receptor-antagonists as possible candidates for SPECT imaging. *Manuscript*

PAPER V

Richard Fjellaksel, Ana Oteiza, Montserrat Martin-Armas, Patrick J. Riss, Ole K. Hjelstuen, Samuel Kuttner, Jørn H. Hansen and Rune Sundset. First *in vivo* evaluation of a potential SPECT brain radiotracer for the gonadotropin releasing hormone receptor based upon the piperazinyl-benzimidazole class of compounds. *Manuscript.*

ABBREVATIONS AND SYMBOLS

%ID	Percentage of injected dose
%ID/g	Percentage of injected dose per gram of tissue
β^+	Positron
γ	Gamma ray photon
AD	Alzheimer`s disease
BBB	Blood-brain barrier
BOC	Tert-butoxycarbonyl
CNS	Central nervous system
CT	Computed tomography
CuAAC	Copper catalyzed azide-alkyne cycloaddition
DIPEA	N,N-Diisopropylethylamine
DMSO	Dimethylsulfoxide
DMF	Dimethylformamide
ESI	Electrospray ionization
FSH	Follicle stimulating hormone
GnRH	Gonadotropin releasing hormone
HPG	Hypothalamus-pituitary-gonads
HPLC	High performance liquid chromatography
IC_{50}	Inhibitory concentration – half maximum
i.p.	Intraperitoneal
i.v.	Intravenously
Ki	Inhibitory constant
LC-HRMS	Liquid chromatography - High resolution mass spectrometry
LH	Luteinizing hormone
LHRH	Luteinizing hormone releasing hormone
MeCN	Acetonitrile

NMR	Nuclear magnetic resonance spectroscopy
PBS	Phosphate buffered saline
PET	Positron emission tomography
QToF	Quadrupole time of flight
RCY	Radiochemical yield
RT	Room temperature
SGF	Simulated gastric fluid
SPECT	Single photon emission computed tomography
TFA	Trilfuoroacetic acid
THF	Tetrahydrofuran
TLC	Thin layer chromatography
UPLC	Ultra performance liquid chromatography
VOI	Volume of interest

TABLE OF CONTENTS

1   INTRODUCTION

1.1   GENERAL INTRODUCTION

In modern medicine, imaging techniques visualize body functions and improve the diagnosis of diseases. This, in turn, influences the clinical outcome and management of the patient. The discovery of X-rays is the fundament for medical imaging and an example of a change of paradigm in medicine. Since the discovery of modern non-invasive molecular imaging techniques such as single photon emission computed tomography (SPECT) and positron emission tomography (PET), the development in molecular imaging has been, and still is, rapid and continuous. The discovery of the [^{18}F]-Fluorodeoxyglucose (FDG) in 1976 was a breakthrough in molecular imaging, and [^{18}F]-FDG is still the most used PET imaging radiotracer to date.[1-2] The success of the technology lies in the ability to visualize body functions on a molecular level without any pharmacological response of the radiotracer. This makes PET and SPECT powerful imaging tools for the diagnosis and therapeutic evaluation of tumors, nervous system diseases and cardiovascular disorders.[3] One of the challenges in these molecular imaging methods lies in the need for new and more specific radiotracers and methods for the development of radiopharmaceuticals. The prerequisites for successful radiopharmaceutical development are the symbiosis between chemistry, radiochemistry, preclinical and clinical trials. These critical factors are equally dependent on each other and are part of the complexity for the development of new, target-specific radiotracers.

1.2   OUTLINE OF THESIS

The thesis is written as a collection of papers I-V. Chapter 1 gives a short introduction into imaging in medicine and the importance of molecular imaging technology in symbiosis with organic chemistry, radiochemistry, preclinical and clinical trials. Chapter 2 goes more into detail on molecular imaging and explains the background information for single photon emission computed tomography (SPECT) and positron emission tomography (PET) imaging in combination with the different available radionuclides used. Furthermore, the knowledge of the hypothalamic-pituitary-gonadal axis (HPG-axis) is explained to give a background for the understanding of the connection to Alzheimer's disease (AD) and the HPG-axis. As an important step in molecular imaging the relevance of radiochemistry, selection of radionuclides and radiochemical methods for this thesis is explained. In Chapter 3 the aims of the thesis are presented. Chapter 4 gives a summary of all papers. Chapter 5 is presenting the results and discussions.

2   BACKGROUND

2.1   MOLECULAR IMAGING

A more detailed presentation of the molecular imaging is presented in this Chapter. Molecular imaging is imaging on a molecular level in contrast to techniques as x-ray and ultra-sound where organ anatomy and movement are visualized. Most of contemporary imaging techniques are not competitors; they are instead used for different purposes and provide complementary information. In nuclear medicine, the use of radioisotopes is necessary to obtain an image. There are several radioisotopes available for medical use. Single photon emission computed tomography (SPECT) radioisotopes emit a single gamma photon at each disintegration as shown in Figure 1, while positron emission tomography (PET) radioisotopes emit a positron that annihilates with its anti-particle, an electron, resulting in the creation of two gamma photons (511 keV) radiating in opposite direction. The photon is captured by scintillator crystals in gamma camera heads or in PET detector rings. In the case of a PET/CT camera, the CT part of the PET/CT scanner provides anatomical images for better localization of the radiotracer uptake. Figure 1 gives a graphical presentation of the two radiation types.[4]
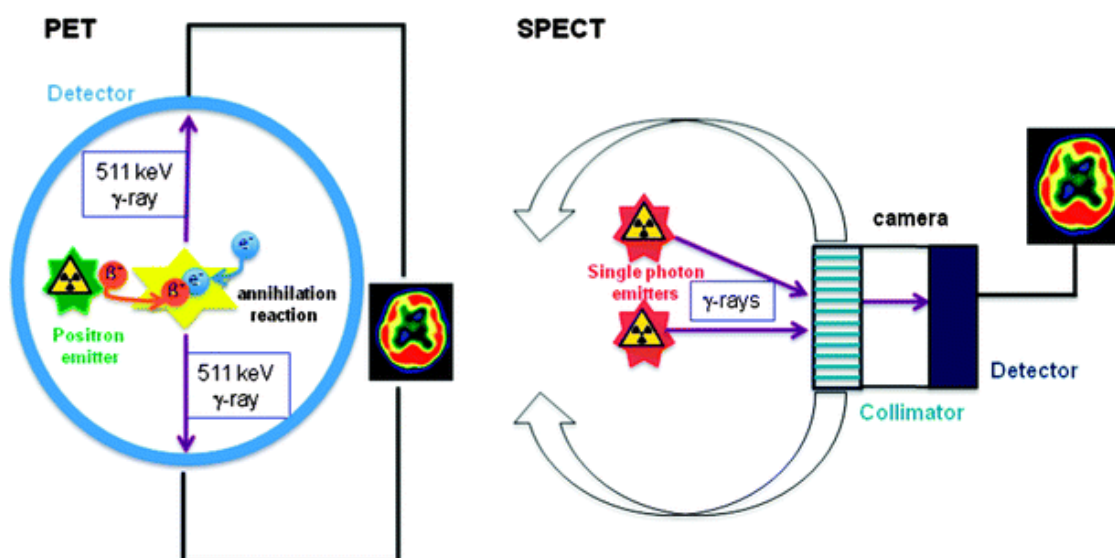
Figure 1: The basic comparison between PET and SPECT. *Left; the emission of a positron from a PET radioisotope is illustrating the annihilation reaction between the positron and the electron resulting in the emission of two gamma rays in opposite direction. The PET detector is the blue ring. Right; the emission of single gamma photons illustrating the SPECT principle allowing only the photons in straight lines to the collimator to pass into the detector and to be included in the processing of the image. Reprinted with permission from Noel, S.; Cadet, S.; Gras, E.; Hureau, C., The benzazole scaffold: a SWAT to combat Alzheimer's disease.* Chemical Society reviews ***2013,*** *42 (19), 7747-7762. Copyright@Royal Society of Chemistry.* [4]

The major differences between PET and SPECT are listed in Table 1. The ability to work with most PET radionuclides is limited to a location within a reasonable distance from a cyclotron due to the relatively short half-life of the radionuclides. However, ^{68}Ga is produced by a generator and could therefore be readily available at laboratories without a cyclotron. SPECT is more widely accessible worldwide and may therefore play an important role also in the future. For the future, these technologies will probably not compete but might supplement each other since there will be opportunities for both new PET and SPECT radiotracers.[5] However, the large increase in the number of cyclotrons and PET/CT scanners over the last few years, and the lack of market penetration of SPECT/CT scanners suggests that PET will be growing more rapidly than SPECT in the years to come.

Table 1: PET and SPECT comparison.[5]

PET	SPECT
Need a nearby cyclotron	Can be shipped over considerable distances
Expensive	Inexpensive compared to PET
Qualitative and quantitative	Qualitative*
Expensive PET detectors	More accessible Gamma cameras
Lack of more readily available radiotracers	More readily available radiotracers

*SPECT quantification is still widely questionable. However, new SPECT-scanners are available with quantification opportunities[6-7]

Several radionuclides for PET and SPECT imaging are available. A selection of radionuclides are presented in Table 2. ^{18}F is the most frequently used radioisotope for PET due to a half-life that allows multi-step chemistry and can as such be used to radiolabel a wide range of molecules. ^{11}C, ^{13}N and ^{15}O are other interesting PET radionuclides that are useful in patient scanning but until now mainly used in academic settings due to the short half-life. ^{99m}Tc is the most frequently used SPECT radionuclide counting for approximately 80% of all SPECT procedures. Various isotopes of iodine can also be used due to their ability to move from SPECT(^{123}I) to PET(^{124}I) diagnostic use and further to therapeutic treatment (^{131}I). Radioisotopes of iodine can therefore be used as theranostics.[8-10]

Table 2: Selected radionuclides and main characteristics of PET and SPECT used in medicine and in biology.[11]

Radionuclide	Main use	Maximum β β+ energy MeV	Energy keV γ	Half-life	Usage
^{18}F	Imaging	0.633		109.8 min	PET
^{123}I	Imaging		γ 159	13.2 h	SPECT
^{124}I	Imaging	2.1	γ 603, 1691	4.15 days	PET
^{125}I	Imaging		γ 35	59.4 days	SPECT
^{131}I	Imaging, therapy		γ 364, 637	8.02 days	SPECT
^{99m}Tc	Imaging		γ 141	6.0 h	SPECT
^{11}C	Imaging	1.0		20.4 min	PET
^{13}N	Imaging	1.2		9.96 min	PET
^{15}O	Imaging	1.7		2.03 min	PET

Nowadays, PET is most often fused with a computed tomography (CT) image. The CT image shows anatomical details, thereby adding structural information to locate the precise position of the radiation. In Figure 2, the fused SPECT/CT image shows a rat injected intravenously with ^{99m}Tc-HMPAO that visualizes the cerebral blood flow. The image on right side is a fused PET/CT picture after injection of 2-deoxy-2-[^{18}F]-fluoro- D-glucose ([^{18}F]-FDG) in mice, in which the metabolic entrapment of [^{18}F]-FDG is imaged.[12-13]
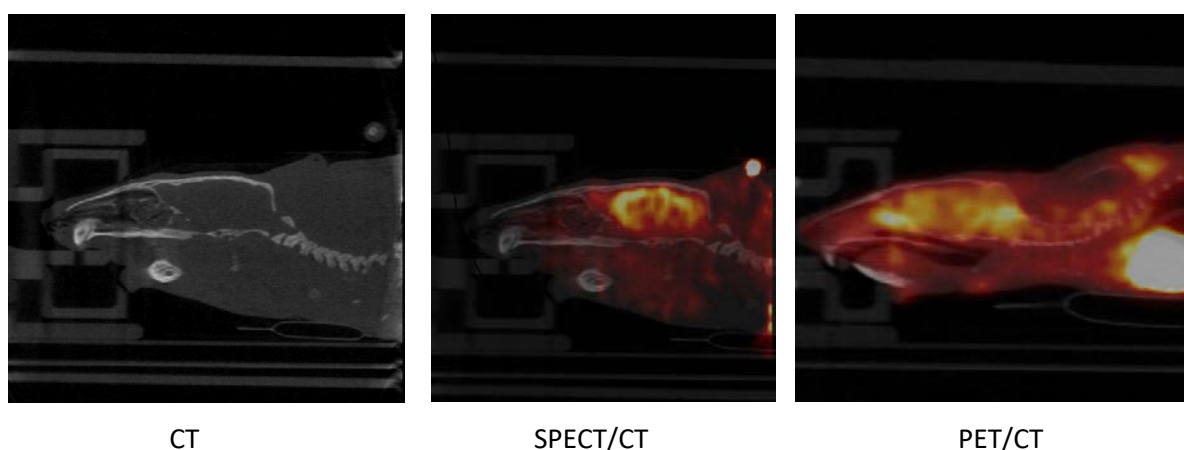
| CT | SPECT/CT | PET/CT |

Figure 2: A comparison between CT, SPECT/CT and PET/CT in rat. The CT shows basic anatomical features while the fused SPECT/CT image shows cerebral blood flow with ^{99m}Tc-HMPOA and the fused PET/CT shows [^{18}F]-FDG metabolic uptake. Images obtained at the Core facility for preclinical SPECT/PET/CT at University of Tromsø – The Arctic University of Norway (with permission).[12-13]

2.2 GONADOTROPIN RELEASING HORMONE AND THE HYPOTHALAMIC-PITUITARY-GONADAL AXIS

It is important to understand the hypothalamic-pituitary-gonadal axis (HPG-axis) to understand the pathophysiological connection to the Alzheimer's disease (AD) discussed in the next section. The HPG-axis is explained by the pulsatile release of gonadotropin releasing hormone (GnRH), gonadotropins and the regulatory feedback mechanism, Figure 3. GnRH, also known as luteinizing-hormone releasing hormone (LHRH), which is a neurohormone that consists of 10 amino acids. GnRH is produced in the hypothalamus and released in a pulsatile manner into the hypophysial portal bloodstream. When it reaches the pituitary gland, it binds to its own G-protein coupled receptor (GnRH-receptor) and stimulates the production of two gonadotropins in the anterior pituitary gland – Luteinizing Hormone (LH) and Follicle Stimulation Hormone (FSH). The release of gonadotropins acts on the gonads to produce androgens and estrogens. The release of gonadotropins is controlled by the pulsatile release of GnRH in the hypophysial portal blood stream and by the feedback mechanism of androgens and estrogens.[14]
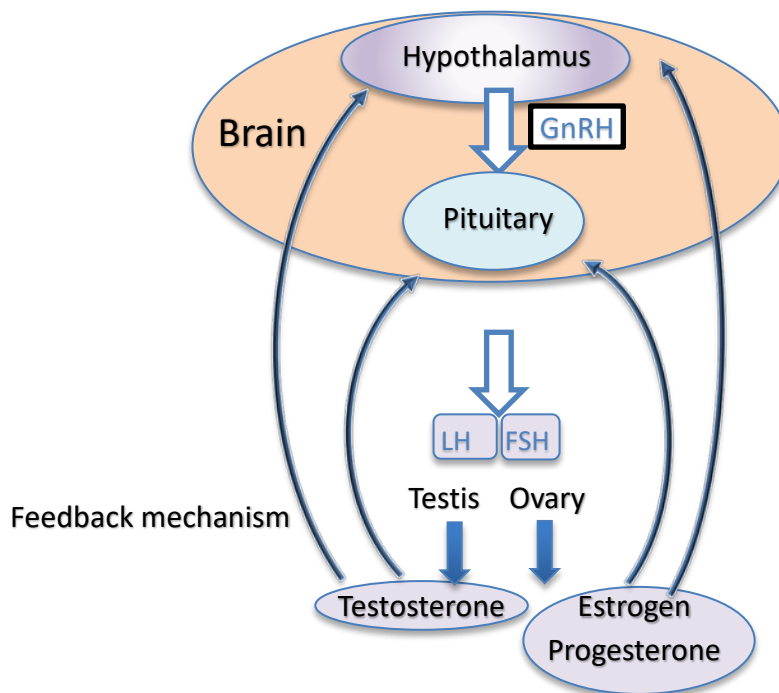
Figure 3: HPG-Axis, showing GnRH release stimulation on the pituitary gland where LH and FSH are produced. LH and FSH then acts in the gonads to produce androgens and estrogens. The regulation of GnRH-release is controlled by the pulsatile release of GnRH in addition to the feedback mechanism of androgens and estrogens.

Disturbance in the HPG-axis can lead to several implications in cognitive and behavioral traits.[15-18] GnRH has multiple actions other than the gonadal functions due to the HPG-axis and the reason can be linked towards its diverse signaling pathways activated by GnRH-R.[19-20] For example, outside the HPG-axis there is a strong evidence for the role of GnRH and GnRH-R in different cancer cells.[21-24] GnRH-R localization in mammals outside the HPG-axis is also well documented. The central nervous system has several areas within the central nervous system (CNS) where GnRH-R has been discovered. Retina, olfactory bulb, cortex, especially piriform, lateral septum, preoptic area, arcuate nucleus, hippocampus, amygdala, cerebral grey, cerebellum and spinal cord.[25] The GnRH-R has also been located in the kidney, liver, heart, bladder, tooth, adrenal, skin, skeletal muscle, spleen and lymphocytes. The HPG axis and GnRH is connected to a wide range of diseases, for example the reproductive functions, sex behavior, cognition, neurodegeneration and ageing.[20] All in all, these physiological and pathophysiological implications of the GnRH and GnRH-R are of high interest for further utilization.

2.3   ALZHEIMER`S DISEASE AND CONNECTION TO HPG AXIS

The connection between the HPG-axis and Alzheimer's disease (AD) is the focus in this section. The role of GnRH in connection to AD is still to be fully examined and more knowledge is needed. AD is the most dominant reason for dementia, it is estimated that as much as 131.5 million people worldwide will be affected by dementia in 2050.[26] High global costs and no treatment for Alzheimer's disease motivates the research. The main hypothesis for the pathophysiology for AD are amyloid plaque, hyper phosphorylation of Tau proteins, cholinergic hypothesis, disturbance of GABA-receptors and disturbance in the serotonergic system.

In the last decades, the focus on AD research has been towards the amyloid plaque hypothesis. The hypothesis postulates that the deposits of β-amyloid plaques are the main reason for developing AD, responsible for the neurotoxicity, which leads to dementia. However, even though the efforts to find a treatment for AD based on drugs that target amyloid plaque have been tremendous, these have so far resulted in failure in several clinical trials.[27] During those efforts, several radiotracers have been developed to target β-amyloid plaque, such as [^{11}C]-PIB and [^{18}F]-Flutemetamol. The failure of therapeutics in several clinical trials have changed the focus towards tubulin associated unit (tau) proteins as a major hallmark in the disease development. The tau protein gets hyper-phosphorylated and detaches from microtubules and self-aggregates into insoluble neurofibral tangles (NFT). This tau specific pattern of insoluble NFTs correlates closely to the clinical symptoms of AD. Several new tau-PET radiotracers are in development, where [^{18}F]-AV1451 is the most promising one to date.[28] There are six known isoforms in humans of tau proteins.[29] Yet to be discovered is which isoform of the tau proteins correlates to AD disease most closely. The implications for the diagnosis related to the tau hypothesis remains

questionable since tau protein isoforms are not specific to AD pathology alone.[29-30] This means there is still a lack of an objective biomarker for the early detection of AD.

In contrast, the GnRH receptor is prevalent in the brain and has been strongly linked to AD.[31-32] As such, radiolabeled antagonists of the GnRH receptor are of interest as imaging agents for early diagnosis of AD. GnRH, Luteinizing hormone (LH) and Follicle stimulating hormone (FSH) are not typically considered as the primary causes of AD. Amyloid plaque and hyper-phosphorylation of tau protein have been the most supported theories for developing AD as previously discussed. However, the relationship between the HPG –axis and AD is gaining more evidence supporting its important role in development of AD. There is a growing evidence supporting the connection of the HPG axis contribution to AD.[32] In addition, LH is known to cross the blood-brain barrier, and the receptors are located in hippocampus.[31] Hippocampus is a part of the limbic system, and this part of the brain is responsible for short-term and long-term memory. This part of the brain is also most vulnerable to AD. In the menopause and andrenopause there is a decreased sex steroid signaling. This leads to changes in the HPG-axis, and this affects alterations in the neuronal cells. This also explains the difference in prevalence of AD reported by the gender differences (2:1) female to male, since this is consistent to the earlier loss of gonadal functions and decrease in sex hormones and increase in serum gonadotropins. It has been found that AD patients have two-folded elevation of LH and FSH in the circulation compared with age-matched controls. This increase of LH and FSH seems to be an early change in disease progression in AD patients.[31] In light of this, the GnRH receptor density and availability may contribute to early detection and understanding of the pathophysiology for AD.

The connection between AD and gonadotropins has made small GnRH antagonists very interesting. Several small GnRH antagonists have shown significant inhibition of the GnRH-receptor, even if they do not use the primary ligand, which is a relatively large peptide, as a template.[33] Small GnRH antagonists can have great potential as PET or SPECT tracers to determine early pathological changes in the brain. Previous work have investigated GnRH-peptides as imaging agents.[34-35] However, Olberg and co-workers have found a brain penetrant non-peptide novel small molecule [^{18}F]-fluorinated GnRH-R antagonist that was permeable to the blood–brain barrier (BBB), but failed to reveal significant specific binding in brain of living rats. Nonetheless, the approach serves as a foundation for using radioligands for further imaging of the GnRH-R distribution in brain.[36-37]

2.4 RADIOCHEMISTRY: IODINE

Radiochemistry is an important field in molecular imaging and the development of radiotracers for imaging is a necessary step towards successful molecular imaging. The selection of radiochemical methods and radionuclides to fulfill the task to radiolabel desired compounds is outlined in this section. Radiochemistry includes production of radionuclides and radiolabeling of chemical compounds. All unstable radionuclides undergo some form of radioactive decay. This radioactive decay leads to the emission of radiation generally in either α, β or γ-rays. Such radiation is all categorized as ionizing radiation, which means that the energy is sufficient to ionize atoms and molecules, even break chemical bonds. This can potentially be harmful to living organisms. An α-particle consists of 2 protons and 2 neutrons. α-particles have a very short range and travel only a few centimeters in air. For protection, they can be stopped with a piece of paper. However, α-particles have high ionization capacity and can be harmful on short distances, for instance when they are inside living organisms. The β-particle can be either an electron or a positron. β-particles have weaker ionizing power than α-particles, but higher than γ-rays. γ-rays are electromagnetic radiation.

Production of these radionuclides requires either a reactor or a cyclotron, dependent on the nuclear reaction. In medicine today, the use of cyclotrons to produce radioactive nuclides is limited to location of the cyclotron due to the short half-life of the isotopes. For example, the production of ^{18}F and ^{123}I requires a cyclotron. The typical production of ^{18}F; ^{18}O-water is bombarded by protons to give a p,n reaction of ^{18}O to ^{18}F.[38] In a similar fashion is enriched $^{124}Xenon$ gas used to produce ^{123}I by several steps in a p,2n nuclear reaction, Figure 4.[3, 39]

a) $^{18}O(p,n)^{18}F$

b) $^{124}Xe(p,2n)\ ^{123}Cs \rightarrow\ ^{123}Xe \rightarrow\ ^{123}I$
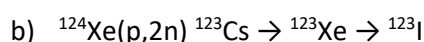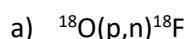
Figure 4: Nuclear reaction by cyclotron production of ^{18}F and ^{123}I. The ^{18}F and ^{123}I are produced in an accelerator by bombardment of enriched $^{18}O_2H$ and ^{124}Xe, respectively, with protons.[3, 38-39]

Important criteria for radiochemical labeling methods are: (1) a rapid reaction with high radiochemical yield (RCY); (2), simplicity, and; (3) high specific activity. This is especially important for radionuclides with a short half-life.[38]

In the present work, we sought after a radionuclide with suitable half-life for our initial biological experiments. The radionuclide ^{123}I has a half-life of 13.2 hours that allowed us to do biological characterization of our compounds with excellent SPECT imaging properties i.e. the gamma radiation energy is quite similar to the widely used ^{99m}Tc. In addition, logistic issues hampers the availability of ^{18}F, if not located to a nearby

cyclotron center, and makes it expensive. In addition, the ability to evaluate the theranostic possibilities for a compound using [131]Iodine is also present. Another potential advantage using ^{123}I as the radionuclide is that it can be made available for sites around the world without a cyclotron. Finally, the possibility to use [124]I which is a positron emitter is also present.[9-10, 40]

The nucleophilic and electrophilic substitution reactions are the most used radiolabeling reactions.[38] In addition, another common radiolabeling method is the use of a prosthetic group, which is discussed later in this section. In fluoride chemistry, the preparative process to turn [18]F$^-$ into a usable nucleophile is a prerequisite. Fluoride is a poor nucleophile compared to Iodine. Fluoride needs to be processed in order to participate in either S_N2 [^{18}F]-labelled fluoroalkanes and S_NAr [^{18}F]-labelled fluoroarenes reactions. In short, a standardized method to prepare fluoride usually involves entrapment of fluoride in an ion-exchange column where the expensive ^{18}O-enriched water is removed for reuse, the [^{18}F]fluoride is then eluted with a mixture of potassium carbonate and kryptofix 222 (K_{222}), the solution once dried gives an anhydrous fluoride that is more reactive and has the ability to participate in either S_N2 and S_NAr as a nucleophile.[3] Iodide is a stronger nucleophile and can be used in S_N2 reactions without any preparative work-up.[41] The S_N2 mechanism is explained by the binding of iodide to a carbon atom next to a chloride, which then acts as a leaving group. Examples of typical good leaving groups are weak bases, such as Cl-, Br- and HSO$_4$-, Figure 5. Nucleophilic substitutions are faster with aliphatic compounds than aromatic compounds. In order to increase the rate of the reaction on aromatic compounds, the reaction is often assisted by electron-withdrawing groups in addition to a good leaving group.
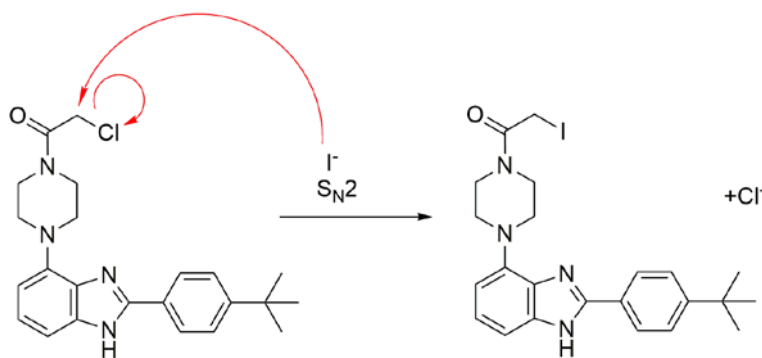
Figure 5: Example of S_N2 nucleophilic iodination.[41]

Electrophilic substitution is usually the preferred method for radioiodination of aromatic compounds. This method is based on the oxidation by mild oxidizing agents (in example: Chloramine-T, ICl, peracetic acid, N-chlorosuccinimide) to I$^+$ and thereby directly labeling by the radionuclide or indirectly by various radio de-metallation where Si, Gn, Sn and organothallium, organomercury usually with high regioselectivity and radiochemical yields. Destannylation is the most favored method due to high radiochemical yield, mild

conditions and the use of small amounts of precursor.[10, 42] The SPECT diagnostic agent ^{123}I-FP-CIT DaTSCAN, ^{123}I-2-β-carbomethoxy-3β-(4-iodophenyl)-N-(3-fluoropropyl)nortropane is radiolabeled by radioiodide-destannylation. DaTSCAN is a commercially available ^{123}I–labeled radiopharmaceutical used to diagnose Parkinson's syndrome and to help differentiate probable dementia with Lewy bodies from Alzheimers disease.[3]

Prosthetic groups are used in radiolabeling as an indirect method of labeling. In short, a small molecule, for example a bis-tosylated ethyl group, is radiolabeled and then reacted with compound that is not well suited for direct radiolabeling.[43] Alkylating agents, amide bond and reactive amines, thiol functionalization, radio-click chemistry and transition-metal catalyzed cross-coupling reactions can be examples of the use of a prosthetic group. The copper-catalyzed azide-alkyne cycloaddition (CuAAC) also known as click-chemistry has been widely used in medicinal organic chemistry to diversify lead molecules where structure activity relationship (SAR) studies are important. The CuAAC has also been used for a long time to radiolabel different molecules mainly due to its reliability, amenability for late-stage radiolabeling, few side products, and good yields.[44] The proposed catalytic mechanism was revealed by Fokin et al., Figure 6. Two copper atoms binds to the alkyne in a two-step manner, whereas the electron rich nitrogen on the end of the azide attracts the alkyne, then after electron rearrangements and intermediate bindings between nitrogen and the two copper ligands, the ring formation is complete and one of the copper atoms leave the triazole.[45]
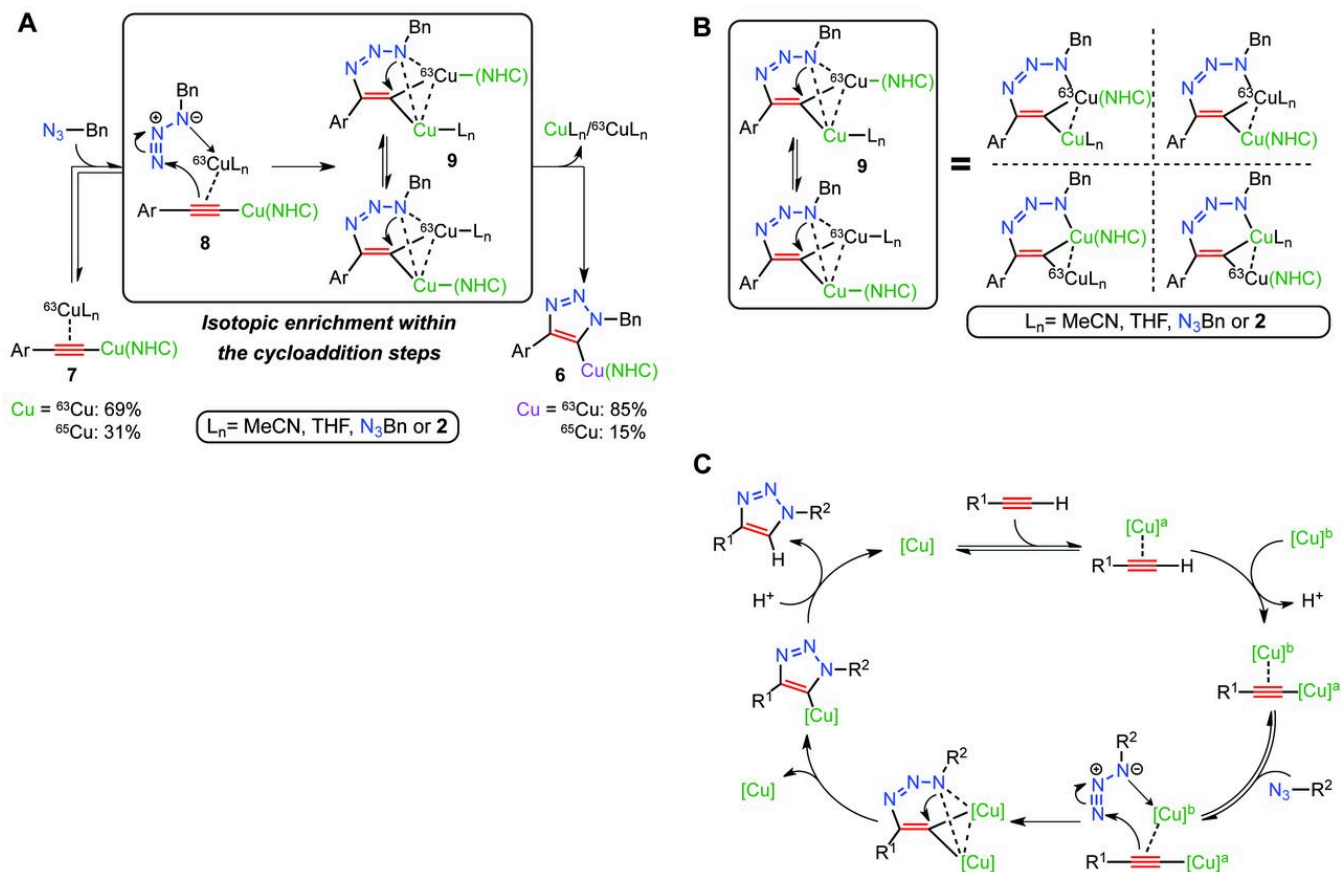
*Figure 6: Proposed catalytic mechanism for CuAAC. **A**) Mechanistic rationale for the isotopic enrichment of triazolide. (**B**) Rapidly interconverting isomers of intermediate **9**. (**C**) Proposed catalytic model for the CuAAC with two copper atoms. Reprinted with permission from Worrell, B. T.; Malik, J. A.; Fokin, V. V., Direct Evidence of a Dinuclear Copper Intermediate in Cu(I)-Catalyzed Azide-Alkyne Cycloadditions. Science **2013,** 340 (6131), 457. Copyright@American Association for the Advancement of Science.[45]*

3   AIMS OF THE THESIS

The overall aim for this thesis is to study the potential of gonadotropin releasing hormone (GnRH) antagonists as radiotracers in the early detection and understanding of Alzheimer's disease, based on their relationship to the hypothalamus-pituitary-gonadal (HPG)-axis. More specifically:

- Develop a library of GnRH antagonists with focus on late-stage diversification and possibilities for late stage radiolabeling (paper I)
- Develop a radiolabeling technology for potential GnRH antagonists (paper II and paper III)
- Assess *In vitro* and *in vivo* the most promising candidates (paper IV and paper V)

4   SUMMARY OF PAPERS AND AUTHOR´s CONTRIBUTION

4.1   PAPER I

Small molecule piperazinyl-benzimidazole antagonists of the gonadotropin-releasing hormone (GnRH) receptor. Richard Fjellaksel, Marc Boomgaren, Rune Sundset, Ira H. Haraldsen, Jørn H. Hansen and Patrick J. Riss. *MedChemComm* **2017**, *8* (10), 1965-1969.

The aim of the initial study was to find a suitable scaffold molecule for late stage diversification and late stage radioiodination with high affinity for the GnRH-R. WAY207024 was selected as a scaffold since WAY207024 has the possibility to apply click chemistry with copper-catalyzed azide-alkyne cycloaddition (CuAAC) and thereby makes a late stage diversification possible. The increase of solubility was a main goal since the literature reported WAY207024 as sparingly soluble. Therefore we had to choose candidates which would make the compound more aqueous soluble. The scaffold and key intermediate was synthesized in a 7 step synthesis and gave 21 different analogues to be tested in a competitive inhibition assay for the affinities to the GnRH receptor. Several compounds showed nanomolar affinities compared to WAY207024 in the assay. We postulated that an addition of a pyranose would increase the aqueous solubility and still have high binding affinity. However, the addition of the pyranose moiety did not show comparable affinities to WAY207024. The addition of a synthetic glycoside resulted only in a 3-fold loss of the affinity and the addition of a 2-fluoroethyl triazole showed comparable affinities to WAY207024. This resulted in 1.5 times more soluble compound than WAY207024 (pH 7.4 PBS).

Author contributions
P.J.R, J.H., M.B. and R.F developed the synthetic strategies. R.F. performed the synthetic work and designed the compounds. The biological assay and the thermodynamic solubility assay was performed by external partners/companies. Analysis of data by R.F., J.H., P.J.R. and M.B. Major contribution in manuscript preparation: R.F., J.H. and P.J.R.

4.2   PAPER II

Copper-mediated late stage iodination and ^{123}I-labelling of triazole-benzimidazole bioactives. Richard Fjellaksel, Rune Sundset, Jørn H. Hansen, Patrick J. Riss. Synlett. Accepted 16 march, 2018

Herein we present the effort to adapt the copper-catalyzed azide-alkyne cycloaddition (CuAAC) to include iodine on the triazole moiety by late stage radiolabeling. The reaction gives two different products one with iodination

in the 5-position on the 1,2,3-triazole, one product without iodine on the triazole and one with iodination on the 7-position on the benzimidazole. We investigated the different reaction conditions known from literature and measured the effects of the copper source, additive, and solvent. Published literature had reported problems with the chelating effects between copper and piperazine. We started the investigation of solvents where H_2O:THF in a 1:9 relationship was found to be the best, $CuSO_4$ $CuCl_2$ and $Cu(ClO_4)_2$ where analyzed and $Cu(ClO_4)_2$ gave the best results, finally a number of bases were tested: TEA, KOAc, KOH, KOtBu and pyridine showed the best yields (27-34%). We then used the best bases, solvent and copper source in a hot experiment with $Na^{123}I$ in water. These experiments showed a serendipitous discovery of radioiodination with high analytical radiochemical yield on the 7-position on the benzimidazole. We further exploited this reaction and iodinated several bioactive compounds with 2-fluoroethyltriazole, a pyranose and a synthetic glucoside. For a further evaluation of the addition of iodine on the benzimidazole the compounds was tested in a competitive binding assay for the GnRH-R and showed a drop in binding affinity by approximately one order of magnitude compared to WAY207024. The compound iodinated on the 5-position on the 1,2,3-triazole showed comparable binding affinities to WAY207024. Both these iodinated triazole retain antagonistic binding properties and are highly interesting candidates for progression into imaging studies.

Author contributions

P.J.R, J.H. and R.F developed the strategies for synthesis and radiolabeling. R.F. performed the synthetic work. R.F. designed the compounds. The biological data was performed by external partners/companies. Analysis of data by R.F., J.H. and P.J.R. Major contribution in manuscript preparation: R.F., J.H. and P.J.R.

4.3   PAPER III

An Acylation-Finkelstein Approach to Radioiodination of Bioactives: The role of amide group anchimeric assistance. Richard Fjellaksel, Damir Dugalic, Taye B. Demissie, Patrick J. Riss, Ole-Kristian Hjelstuen, Rune Sundset, and Jørn H. Hansen. *Journal of Physical Organic Chemistry* **2018**, e3835-n/a DOI: 10.1002/poc.3835

In this paper we investigated the acylation-Finkelstein approach to radioiodination of bioactives. Little is known about the amide group participation in anchimeric assistance. Our hypothesis was that anchimeric assistance could increase the rate of reaction. We present a thorough mechanistic study of the anchimeric assistance on the amide group. The Finkelstein reaction is driven forward by precipitation of sodium chloride in the solvent (acetone) despite the weak bond strength of C-I compared to C-Cl. The precipitation of sodium chloride makes the reaction irreversible. For the different chain lengths (carbon n=2-7) one might expect that the nearby amide group will engage in anchimeric assistance in the displacement of the chloride ion in competition to direct

bimolecular substitution (S_N2 reaction). The different chain lengths of an acyl group (n=2-7) was evaluated kinetically, monitored by ^{1}H-NMR and the reaction rates were determined. The reaction rate for n=2 was very high. The DFT-study revealed that the reaction clearly follows a classical S_N2 substitution reaction. For the longer chain lengths n=3-7 the fastest reaction rate was observed for n=6. For n=5 and n=3 in chain length the reaction rates were undistinguishable. The calculated energy barrier for the n=3 is quite similar to the n=2, however, the calculation lead us to a conclusion that the contribution of both the S_N2 and the anchimeric assistance is quite similar since the formation of the n=3 is a bit faster than the n=5 in our study.

Author contributions

R.F. D.D., O.K.H. and J.H. developed the strategies for synthesis and radiolabeling. R.F. and D.D. performed the synthetic work. D.D. and R.F. designed the compounds. The computational analysis was performed by T.B.D. Analysis of data by R.F., D.D., O.K.H. P.J.R., T.B.D. and J.H. Major contribution in manuscript preparation: R.F. and J.H.

4.4   PAPER IV

***In vitro* evaluation of two promising bioactive triazole-benzimidazole GnRH Receptor-antagonists as possible candidates for SPECT imaging.** Richard Fjellaksel, Angel Moldes-Anaya, Ana Oteiza, Montserrat Martin-Armas, Terje Vasskog, Ole K. Hjelstuen, Jørn H. Hansen and Rune Sundset. *Manuscript*

The two promising candidates from paper II were evaluated for their potential for preclinical trials. The serum stability, metabolic study (liver microsomes, phase 1) and autoradiography were applied. Serum stability analysis was performed with both rat and human serum and revealed that the compounds are stable for up to 22 hours at 37 °C. Metabolic studies were performed with rat liver microsomes and human liver microsomes and revealed several metabolites for the two compounds. The remaining amount of compound was quantified and the compounds where found stable for the use as imaging agents. In addition, autoradiography was performed and showed binding of tracers within several brain sections.

Author contributions

R.F, A.O., M.M.A., A.M.A., O.K.H., and R.S. developed the study design. R.F. performed the synthetic work. The serum stability assay was performed by R.F. The metabolic study was performed A.M.A. and R.F. Analysis of the metabolic data was performed by T.V. A.M.A. R.F. The autoradiography studies was performed by A.O., M.M.A., and R.F. Analysis of data by R.F., J.H., O.K.H., A.O., M.M.A., A.M.A, T.V. and R.S. Major contribution in manuscript preparation: R.F.

First *in vivo* evaluation of a potential SPECT brain radiotracer for the gonadotropin releasing hormone receptor based upon the piperazinyl-benzimidazole class of compounds. Richard Fjellaksel, Ana Oteiza, Montserrat Martin-Armas, Ole K. Hjelstuen, Samuel Kuttner, Jørn H. Hansen and Rune Sundset. *Manuscript.*

The promising compound 1-(4-(2-(4-tert-butylphenyl)-1H-benzo[d]imidazol-4-yl) piperazin-1-yl)-2-iodoethanone which was radiolabeled with high yield was further examined. A promising literature finding paved way for the examination of the α-halogenated compound-1. Human and rat serum stability assay in addition to saline stability were performed and revealed a surprisingly good stability. In addition, a competitive binding assay was performed which showed nM affinity to the GnRH-R. The literature finding, serum stability and the binding affinity results were indication for *in vivo* evaluation. Rat brain single photon emission tomography imaging (SPECT) and biodistribution studies gave further insight on the nature of the compound as a radiotracer and the compound were not found suitable as a radiotracer.

Author contributions

R.F., A.O., and M.M.A., developed the study design. R.F. performed the synthetic work. The serum and saline stability assay was performed by R.F., The biodistribution study was performed by A.O., and M.M.A. The biological data were performed by external partners/companies. The SPECT/CT imaging was performed by A.O., and M.M.A. Analysis of data by R.F., J.H., A.O., M.M.A., and R.S. Major contribution in manuscript preparation: R.F., A.O., and M.M.A.

5 RESULTS AND DISCUSSION

5.1 DEVELOPMENT OF A GnRH-RECEPTOR ANTAGONISTS LIBRARY (PAPER I)

The main aim for the initial study was to generate a library of potential GnRHR antagonist. Our interest was directed towards the already known compound **WAY207024** because of its high affinity for the GnRH-R and the ability to be used as a scaffold for CuAAC as late stage diversification and late stage radiolabeling at the B (green) moiety, Figure 7.[46] Solubility was cited as a shortcoming by Pelletier and co-workers.[33, 47] Our design strategy was to make triazoles from different functionalized azides, still beneficial for the potency while improving the limited aqueous solubility.[33, 46-47] We included a wide range of azides in the study as means to improve the aqueous solubility.[48-51]
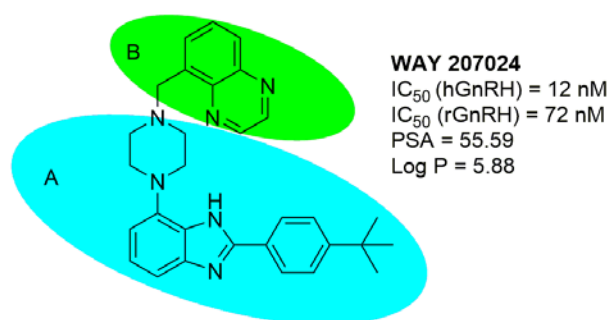
*Figure 7: WAY207024 as starting point for our synthetic strategy. A (Blue) moiety has been identified as the scaffold specific for binding to GnRH-R.B (green) is the moiety of interest for late stage diversification. The key properties as IC_{50} in rat and human GnRH, PSA and Log P are displayed on right side. Reprinted with permission from Fjellaksel, R.; Boomgaren, M.; Sundset, R.; Haraldsen, I. H.; Hansen, J. H.; Riss, P. J., Small molecule piperazinyl-benzimidazole antagonists of the gonadotropin-releasing hormone (GnRH) receptor. MedChemComm **2017,** 8 (10), 1965-1969. Copyright@Royal Society of Chemistry.[52]*

In a six step synthesis the key intermediate **7** was synthesized with 19% overall yield, Scheme 1. Several modifications were done in comparison to literature.[33, 47] The oxidative conversion of **4** into **6** proceeded smoothly with air as an oxidant and in absence of transition metal catalyst.
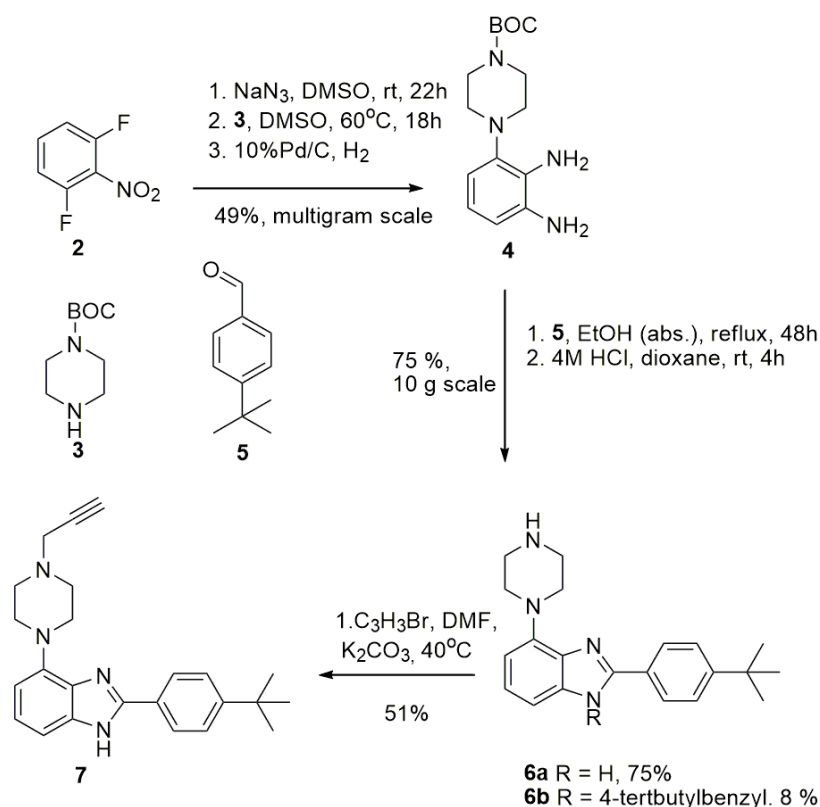
Scheme 1: Synthetic route to alkyne intermediate **7**. Reprinted with permission from Fjellaksel, R.; Boomgaren, M.; Sundset, R.; Haraldsen, I. H.; Hansen, J. H.; Riss, P. J., Small molecule piperazinyl-benzimidazole antagonists of the gonadotropin-releasing hormone (GnRH) receptor. MedChemComm **2017**, 8 (10), 1965-1969. Copyright@Royal Society of Chemistry.[52]

The synthetic route to the key intermediate **7** paved way for further diversification by the use of copper-catalyzed azide-alkyne cycloaddition (CuAAC) with a wide range of commercially available azides which gave piperazinyl-benzimidazole triazoles GnRH-R antagonists (**8a**-**8j**) in yields from 4-72%, Scheme 2. The side product **6b** is explained by a canizarro-like reaction.[53]
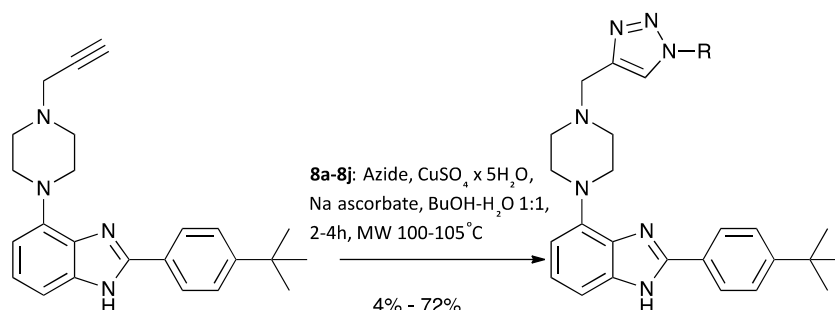
Scheme 2: Diversification using CuAAC as a synthetic strategy. Reprinted with permission from Fjellaksel, R.; Boomgaren, M.; Sundset, R.; Haraldsen, I. H.; Hansen, J. H.; Riss, P. J., Small molecule piperazinyl-benzimidazole antagonists of the gonadotropin-releasing hormone (GnRH) receptor. MedChemComm **2017**, 8 (10), 1965-1969. Copyright@Royal Society of Chemistry.[52]

5.2 INHIBITION ASSAY (PAPER I, PAPER II AND PAPER V)

A competitive inhibition assay was applied after the synthesis and characterization. The division arrested cell lines bought from Multispan Inc. were used to measure the inhibition of receptor activation by LHRH/GnRH with a fluorescence based FLIPR assay. The compounds were tested in concentrations from 50 μM to 0.5 nM with 5 nM LHRH as the competitor. Two well-known positive controls where added (T98475 (**8k**) and AG04557 (**8l**) to validate the assay. The metabolic stable agonist Buserelin was used as a negative control. The lead compound **WAY207024** (**1**) was included in the assay as a reference. Figure 8 shows the compounds that were found to compete with the endogenous agonist GnRH. The K_i was calculated using the Cheng-Prusoff equation.[54] The alkyl piperazines showed only moderate potency, however the Clog P indicates a slight increase in solubility. The introduction of a planar triazole core had a positive effect for the potency as the K_i was measured to be 13.8 nM for compound **8a** (2-fluoroethyl triazole), similar to **WAY207024** (K_i = 12.2 nM). In addition, the Clog P indicates a more soluble compound. Next, the introduction of a functionalized N-Boc-ala triazole improved solubility; however the cost was a loss in the binding affinity of one order of magnitude. A range of pyranose functionalized azides was employed to the triazole because of their improvement for the solubility as shown for the Clog P for compounds **8c-8f**. Unfortunately, the binding affinities dropped out of the desired range. When we masked the polyol as a tretraacetate, the potency increased. However, when we applied a synthetic glycoside we achieved a compromise between solubility improvement and binding affinity (**8g**). Compound **8h**-**8j** from aromatic and heteroaromatic azides did not exhibit the desired solubility or binding improvement.
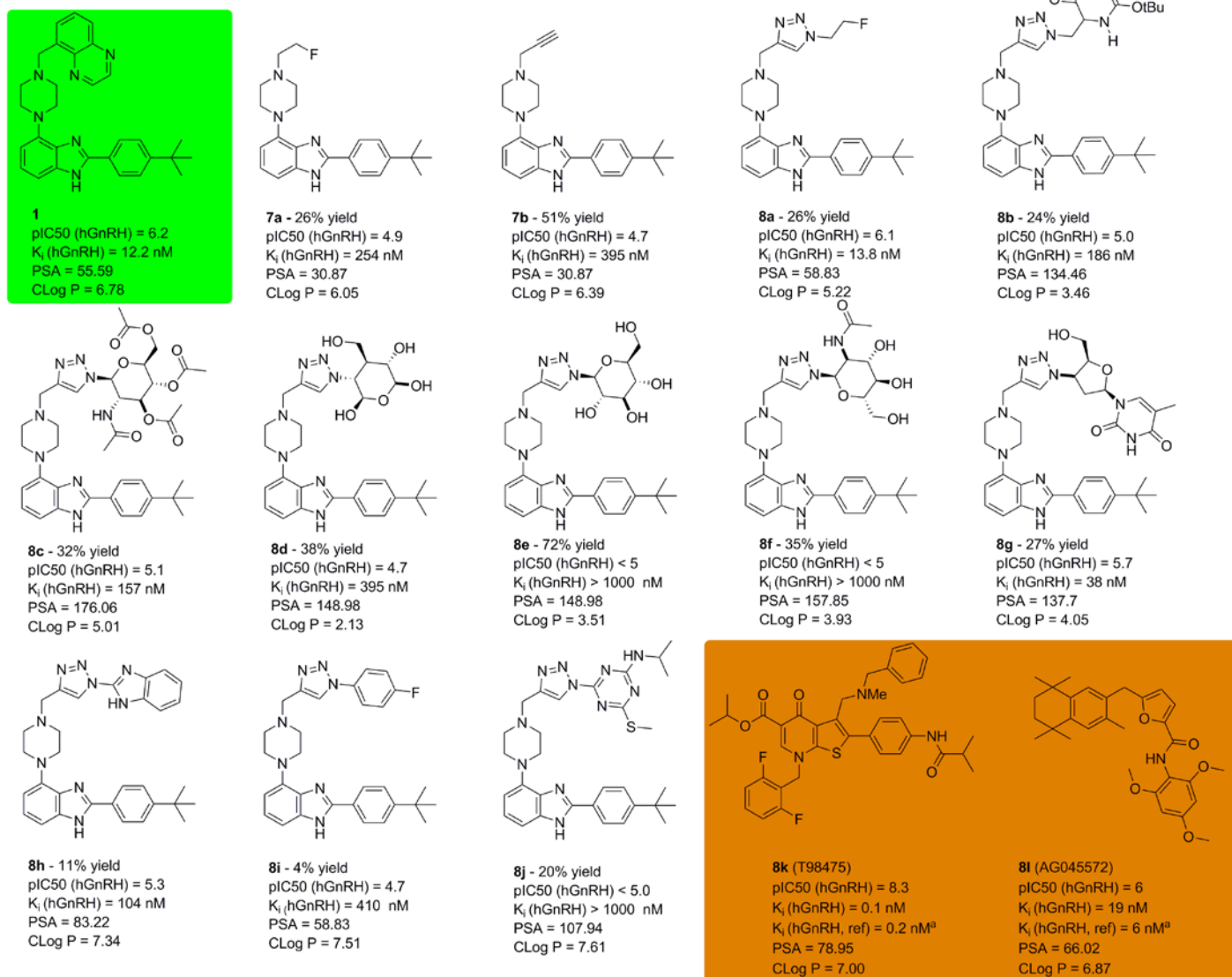
Figure 8: Library of different GnRHR-antagonists showing Ki obtained from Cheng-Prusoff.[52] [a]Reference value from literature.[55-56] Reprinted with permission from Fjellaksel, R.; Boomgaren, M.; Sundset, R.; Haraldsen, I. H.; Hansen, J. H.; Riss, P. J., Small molecule piperazinyl-benzimidazole antagonists of the gonadotropin-releasing hormone (GnRH) receptor. MedChemComm **2017,** 8 (10), 1965-1969. Copyright@Royal Society of Chemistry.[52]

In the same assay, compounds **4** and **5** in paper II were biologically evaluated for their affinity for the GnRH-R. The method described in the previous part was used and the binding affinities determined. K_i for compound **4** was found to be 82.0 nM and for compound **5** 12.9 nM, Figure 9. We have previously reported that Compound **8a** (K_i = 13.8 nM) is equally potent as **WAY207024** (K_i = 12.2 nM).[52] In conclusion, compound **5** is equally potent as **WAY207024**. The antagonistic properties of the 7-iodobenzimidazole **4** dropped approximately one order of magnitude. However, both of the iodinated compounds still retained favorable nM affinities for the GnRH-R.
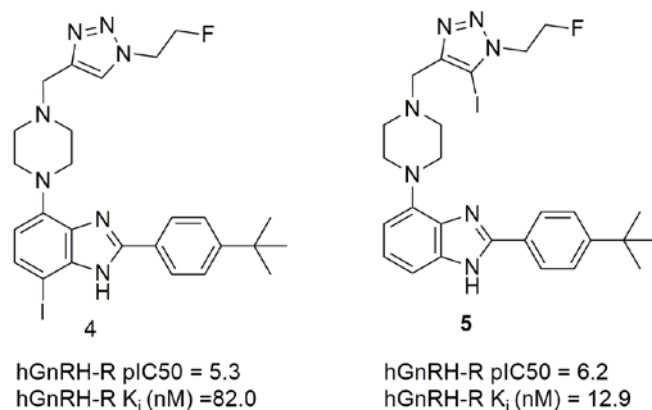
*Figure 9: Inhibition potencies and inhibition constant for compound **4** and **5** from paper II. IC$_{50}$ values are given as the geometric mean of two experiments. K$_i$ was calculated from mean value using the Cheng-Prusoff equation (Ki = IC$_{50}$/(1+[L]/Kd).[54] Reprinted with permission from Richard Fjellaksel, Rune Sundset, Jørn H. Hansen, Patrick J. Riss. Copper-mediated late stage iodination and ^{123}I-labelling of triazole-benzimidazole bioactives. Synlett. Accepted 16 march, 2018. Copyright@Thieme gruppe.*

Furthermore, compound **1** was evaluated in the same competitive binding assay in paper V as described with reference compound **WAY207024**.[52] We obtained a K$_i$ value of 82.0 nM for compound **1** in the concentration dependent competition study using HEK293T cell lines, Figure 10. The affinity for the GnRH-R dropped only a drop of magnitude in order compared to **WAY207024** K$_i$ = 12.2 nM.
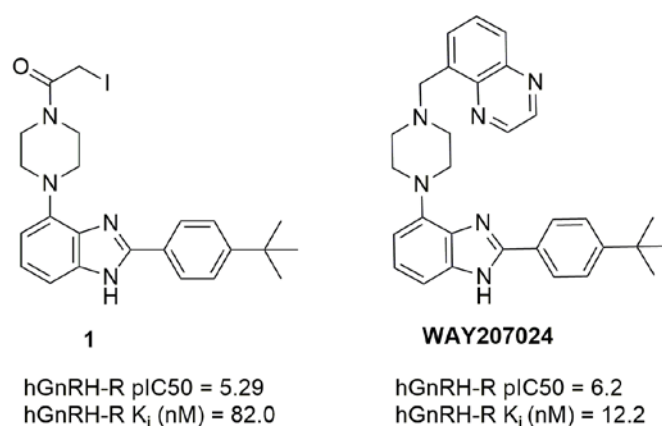
*Figure 10: Inhibition potencies and inhibition constant for compound **1** compared to the reference **WAY207024** from paper V. IC$_{50}$ values are given as the geometric mean of two experiments. K$_i$ was calculated from mean value using the Cheng-Prusoff equation (K$_i$ = IC$_{50}$/(1+[L]/Kd).[54]*

5.3 THERMODYNAMIC SOLUBILITY ASSAY (PAPER I)

Further *in vitro* ADME determination of the aqueous solubility became necessary for the evaluation of compound **8a** and **8g**. Thermodynamic solubility assay was performed for compounds **8a** and **8g**. In short, the compound was dissolved overnight in the desired aqueous buffer system (phosphate buffered saline (PBS) and simulated gastric fluid (SGF). The mixture was then filtrated before quantified by HPLC HRMS. The thermodynamic solubility assay investigates the solubility of a compound as a saturated solution in equilibrium.[57] Interestingly, the thermodynamic solubility assay showed that compound **8a** is 1.5 times more soluble than **WAY207024** at pH 7.4 (PBS) in line with our working hypothesis. Compound **8a** showed a solubility of 3 µg ml^{-1} at pH 7.4 (PBS) and 2.1 mg ml^{-1} at pH 1.2 (SGF). **8g** showed a solubility of 1.2 mg ml^{-1} at pH 1.2 in SGF and <1 µg ml^{-1} at pH 7.4 in PBS.

5.4 COPPER MEDIATED LATE-STAGE IODINATION AND ^{123}I-LABELLING OF TRIAZOLE-BENZIMIDAZOLE BIOACTIVES (PAPER II)

In the initial study we disclosed a library of gonadotropin releasing hormone (GnRH) receptor antagonists using copper-catalyzed azide-alkyne cycloaddition (CuAAC) as a late stage diversification strategy resulting in compound **1** (13.8 nM) and compound **2** (38 nM) affinity for the GnRH-R, Figure 11.[52] In this study we examined a modified CuAAC to make 5-iodo-1,2,3-triazoles. We wanted to introduce a long-lived radionuclide for a straightforward biological evaluation. Direct nucleophilic Radioflurination with [^{18}F] fluoride ion ($t_{1/2}$ = 110 min), ^{3}H-labelling ($t_{1/2}$ = 12.3 years) and iodine-labeling (13.2 hours) were considered for our study. Radiofluorination is an essential step towards PET-imaging, the short half-life and the troublesome logistics makes the biological evaluation problematic. Tritiation would require synthesis of starting material by introducing bromine atoms. The radioiodination is less troublesome since none of the requirements are necessary and in addition there are three highly attractive isotopes of iodine, ^{123}I, ^{124}I and ^{125}I. The ^{123}I in addition to ^{125}I provides longer half-life (13.2h and 60 days), in addition the ^{124}I could be used for PET studies with a half-life of 4 days.
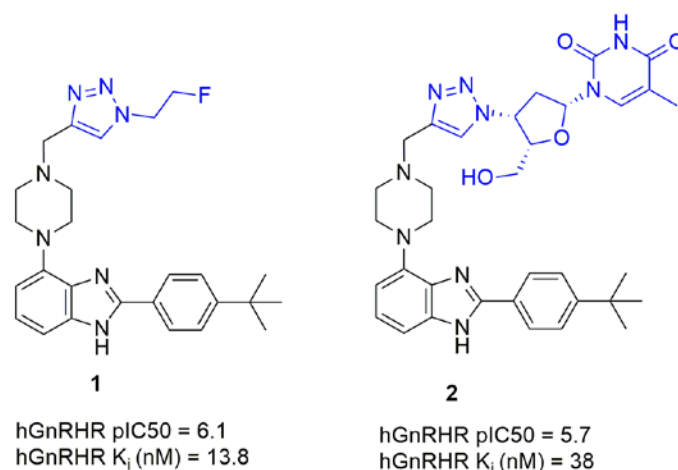
Figure 11: Novel GnRH-antagonists with high affinities to the GnRH receptor.[52] The blue marking shows the triazole moiety. **Reprinted with permission from Richard Fjellaksel, Rune Sundset, Jørn H. Hansen, Patrick J. Riss. Copper-mediated late stage iodination and ^{123}I-labelling of triazole-benzimidazole bioactives. Synlett. Accepted 16 march, 2018. Copyright@Thieme gruppe.**

Several methods exists for making 5-iodo-1,2,3-triazoles and particularly the work by Yan and co-workers caught our attention. They used a one-pot, three component radiochemical reaction variant of the CuAAC to afford 5-[^{125}I]iodo-1,2,3-triazoles in high radiochemical yields (39-99%).[58] However, when we applied the same conditions to our substrates we got compounds **4** and **5** in very low analytical radiochemical yields (8 and 3%, respectively). Notably, compound **4** has not previously been reported. Yan and co-workers reported problems when they tried to radiolabel another piperazine-containing molecule were they observed very low analytical radiochemical yield. They proposed that the piperazine displays a Cu-chelating effect and thereby is inhibiting the CuAAC-iodination.[45, 58-61] Several other studies for the formation of 5-iodo-1,2,3-triazoles suggested a variety of reaction conditions.[58] We wanted to examine this further and designed a small study to evaluate the effect of the copper (II) salt, the additive and solvent effect on the formation of the 5-iodo-1,2,3-triazoles, Table 3. Based on the literature we selected the following solvents: 1:9 mixture of solvents H_2O:t-BuOH, H_2O:MeCN and H_2O:THF as the solvent system. The molar ratio of the reactants alkyne:azide:base:copper salts was 1.0:3.0:1.0:1.0.

Table 3: *Effect of the solvent, copper (II) salts and additive on the formation of small molecule triazoles using Cu-mediated azide-alkyne cycloaddition.*

Entry	Solvent	Copper source	Additive	Isolated yield 1 (%)	Isolated yield 5 (%)[a]
1	H_2O:tBuOH(1:9)	$CuSO_4$	no base	22	NP
2	H_2O:tBuOH (1:9)	$CuSO_4$	TEA	NP	9
3	H_2O:MeCN (1:9)	$CuSO_4$	TEA	NP	NP
4	H_2O:THF (1:9)	$CuSO_4$	TEA	8	11
5	H_2O:THF (1:9)	$CuCl_2$	TEA	NP	NP
6	H_2O:tBuOH (1:9)	$Cu(ClO_4)_2$	TEA	5	3
7	H_2O:THF (1:9)	$Cu(ClO_4)_2$	TEA	21	28
8	H_2O:THF (1:9)	$Cu(ClO_4)_2$	K_3PO_4	48	8
9	H_2O:THF (1:9)	$Cu(ClO_4)_2$	Cs_2CO_3	2	12
10	H_2O:THF (1:9)	$Cu(ClO_4)_2$	DBU	NP	NP
11	H_2O:THF (1:9)	$Cu(ClO_4)_2$	K_2CO_3	35	12
12	H_2O:THF (1:9)	$Cu(ClO_4)_2$	KOAc	14	34
13	H_2O:THF (1:9)	$Cu(ClO_4)_2$	KOH	38	37
14	H_2O:THF (1:9)	$Cu(ClO_4)_2$	KOtBu	37	27
15	H_2O:THF (1:9)	$Cu(ClO_4)_2$	Pyridine	39	31
16	H_2O:THF (1:9)	$Cu(ClO_4)_2$[b]	Pyridine	13	11
17	THF	$Cu(ClO_4)_2$	Pyridine	NP	6

[a]Compound 4 was not detected unambiguously in the HPLC-UV chromatogram [b]4 equivalents of $Cu(ClO_4)_2$ were used

The use of water:t-butanol as solvent and no base resulted in lack of formation of compound **5**. The uniodinated product **1** was formed in 22% yield. The addition of TEA resulted in 9% formation of product **5**. The change of solvent to water:acetonitrile gave no increase in yield. The change of copper (II) salt to $CuCl_2$ resulted in no product formation. Applying $Cu(ClO_4)_2$ with TEA and water:THF gave an increase in yield to 28% for product **5**. The increase in yield when using $Cu(ClO_4)_2$ may be due to the oxidative effect the perchlorate has towards iodine. The change of solvent to water:t-butanol did not increase the yield. Having found that water:THF and $Cu(ClO_4)_2$ worked best, a series of bases were tried: KOAc, KOH, KOtBu and pyridine gave increased yields for compound **5**, respectively 34%, 37%, 27% and 31%. An attempt to boost the yield was tried when applying 4 equivalents of $Cu(ClO_4)_2$, however the yield did not increase. THF alone as the solvent was also tried and did not increase the yield. Our main focus was directed to the formation of compounds **1** and **5**, however the compound **4** was discovered in some entries after a more careful analysis of the reaction mixtures, this was not pursued further.

After the initial study of the effect of solvent, copper (II) salt and additive our focus was turned towards radiolabeling. We applied the same conditions as entry 12, 13 and 15 which gave the surprisingly high analytical yield of **[¹²³I]-4.** This serendipitous discovery of the radioiodination in the 7-position on the benzimidazole was investigated further with the addition of a few more bases to ensure consistency in our data. The analytical

radiochemical yields were ranging from 48-76%, Table 4. The best yield for the iodination on the triazole of compound **5** was found to be pyridine with 11% analytical RCY, Scheme 3.

*Table 4: Analytical radiochemical yields of compound **4** and **5** with [123]I.*

Entry	Base	RCY [123I]-4(%)[d]	RCY [123I]-5(%)[d]
1	KOH[a]	71	5
2	KOAc[a]	76	2
3	Pyridine[a]	68	11
4	TEA[b]	65	7
5	K_2CO_3[b]	48	3
6	KOH[b,c]	69	2
7	Pyridine[b,d]	59	12

[a]Experiments done in duplicates. [b]One experiment.
[c]Na[123]I was added before the 2-fluoroethyl azide.
[D]4 equivalents of $Cu(ClO_4)_2$.
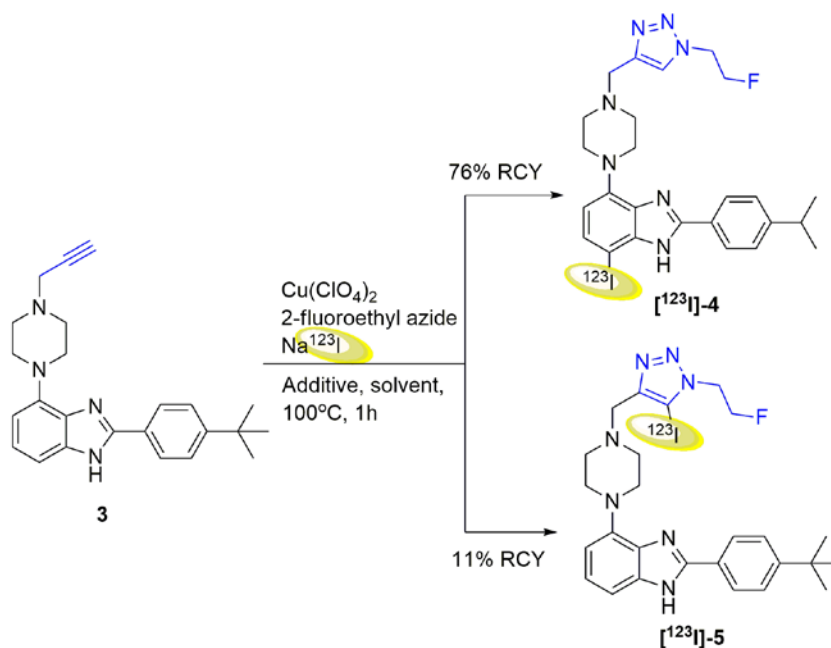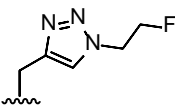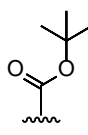
*Scheme 3: Radiolabeling of compounds **4** and **5**, $Cu(ClO_4)_2$, 2-fluoroethyl azide, Na[123]I, different additives as shown in Table 3, H_2O:THF (1:9) as solvent, 10 0ºC for 1 hour. Reprinted with permission from Richard Fjellaksel, Rune Sundset, Jørn H. Hansen, Patrick J. Riss. Copper-mediated late stage iodination and ^{123}I-labelling of triazole-benzimidazole bioactives. Synlett. Accepted 16 march, 2018. Copyright@Thieme gruppe.*

5.5 REGIOSELECTIVE IODINATION ON DIFFERENT COMPLEX TRIAZOLE-BENZIMIDAZOLE BIOACTIVES (PAPER II)

As mentioned previously, the regioselective iodination on the 7-position on the benzimidazole part of the molecule was a major discovery in this study. We wanted to examine this independent process in comparison to the iodination on the triazole. The study of this late-stage iodination was performed using a protocol following the same conditions as entry 15 (Table 5) and was applied to several different bioactive compounds. Compound **2** was formed in 38% yield and compounds **7**, **8**, **9** and **10** gave 20-29% yields, non-optimized. The moderate yield may be explained by the complexity of the test substrates or the inability of the reagents to maintain turnover. As a control, the exclusion of Cu(ClO$_4$)$_2$ resulted in no product formation.

Table 5: Regioselective iodination of different GnRH antagonists at the 7-position of the benzimidazole.
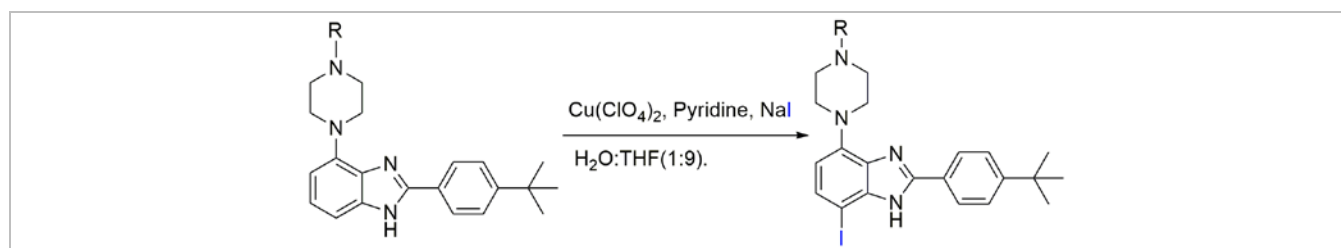
Entry	R=	Isolated yield %
1	**2**	38
2	**7**	20
3	**8**	28

4   **9**   23

5   **10**   29
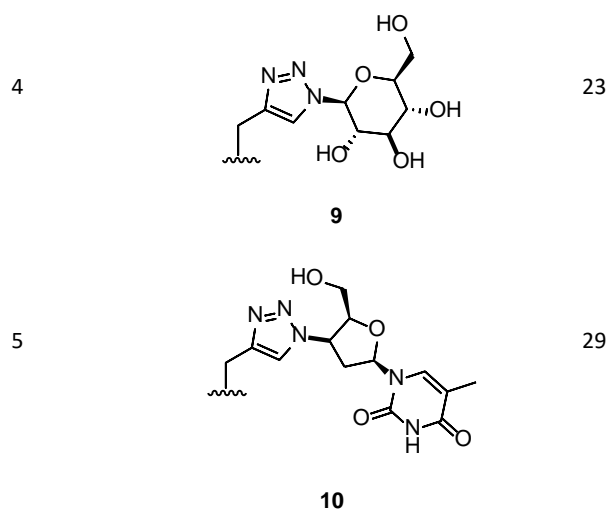
The major discovery was the direct Cu-mediated late-stage iodination of the benzimidazole, which gave novel advanced analogues and an interesting route to iodination for such compounds.

5.6   THE ACYLATION-FINKELSTEIN APPROACH AND SYNTHESIS (PAPER III)

The ability of functional groups to participate in intramolecular nucleophilic reaction to neighboring reactive centers, which is known as anchimeric assistance, was assessed in paper III. Anchimeric assistance is widely known in physical organic chemistry and has been thoroughly studied.[62-68] The participation of amide groups in this context are sparsely reported in the literature.[69] A general and well documented understanding of the amide group participation in anchimeric assistance is lacking, even though Garavelli and co-workers reported experimental and computational evidence for amide group anchimeric assistance in acid-catalysed ether cleavage.[70]

Our main aim here was to assess the acylation-Finkelstein approach for iodination and radioiodination of a bioactive model molecule. We also aimed to disclose the mechanism for the involvement of the amide group in anchimeric assistance. We have used the combination of experimental and computational techniques. The design of the study was based on the experimental comparison between relative rates for the substitution depending of chain lengths and the ring size of the activated intermediate electrophile and a detailed computational study of the mechanistic details of the processes using density functional theory (DFT) calculations. The study would bring fundamental insight into the mechanism of the anchimeric assistance participation of the amide group.

Intermediate **1** was synthesised according to previously published procedures in 37% overall yield from 2,6-difluoronitrobenzene. In addition, this bioactive template has shown nM binding affinities to the GnRH

receptor.[52] In addition, the N–H moiety of the test model substrate is highly suitable for acylation chemistry which makes compound **1** an ideal model substrate. Compounds **2a-e** were synthesized as shown in Scheme 5. The key intermediate **1** gave compounds **2a-e** in yields from 24-67% when reacted with excess of chloroacyl chlorides (**3a-e**), Diisopropylethylamine (DIPEA) and DMF as solvent, Scheme 4.
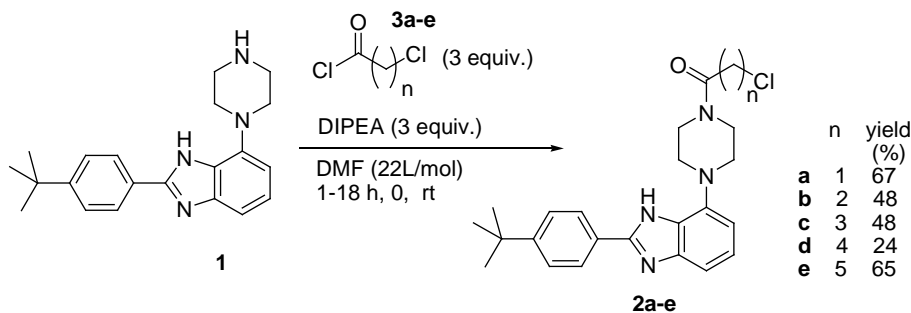
Scheme 4: Acylation of key intermediate 1. Reprinted with permission from Richard Fjellaksel, Damir Dugalic, Taye B. Demissie, Patrick J. Riss, Ole-Kristian Hjelstuen, Rune Sundset, and Jørn H. Hansen. An Acylation-Finkelstein Approach to Radioiodination of Bioactives: The role of amide group anchimeric assistance. Journal of Physical Organic Chemistry 2018, e3835-n/a DOI: 10.1002/poc.3835 Copyright©John Wiley & Sons Ltd.[41]

Compounds **4a-e** were synthesized with the excess of NaI until full conversion of materials. The isolated yields were poor (11-37%), Scheme 5. In an attempt to shorten the reaction time we tried microwave assisted reaction for the formation of **4d** from **2d**, 160 °C and 5 minutes, gave **4d** in 26% isolated yield. ^{1}H-NMR showed full conversion of all substrates so the poor isolated yield is most likely due to instability issue in the work-up or isolation step. Interestingly, we were unable to isolate the expected product **4c**, the isolated product was **5** and the acyl chain was gone.
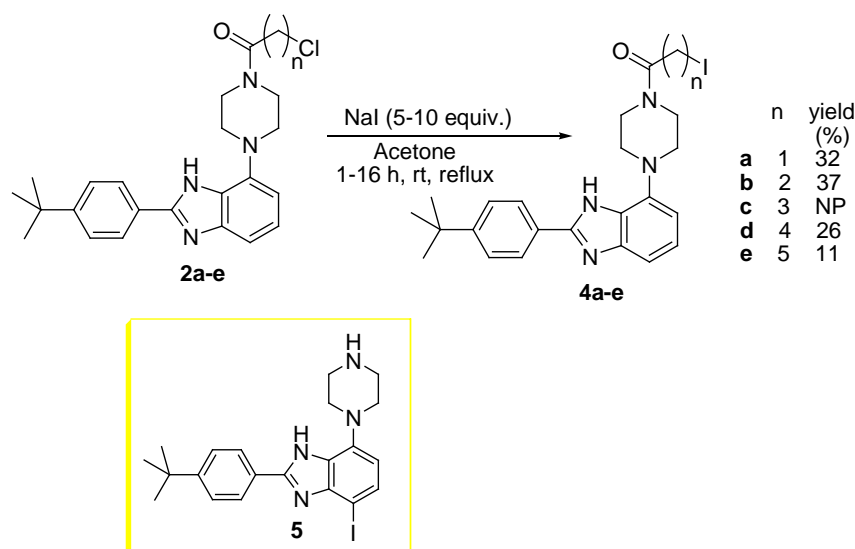
Scheme 5: Finkelstein reactions on chloroamides 2a-e, and the identified compound 5 from the reaction of 2c. Reprinted with permission from Richard Fjellaksel, Damir Dugalic, Taye B. Demissie, Patrick J. Riss, Ole-Kristian Hjelstuen, Rune Sundset, and Jørn H. Hansen. An Acylation-Finkelstein Approach to Radioiodination of Bioactives: The role of amide group anchimeric assistance. Journal of Physical Organic Chemistry **2018***, e3835-n/a DOI: 10.1002/poc.3835 Copyright©John Wiley & Sons Ltd.[41]*

5.7 MECHANISTIC ANALYSIS OF THE ROLE OF AMIDE GROUP IN ANCHIMERIC ASSISTANCE (PAPER III)

The amide group anchimeric assistance is sparsely reported in the literature.[70-71] Therefore, we decided to conduct a mechanistic study to gain a deeper understanding of the complexity involved in this phenomenon based on experimental and computation analysis. The experimental reaction rates were determined by analyzing the relative rates of halide substitution in the substrates. The semi-logarithmic plots of the disappearance of the CH_2-Cl peak in ^{1}H-NMR versus reaction time where graphically illustrated and the method of least square was used to calculate the regression, then calculate the rate constant, Figure 12. The reactions were performed in NMR-tubes in deuterated acetone. Compound **2b**, **2d**, and **2e** displayed clear pseudo-first order kinetics, Figure 12. The observed rate constants are quite similar, however **2e** (0.0612 h^{-1}) were the most rapid after **2a** which was completed after 10 minutes. The rate constant must be understood by a contribution of the two mechanistic pathways direct S_N2-substitution and cyclization of the amide (anchimerically assisted).
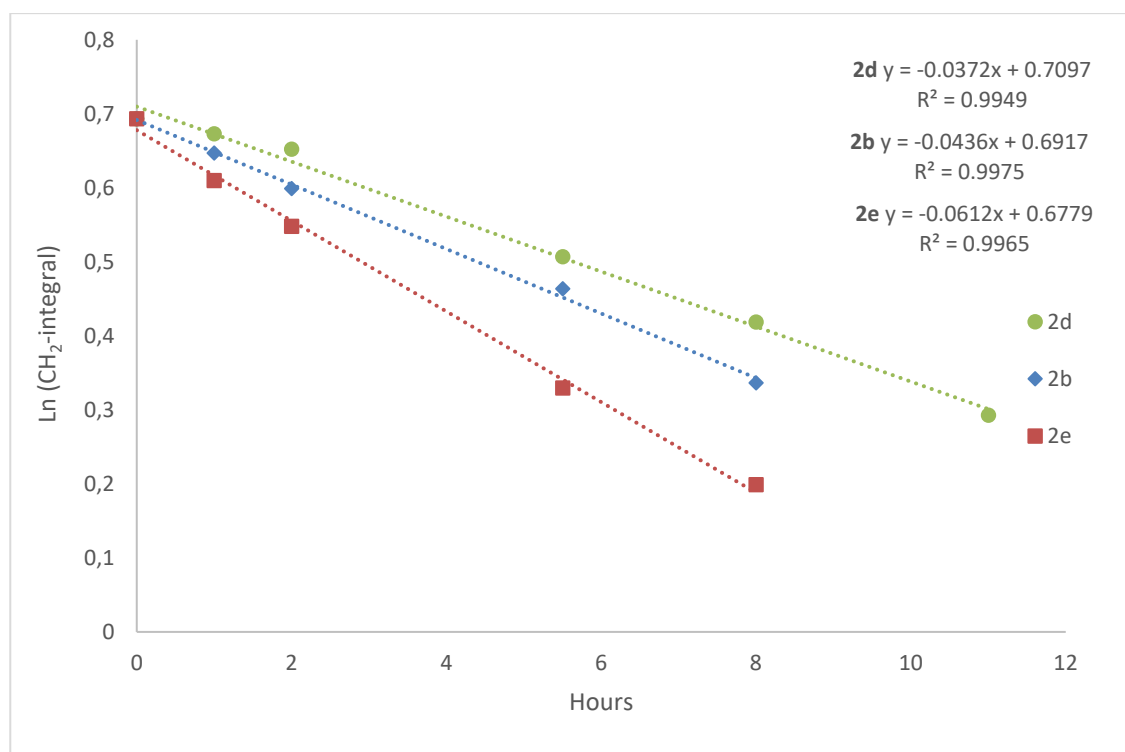
*Figure 12: Semi-logarithmic plots for the disappearance of **2b, 2d** and **2e** with corresponding linear regression analyses. Reprinted with permission from Richard Fjellaksel, Damir Dugalic, Taye B. Demissie, Patrick J. Riss, Ole-Kristian Hjelstuen, Rune Sundset, and Jørn H. Hansen. An Acylation-Finkelstein Approach to Radioiodination of Bioactives: The role of amide group anchimeric assistance. Journal of Physical Organic Chemistry 2018, e3835-n/a DOI: 10.1002/poc.3885. Copyright©John Wiley & Sons Ltd.[41]*

In order to evaluate the observed relative rate constants, we performed computer-aided calculations based on density functional theory (DFT). Both of the two mechanistic pathways for the model chain lengths using ωB97XD functional,[72] 6-311G(d,p) basis sets[73-74] together with the polarizable continuum model (PCM)[75] with acetone as a solvent. A simplified molecule was applied, in which the tert-butyl benzimidazole part is replaced by a H since this part is likely to not affect the reactive center molecule **6a-e**, Scheme 6.
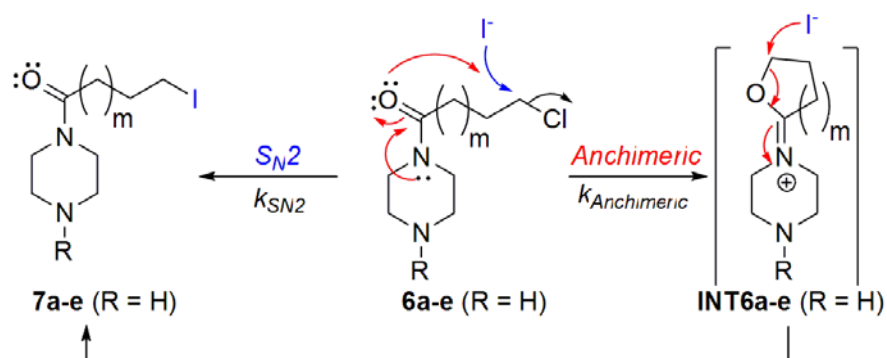
The conversion of **6a** into iodinated product clearly follows a classical S_N2 pathway due to the lack of stability in the ring formation for the hypothetical 3-membered ring. This is supported by the potential energy surface as shown in Figure 13.

Moving to the iodination of molecule **6b**, the situation is more complex. The S_N2 pathway has a barrier of 29 kcal/mol and the anchimerically-assisted pathway has a barrier of 28.4 kcal/mol, Table 6. The anchimerically-assisted pathway is slightly faster, however, at high iodide concentrations the direct substitution could predominate. The contributions of both mechanistic pathways could explain the higher rate constant of **2b** compared to **2d** in the experimental part. **2c** did not give any product formation; interestingly the computer-aided calculations could explain the nature of reaction. Compound **2c** has a predominant anchimerically assisted pathway due to the 7.2 kcal/mol lower free energy barrier. The intermediate is considerably more stable for this

31

molecule than any other is. The relative high-energy barrier for the formation of the iodinated product renders is more vulnerable for hydrolysis and other side reactions in the reaction mixture and this would explain the observation of the side product **5** containing no acyl group. For molecule **6d** the anchimerically assisted pathway (22.5 kcal/mol) is predominant due to is lower energy barrier compared to the energy barrier for the S_N2 reaction (27.2 kcal/mol), Table 6. The intermediate can rapidly react with iodide to form the corresponding product with a barrier of only 17.4 kcal/mol. At low iodide concentrations, this pathway is certainly the predominant one. Moving to **6e** the energy barrier goes up to 25.3 kcal/mol and is quite similar to **6d**.

*Table 6: Computer calculated energy barriers for the S_N2 and anchimerically assisted pathways for the iodination of the substrates **6a-e**.*

Molecule	S_N2 kcal/mol	Anchimercally assisted pathway kcal/mol[a]
6a	25.6	-
6b	29	28.4 (14.8)
6c	28.1	20.9 (31.4)
6d	27.2	22.5 (17.4)
6e	26.8	25.3 (22.9)

[a]In brackets: Calculated energy barriers for the iodine attack on the intermediate.

5.8   RADIOLABELING BY USING ACYLATION FINKELSTEIN APPROACH (PAPER III)

Inspired by Médoc and co-workers who have recently described the use of anchimeric assistance to nearby amino groups as a strategy to introduce radioactive fluoride [^{18}F],[76] we attempted radiolabeling of compound **2a** to demonstrate the validity of the acylation-Finkelstein approach for the radioiodination. Na^{123}I is delivered commercially with water; thereof evaporation of water was performed to maximize the RCY. Compound **2a** was reacted with Na^{123}I in acetone for 1h in reflux, which gave **[^{123}I]-4a** in high analytical radiochemical yield 80%, Scheme 7.
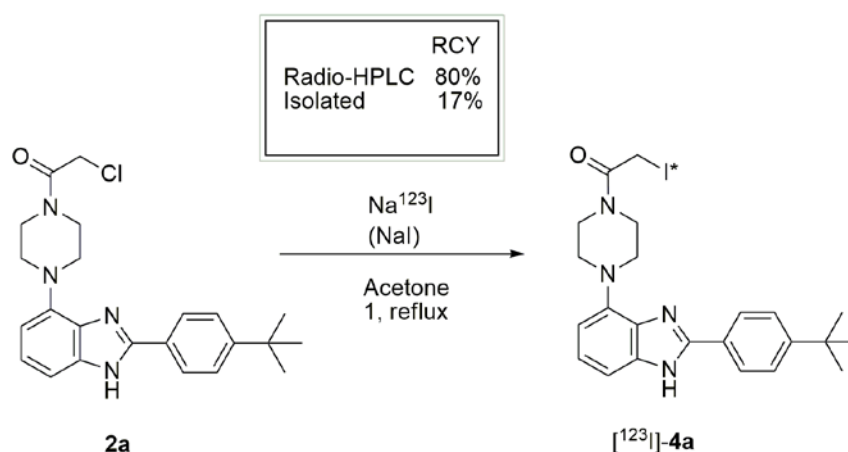
Scheme 7: Radiochemical yields (RCYs) observed for **[^{123}I]-4a**.

The identity of the compound was confirmed by radio-HPLC, Figure 14. Radiolabeling must have a reasonable reaction rate and compound **2a** underwent radioiodination at a high rate. However, the weakness with α-iodo substrate is that it is reactive and may be deiodinated in physiological settings. As such the longer chain analogues may be more stable in physiological settings in order to retain the iodine for a longer time. The longer chained ones are however slower in reaction time and not as suitable for radiolabeling. However, we applied microwave-assisted reaction to overcome this challenge and all substrates **2b, 2d** and **2e** showed full conversion, measured by ^{1}H-NMR, rates only after 5 minutes in microwave. This would render the longer chained ones more accessible for radiolabeling with iodine and due to the slower reaction rates we could expect them to be more tolerable in physiological settings.
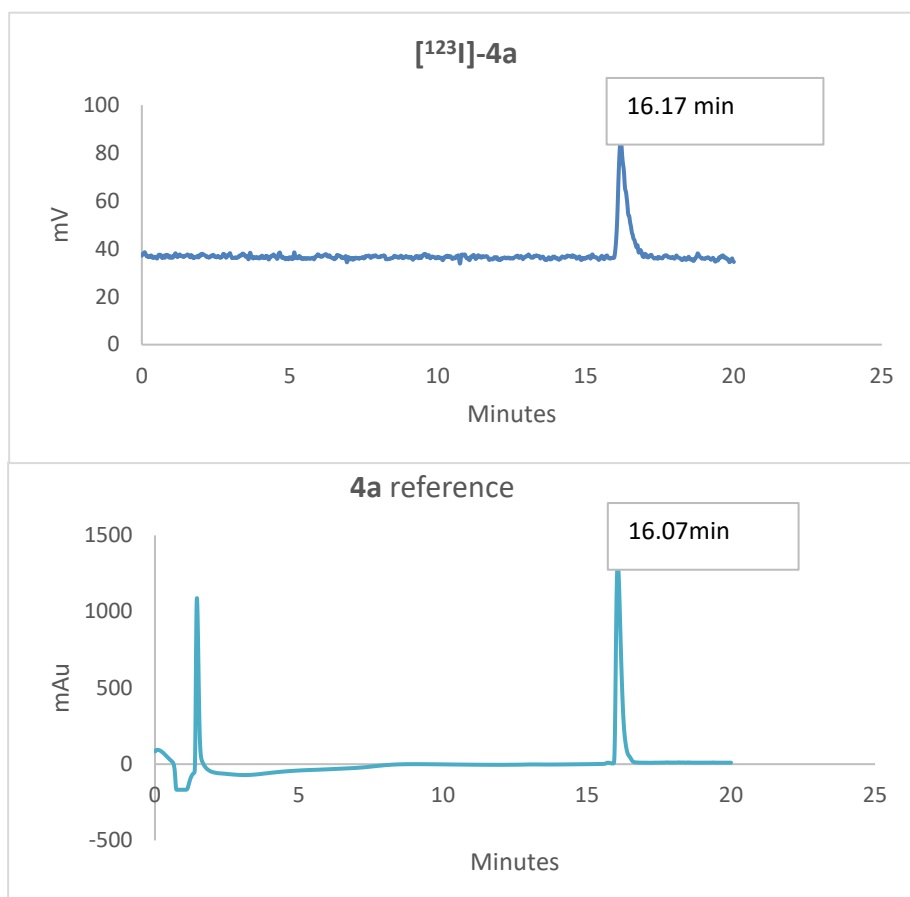
Figure 14: Analytical radiochromatogram of compound [¹²³I]-4a compared to HPLC-UV (214nm) trace of cold 4a reference.

5.9 *IN VITRO* EVALUATION OF TWO BIOACTIVE TRIAZOLE-BENZIMIDAZOLE GnRH-ANTAGONISTS AS SPECT RADIOTRACERS – INTRODUCTON AND STUDY DESIGN (PAPER IV)

In this paper, we have performed the *in vitro* evaluation of two bioactive triazole-benzimidazole GnRH-antagonists. On the basis of the previously reported GnRH-antagonists **1** and **2** (paper I) we developed compound **3** and **4** were we disclosed the synthesis, radiolabeling and binding affinity to the GnRH-R, Figure 15.[52, 77] All of these molecules have nM affinity to the GnRH-R and are designed to be possible imaging agents. In this study we have evaluated compounds **3** and **4** as possible imaging agents. Their serum stability in rat and human serum, the metabolic profiling in rat and human liver microsomes and autoradiography where evaluated for these compounds before preclinical trials.
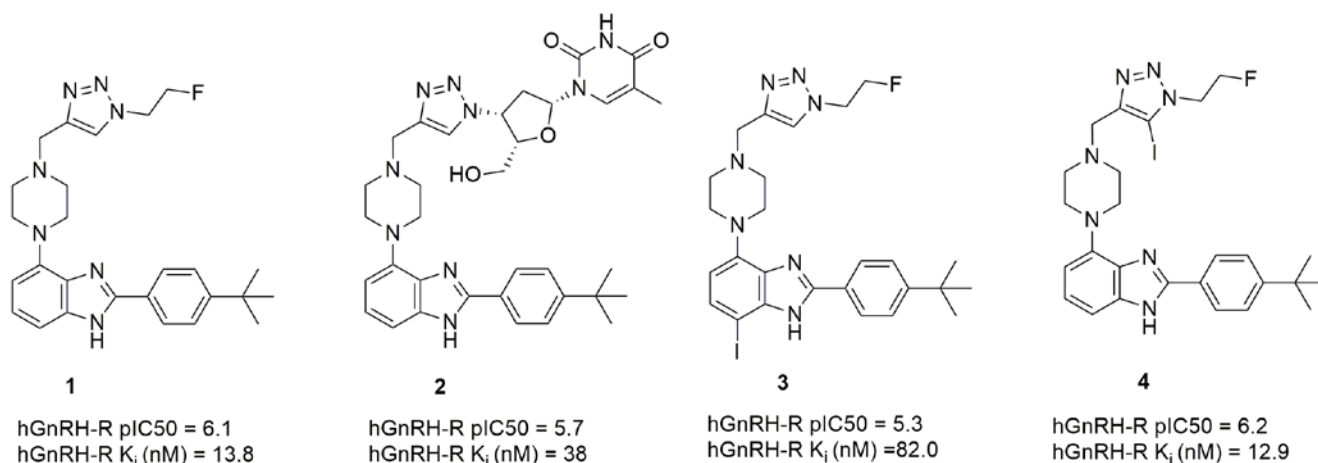
*Figure 15: Previously disclosed compounds **1** and **2** from the initial study (paper I)[52], compounds **3** and **4** were developed in the continuation of the initial study (Paper II).[77]*

5.10 SERUM STABILITY STUDIES (PAPER IV AND PAPER V)

Serum stability of compounds **3** and **4** from paper IV (Figure 15) was analysed by LC-MS, Table 7. The compounds were found stable with more than 70% in rat serum, and more than 84% in human serum, of the original compound remaining after 22 hours, respectively. The serum stability study confirmed sufficient stability for imaging.

Time (minutes)	Compound 3 (%)		Compound 4 (%)	
	hSerum[a]	rSerum[a]	hSerum[a]	rSerum[a]
0	100	100	100	100
30	97	98	109	101
60	107	92	99	94
120	103	81	106	98
1320	84	70	91	86

[a]Stability given as the mean of two independent experiments.

Compound **1** from paper V (Figure 23) was analysed for stability by LC-MS in saline, rat and human serum, Table 8. The stability measurements in saline showed that after 1 hour, 46% of the compound remained, after 120 minutes 10% and after 1320 minutes only 2% of the compound remained. Furthermore, the LC-MS measurements revealed that for rat and human serum 50% of compound **1** remained and after two hours 23% (human serum) and 30% (rat serum) of the compound remained, respectively.

Table 8: Stability of compound 1 in human and rat serum (Paper V), n=3.

Time (minutes)	Human serum (%)	Rat serum (%)	Saline[a] (%)
0	100	100	100
10	88±1.6	86±7.3	-
30	74±8.1	82±11.5	-
60	52±1.5	44±5.5	46
120	23±1.6	30±4.8	10
240	3±0.3	8±1.6	-
1320	0	0	-
1440	-	-	1.6

These results indicate that compound **1** possess serum stability sufficient for imaging.

5.11 METABOLIC PROFILING (PAPER IV)

In addition to the serum stability analysis we performed a metabolic profiling for compounds **3** and **4** (paper IV). MS/MS fragmentation for compounds **3** and **4** were identified by LC-MS/MS shown in Figure 16. The fragmentations of the metabolites were then identified based on the fragmentation of the parent compounds, and the structures were partly determined. MS/MS spectra with structural information of metabolites can be found in the supporting information. Molecular ions and main fragment ions of the metabolites are given in Table 9 and Table 10.
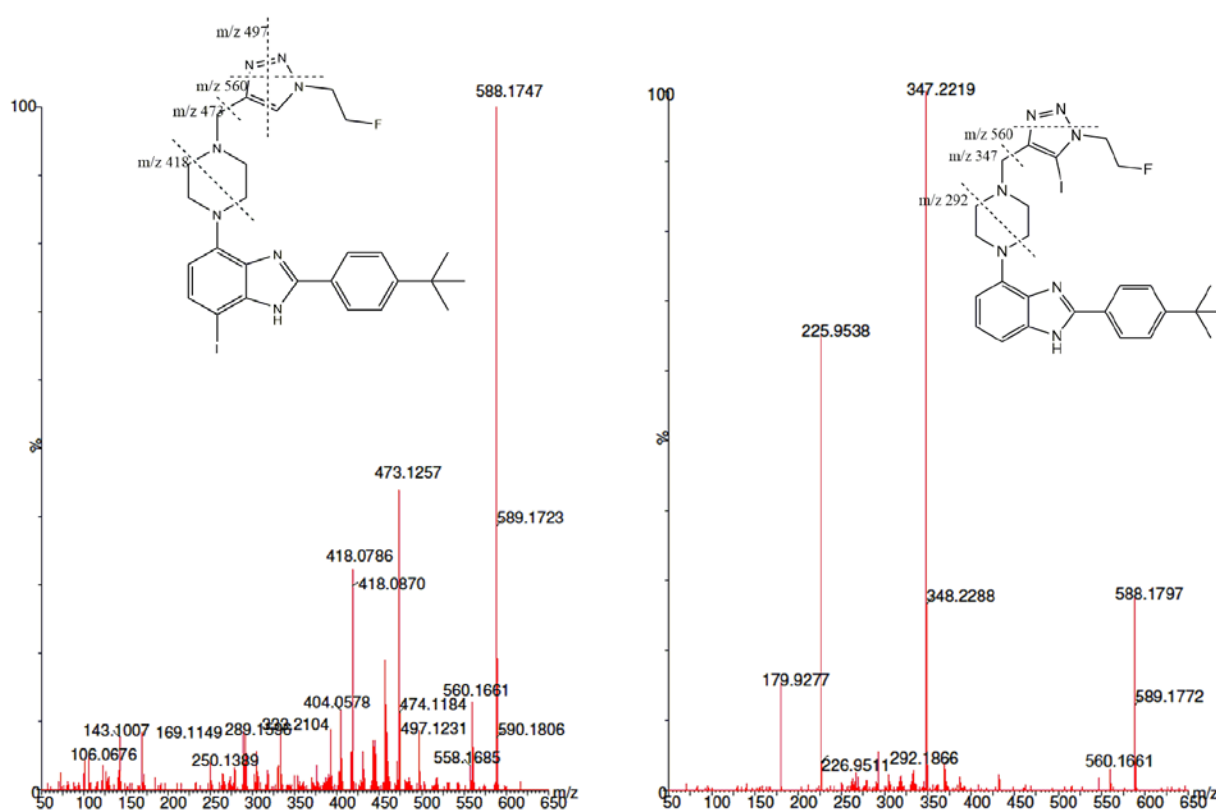
*Figure 16: Structural information obtained by LC-MS/MS. MS/MS spectrum of compound **3** to the left and compound **4** to the right. Major product ions are shown in the structures as mass to charge ratio (m/z).*

Major fragment ions for compound **3** were identified as *m/z* 560, 497, 473 and 418. The fragment ion *m/z* 560 is a loss of two nitrogen's, most likely from the triazole-ring. The *m/z* 497 fragment is probably due to a fragmentation of the triazole-ring where the fluoroethyl group in addition is lost, while the fragment m/z 473 is most likely loss of the entire triazole-ring including the fluoroethyl group. Signal *m/z* 418 is probably a fragmentation of the piperazine.

The metabolites from compound **3** were identified as M1 *m/z* 604 (hydroxylation), M2 *m/z* 578 (hydration and two demethylations), M3 *m/z* 584 (two sequential desaturations), M4 *m/z* 461 (loss of the fluoroethyl-group) and M5 *m/z* 477 (hydroxylation and loss of the fluoroethyl-group) as shown in Table 9.

M1 shows a typical difference of 16 amu compared to compound **3** *m/z* 588, which presumably is a hydroxylation. The MS/MS spectrum shows a fragment signal at *m/z* 576, equal to fragment *m/z* 560 of compound **3**. The signal at *m/z* 489 and *m/z* 434 is equal to the signal *m/z* 473 and *m/z* 418 of compound **3**. M2 is 10 amu less than for compound **3** *m/z* 588, most likely due to hydration and two demethylations. The signal at *m/z* 461, *m/z* and 434 is equal to *m/z* 473 and *m/z* 418 for compound **3**. The signal *m/z* 307 is equal to *m/z* 418 for compound 3, most likely without iodine on the benzimidazole. The signal *m/z* of 295 is equal to the fragment *m/z* 418 for compound 3, however most likely with the additional loss of 12 amu, which is probably a loss of a carbon nearby the nitrogen in the piperazine. The metabolites M3, M4 and M5 were identified by the LC-MS analysis of the fragment ion and additionally by the Metabolyx software.

Table 9: Compound 3 incubated with human liver microsomes. Structural information obtained by LC-MS and LC-MS/MS of metabolites.

Identity	Retention time (minutes)	[M+H]+	Metabolite description	Major fragment ions (*m/z*)[a]
3	4.01	588	Parent	560, 497, **473,** 418,
M1	3.05	604	3 [+OH]	576, **489,** 434
M2	2.91	578	3 [+H$_2$O-CH$_2$-CH$_2$]	461, 434, 307, **295**
M3	3.82	584	3 [two sequential desaturations]	*
M4	3.79	461	3 [-C$_5$H$_6$N$_3$F]	*
M5	2.82	477	3 [+OH-C$_5$H$_6$N$_3$F]	*

*Unable to obtain reliable MS/MS data due to too low concentration. [a]In **bold** diagnostic fragment ions

There is a remarkably similarity between metabolism by rat and human liver microsomes for compound **3**, as shown in Figure 17. Notably, compound **3** is metabolised at a slightly lower rate in human liver microsomes compared to rat liver microsomes. The maximum amount of M1 is produced within 15-30 minutes. In addition, M1 and M2 is produced at a lower rate in human- than in rat- liver microsomes. Additionally, the half-life of compound **3** incubated in human liver microsomes was found to be 43 minutes and for rat liver microsomes 47 minutes. The metabolites M3-M5 were produced in minor amounts (Figure 17).
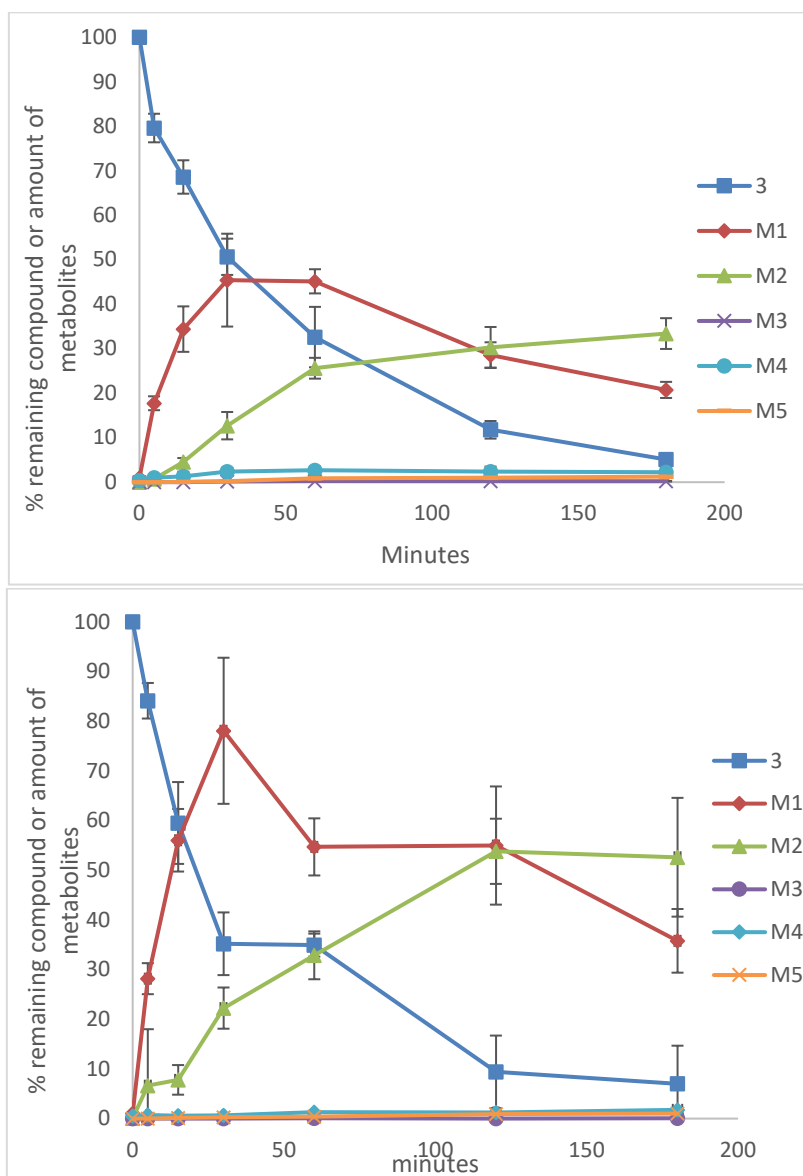
Figure 17: Metabolic transformation of compound 3 with metabolites. Upper graph presents the compound incubated with human liver microsomes and the lower graph with rat liver microsomes. The experiment was performed as two independent experiments with four injections on LC MS-MS.

The ion chromatograms for the compound **3** and metabolites M1-M6 are shown in Figure 18. The increase in the metabolites are seen at the selected time points 15 and 180 minutes for compound **3**.

*Figure 18: Ion chromatogram for compound **3** incubated with human liver microsomes at time points 0, 15 and 180 minutes.*

For compound **4** the fragmentation by LC-MS/MS revealed the major fragment ions as *m/z* 560, 347, 292, 226 and 180. Similarly as for compound **3,** the loss of two nitrogen's probably resulted in the fragment signal of *m/z* 560 from compound **4**. The m/z 347 fragment ion is most likely a loss of triazole with the fluoroethyl group in addition to the loss of iodine. The signal m/z 292 is possibly due to a cleavage of the piperazine. The m/z of 226 and 180 is most likely a fragmentation in the triazole, the signal at *m/z* 226 is probably fluoroethyl group is still present.

The metabolites from compound **4** were identified as M1 *m/z* 604 (hydroxylation), M2 *m/z* 478 (hydroxylation and deiodination), M3 *m/z* 335 (loss of the triazole with the fluoroethyl group in and iodine), M4 *m/z* 558 (hydroxylation and loss of the fluoroethyl group), M5 *m/z* 578 (hydration and demethylation), Table 10.

M1 show a difference of 16 amu from compound **4**, which most likely is hydroxylation. Furthermore, fragment ions of M1 corresponds to a large degree on the fragments of compound **4** (fragment *m/z* 363 corresponds to *m/z* 347, fragment *m/z* 308 corresponds to *m/z* 292, fragment *m/z* 226 corresponds to *m/z* 226 and fragment *m/z* 180 corresponds to *m/z* 180). M2 (*m/z* 478) is probably hydroxylated in addition to a deiodination. The fragment ions of M2 corresponds to a large degree on the fragments of compound **4** (fragment *m/z* 363 corresponds to *m/z* 347, fragment *m/z* 308 corresponds to *m/z* 292). In addition signals *m/z* 226 and *m/z* 180 are missing, which most likely makes iodine on the triazole important for the fragmentation. M3 (*m/z* 335) is most likely the loss of the triazole with the fluoroethyl group and the iodine. The fragment ions for M3 corresponds to a large degree on the fragments for compound **4** (fragment *m/z* 292 corresponds to *m/z* 292, fragment *m/z* 277 and *m/z* 262 corresponds to *m/z* 292, most likely due to the loss of one CH$_2$-group and subsequently another CH$_2$-group. In addition the signals *m/z* 226 and *m/z* 180 is missing here as well, again indicating the importance of the iodine on the triazole for the fragmentation. M4 corresponds to the signal *m/z* 558, which is probably a hydroxylation with the loss of the fluoroethyl group at the triazole. Additionally, the fragment ions for M4 corresponds to a large degree on the fragments for compound **4** (Fragment *m/z* 402 corresponds to *m/z* 560 for compound **4** with the additional loss of iodine, fragment *m/z* 351 corresponds to 347, however with the additional loss of a carbon, *m/z* 308 corresponds to *m/z* 292, fragment ion *m/z* 277 corresponds to *m/z* 292, most likely due to the loss of one CH$_2$-group). The signal for M5 (*m/z* 578) is most likely hydration and demethylation. The fragment ions for M5 corresponds to a large degree to the fragment ions for compound 4 (signal *m/z* 337 corresponds *m/z* 347, *m/z* 308 corresponds to *m/z* 292, *m/z* 226 corresponds to *m/z* 226 and *m/z* 180 corresponds to *m/z* 180). M6 corresponds to the signal *m/z* 542, which probably is a fragmentation of the fluoroethyl group. The fragment ions for this metabolite correspond also to a large degree on the fragment ions for compound **4** (*The m/z* 386 is probably the loss of iodine and two nitrogen's. The *m/z* 335 corresponds to *m/z* 347 with the additional loss of a carbon, signal *m/z* 292 corresponds to *m/z* 292. The *m/z* 278 and *m/z* 266 corresponds to *m/z* 292 (difference of 12 amu) is most likely due to a fragmentation on the piperazine where only a nitrogen is left for *m/z* 266.

Table 10: Compound 4 incubated with human liver microsomes. Structural information obtained by LC-MS and LC-MS/MS of metabolites in human microsomes.

Identity	Retention time (minutes)	[M+H]$^+$	Metabolite description	Major fragment ions (*m/z*)[a]
4	3.17	588	Parent	560, **347,** 292, 226, 180
M1	2.26	604	4 [+OH]	560, **363**, 308, 226, 180
M2	1.98	478	4 [+OH-I+H]	363, **308**,
M3	2.52	335	4 [-C$_5$H$_5$N$_3$FI]	**292**, 277, 262,
M4	2.16	558	4 [+OH-C$_2$H$_3$F]	**402**, 351, 308, 277
M5	2.08	578	4 [+H$_2$O-CH$_2$-CH$_2$]	**337**, 308, 226, 180
M6	3.07	542	4 [-C$_2$H$_3$F]	386, **335**, 292, 278, 266

[a]In **bold** diagnostic fragment ions

The metabolism of compound **4** is quite similar in human and rat liver microsomes. However, it seems like the metabolism is a bit slower in rat liver microsomes than in humans liver microsomes for compound **4,** Figure 19. The main metabolites are M1, M2 and M4. More M1 is formed than M2 and M4 in human and rat liver microsomes. The minor metabolites were M3, M5 and M6. Additionally, the half-life for compound **4** incubated in human liver microsomes was found to be 64 minutes and for rat liver microsomes 86 minutes.
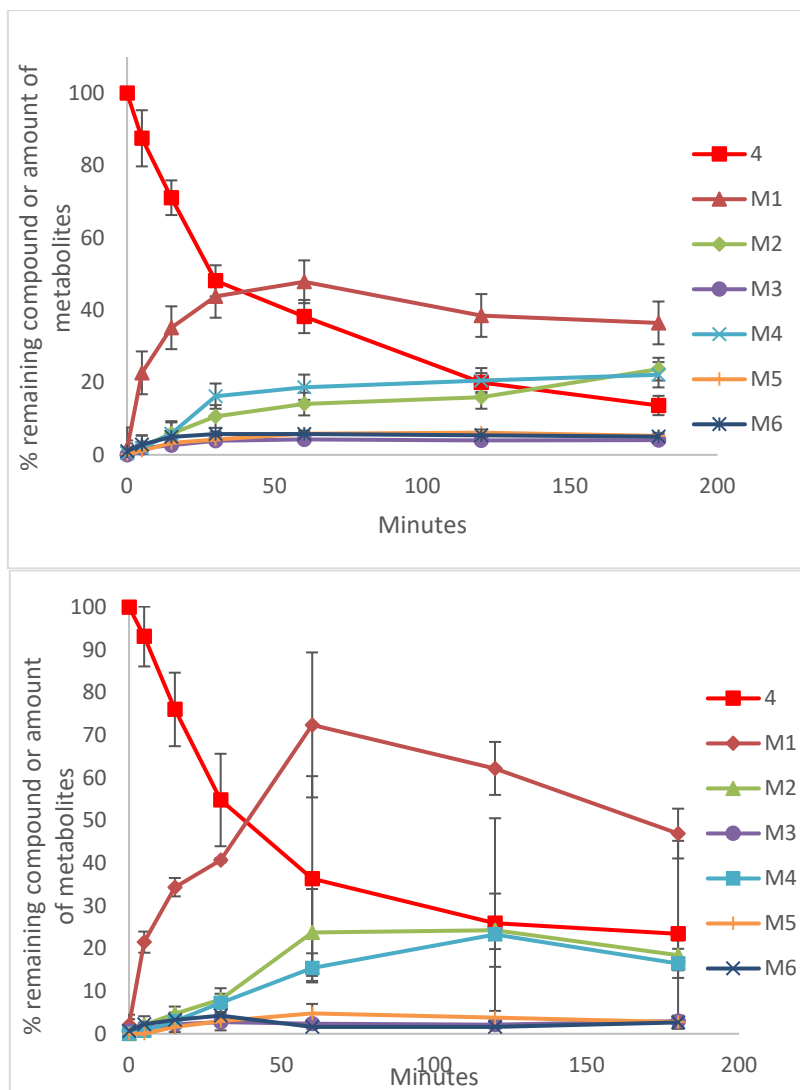
Figure 19: Metabolic transformation of compounds ***4*** *incubated with rat and human liver microsomes. The results are from two different experiments with four injections on LC MS-MS.*

The ion chromatograms for the compound **4** and metabolites M1-M6 are shown in Figure 20. The increases in the metabolites are seen at the selected time points 15 and 180 minutes for compound **4**.
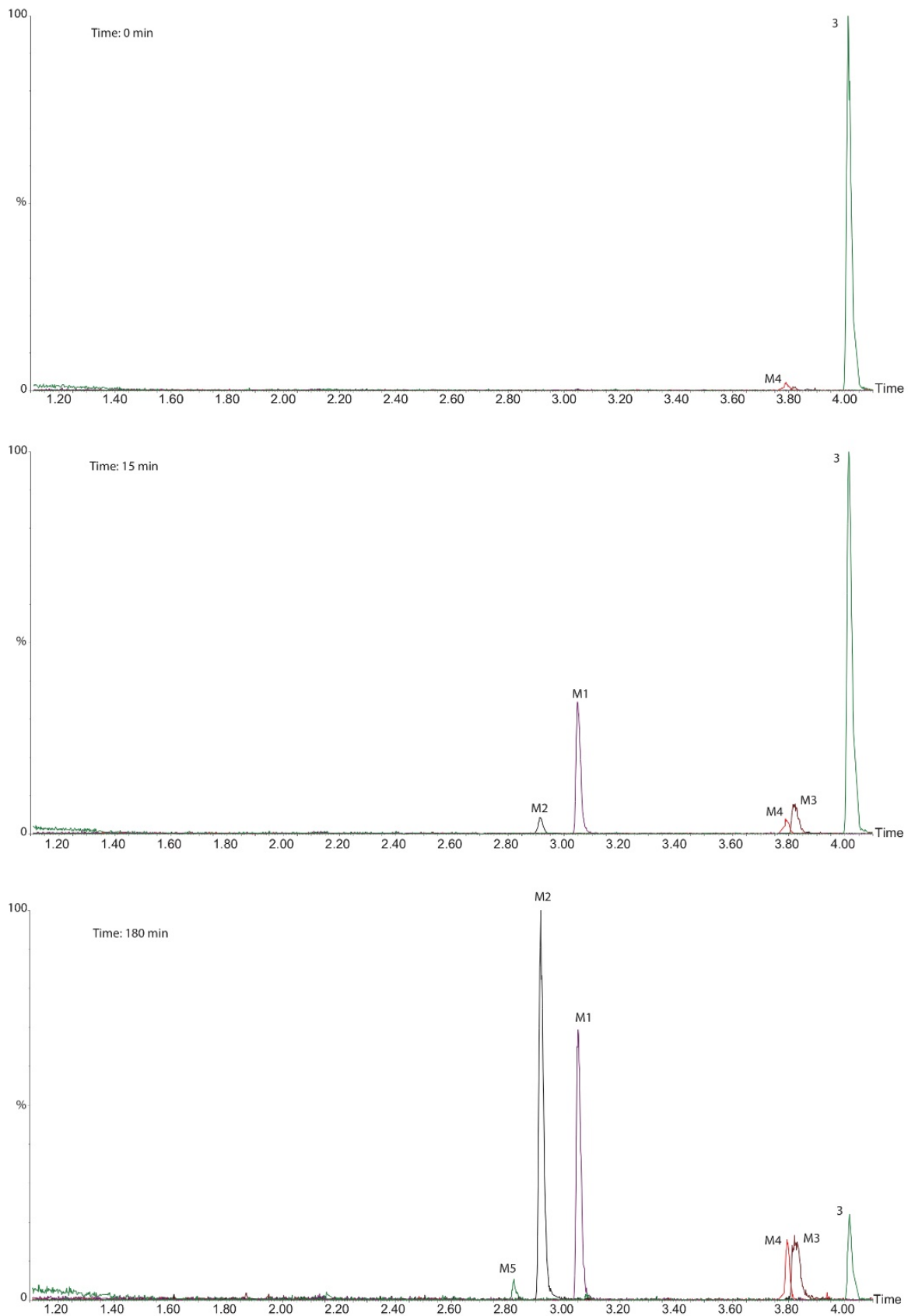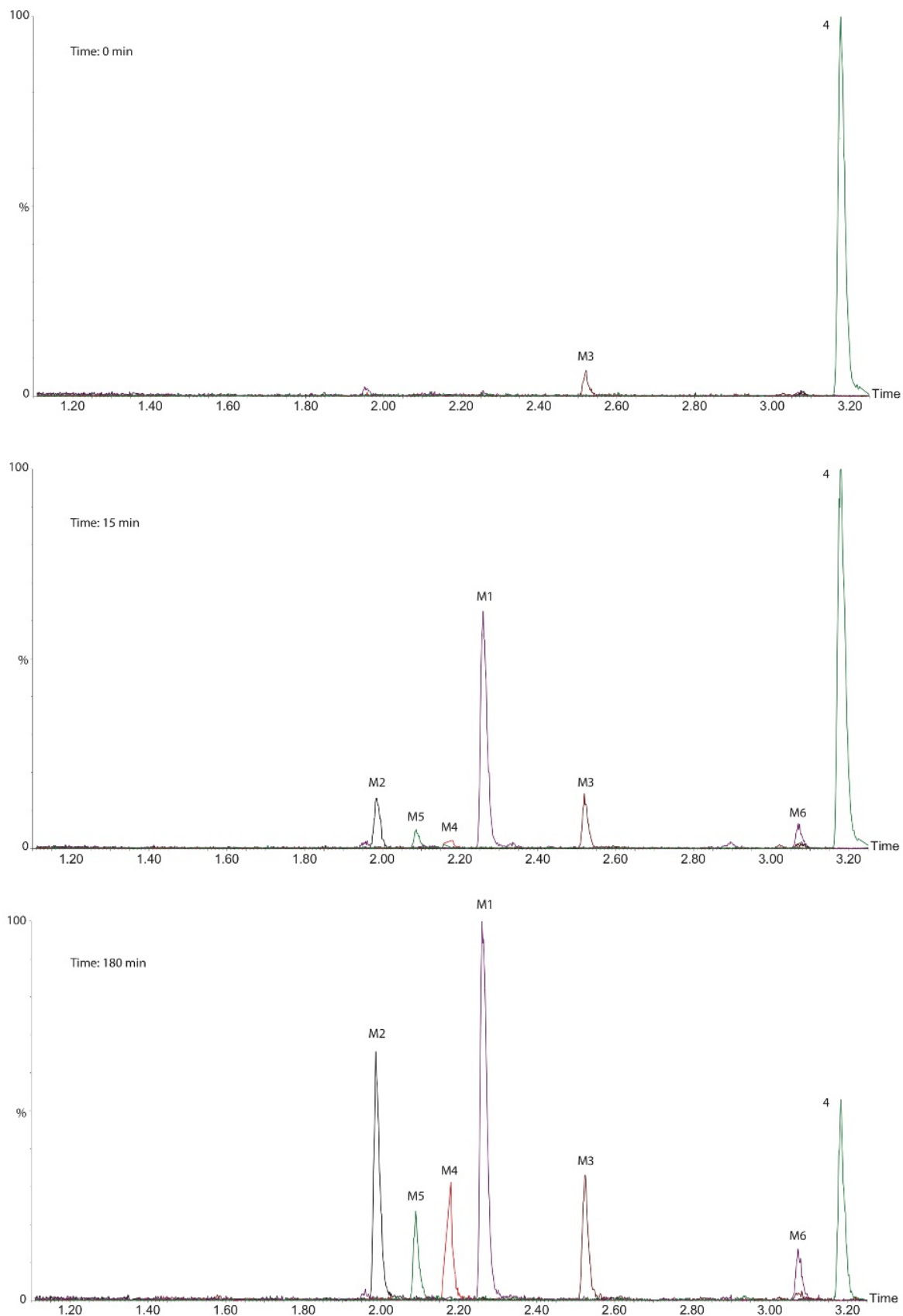
*Figure 20: Ion chromatogram for compound **4** incubated with human liver microsomes at time points 0, 15 and 180 minutes. The increase of metabolites M1-M5 are shown in the comparison to the decrease of the concentration of compound **4***

44

The metabolic profile identified five metabolites for compound **3** and six metabolites for compound **4**. In the light of the metabolic profiling, the metabolism for compounds **3** and **4** both in rat- and human- liver microsomes were found suitable as imaging agent in human and rat. The metabolic half-life was found to be 43 minutes (human liver microsomes) and 47 minutes (rat liver microsomes) for compound **3**. The half-life for compound **4** incubated in human liver microsomes was found to be 64 minutes and for rat liver microsomes 86 minutes. Even though the half-life for compound **4** is a bit longer than compound **3**, the half-life's for both compounds are more than sufficient enough for imaging agents.

5.12 *IN VITRO* AUTORADIOGRAPHY (PAPER IV)

The potential for compounds **3** and **4** to bind to GnRH-R in rat brains were performed in paper IV. Initially, we designed an indirect autoradiography study of binding to rat brain sections. Which means that the competitive agonist [^{125}I]-[D-Trp6]-LH-RH were incubated with the GnRH-R first and then compounds **3** and **4** were incubated with the GnRH-R so that they could compete for the binding to the GnRH-R. The images show the bound ^{125}I[D-Trp6]-LH-RH in competition with compounds **3** and **4**. Compound **3** showed a decrease in signalling when increasing amounts (from 0.1 nM to 100 mM) of compound **3** were added, Figure 21. There is a clear diminution of the activity; not even at concentration of 100 mM compound **3** is able to inhibit totally the binding of the hormone. Compound **4** shows a decrease in signalling when increasing amounts of compound **4** were added. Compound **4** shows a stronger inhibition of the binding of the hormone to the brain sections already at a concentration of 1 nM of and almost no activity when in competition with 10 mM. This is in consistency with our competitive binding assay where compound **3** have a K_i of 82 nM and compound 4 a K_i of 12.9 nM.
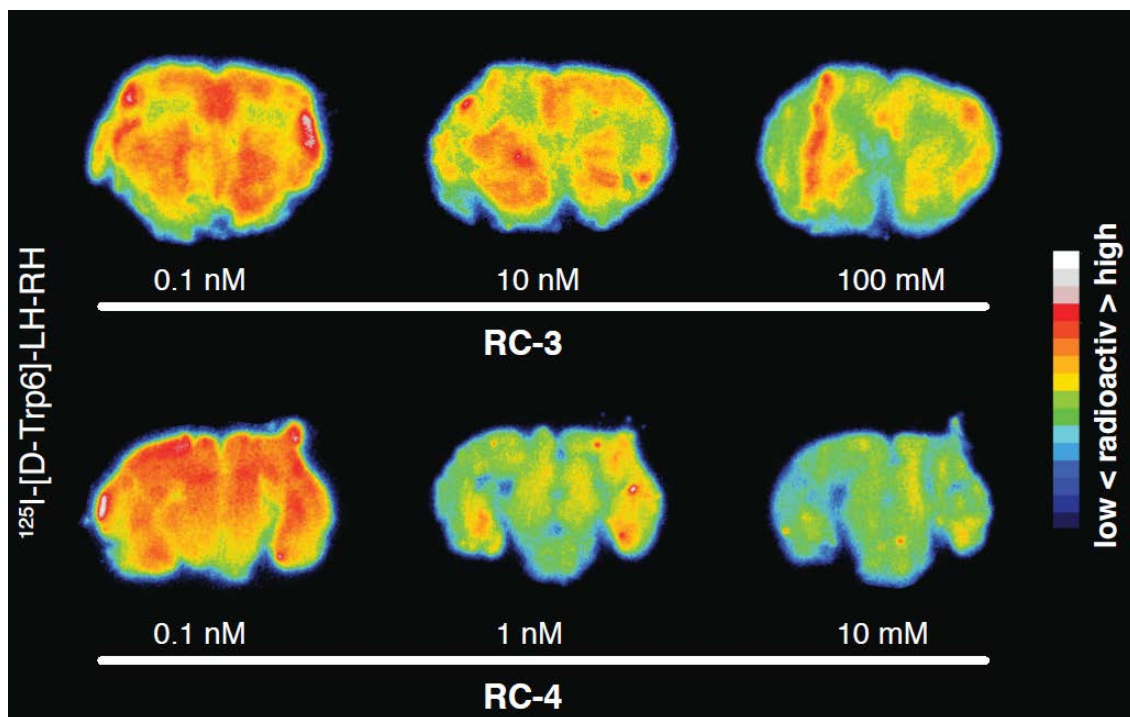
Figure 21: Example of initial autoradiography showing the competition of compounds 3 and 4 against the competitive agonist $^{125}I[D\text{-}Trp6]\text{-}LH\text{-}RH$, n=3.

To confirm our results in the indirect autoradiography study of compounds **3** and **4** we radiolabeled compound **4** with ^{123}I as previously described (paper II) and performed an direct autoradiography study in rat brain sections, Figure 22. By directly labelling the **4** with ^{123}I we were able to visualize the binding in the rat brain region.
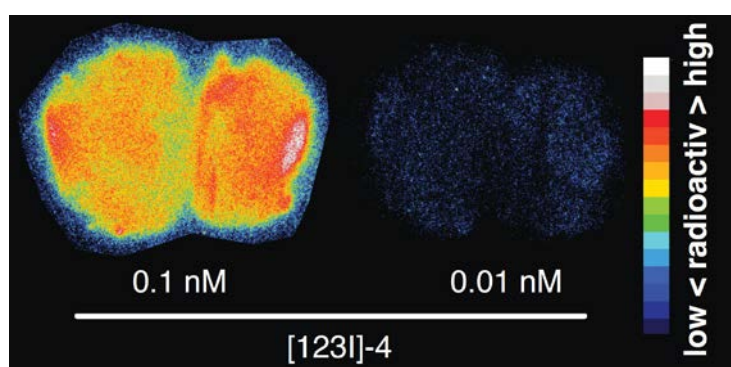
*Figure 22: Autoradiography of **[123I]-4** in rat brain, n=1.*

5.13 *IN VIVO* EVALUATION OF [¹²³I]-1-(4-(2-(4-tert-butylphenyl)-1H-benzo[d]imidazol-4-yl) piperazin-1-yl)-2-iodoethanone (Paper V) – STUDY DESIGN

Initially the reactive compound **[¹²³I]-1** was not found to be stable enough for physiologically settings. However, literature findings of similar compounds **S70254** and **SD6** (Figure 23**)** initiated further investigation of compound 1. Legros and co-workers reported the discovery and receptor specificity evaluation of **S70254** and **SD6** by cell membrane binding assay, tissue membrane saturation assays and *in vitro* autoradiography of rat and sheep brain and retina.[78-79] Paper V is based on the study of the α-halogenated compound-1 and its suitability for *in vivo* testing, followed by *in vivo* evaluation. The serum stability was the prerequisite for further investigations on SPECT-CT imaging and biodistribution.[80]
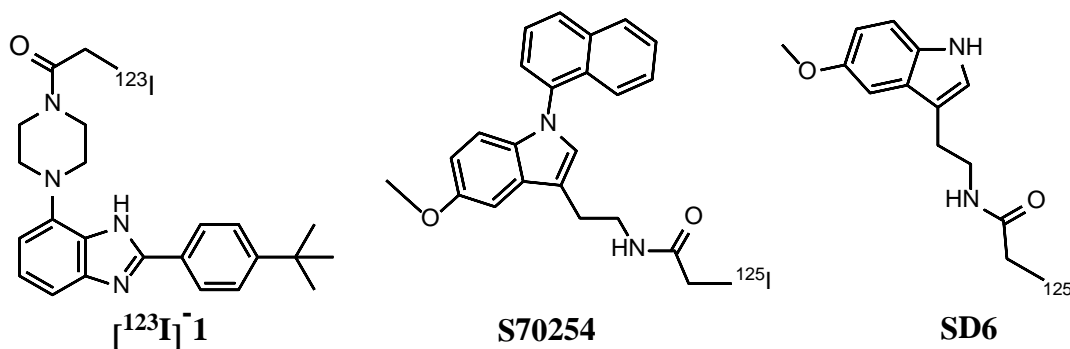
*Figure 23: Structural comparison between **[¹²³I]-1**, **S70254** and **SD6**.*

5.14 *IN VIVO* EVALUATION OF [123I]-1-(4-(2-(4-tert-butylphenyl)-1H-benzo[d]imidazol-4-yl) piperazin-1-yl)-2-iodoethanone (Paper V) – SPECT/CT IMAGING AND BIODISTRIBUTION

The SPECT images were evaluated visually for the uptake in the brain region, Figure 24. An uptake in the thyroid and nose can be seen on pictures A and B. However, we were not able to visually confirm any uptake in the brain region for compound **[123I]-1** and Na123I. Intraperitoneal injections were tried to evaluate the possible accumulation of the compound, however no visual difference were seen in any of the SPECT images.

Figure 24: SPECT Images of male Wistar rat brain. A: Injection of Na123I. B: Intra venous injection of compound [123I]-1 C: Intraperitoneal injection of [123I]-1.

To investigate this further, we designed a semi quantitative study to evaluate the uptake. Three volumes of interests (VOI), namely brain, non-brain and background region were selected, Figure 25. The intensity for these regions was determined and evaluated for difference. The intensity ratio for the signal between brain to non-brain and brain to background values for Na123I were compared with the intensity ratios for 123I-1. The statistical analysis showed no significant differences, paired two-tailed t-test (GrapPad Prism software).
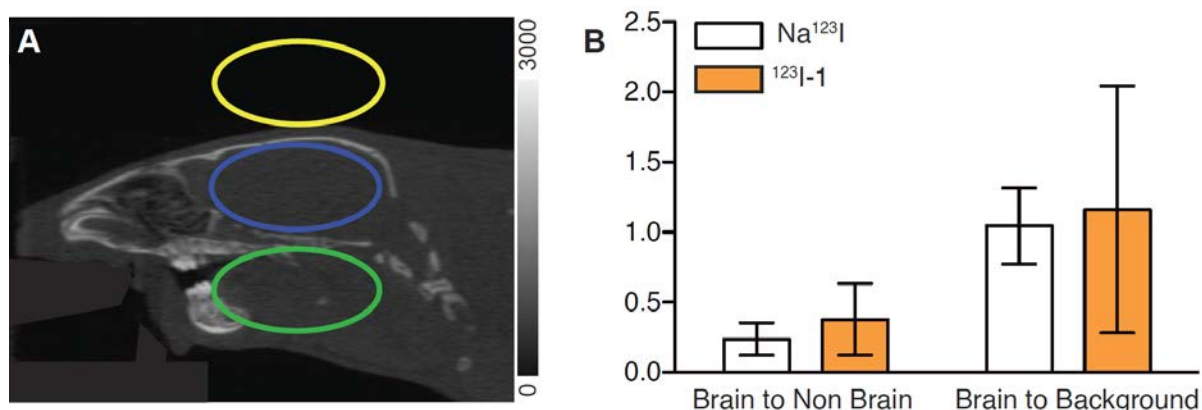
Figure 25: A: The areas selected for the VOIs where brain, non-brain and background were selected. B: Comparison of the selected VOIs measured as intensity which was used to analyze the difference for compounds [123I]-1 and Na123I, n=3.

The biodistribution study for 1 hour post i.v. injection revealed a high uptake in the thyroid (1.2% ID/g) and stomach (3.6 %ID/g), uptake in brain was only 0.03 %ID/g. We also performed a biodistribution of Na^{123}I 1 hour post i.v. injection since we were not able to find literature discussing the biodistribution of Na^{123}I in male Wistar rats, Table 11. The uptake for Na^{123}I in the thyroid was 3.6 % ID/g. The statistical paired, two-tailed t-test showed no statistical difference between **[^{123}I]-1** and Na^{123}I for the uptake in any organs.

*Table 11: ^{123}**I-1** and Na^{123}I biodistribution 1h post i.v. injection*

Organs	Na^{123}I %ID/g	SD±	^{123}**I-1** %ID/g	SD±
Blood	0.66	0.19	0.54	0.22
Urine	1.07	0.34	0.70	0.57
Bladder	0.45	0.16	0.35	0.14
Heart	0.24	0.08	0.22	0.10
Thyroid	3.59	2.63	1.21	1.48
Thymus	0.19	0.06	0.16	0.07
Saliv. Glands	0.25	0.08	0.22	0.12
Lungs	0.37	0.08	0.33	0.16
Pancreas	0.22	0.10	0.21	0.13
Spleen	0.27	0.08	0.24	0.10
Kidneys	0.37	0.10	0.34	0.19
Large I	0.32	0.08	0.30	0.14
Small I	0.57	0.11	0.93	0.89
Stomach	3.40	1.63	3.62	1.70
Feces	0.23	0.23	0.07	0.04
Brain	0.04	0.01	0.03	0.00
Bone	0.30	0.09	0.33	0.20
Liver	0.25	0.07	0.25	0.08
Muscle	0.14	0.06	0.11	0.05
Skin	1.24	1.18	0.38	0.29
Fat	0.06	0.03	0.09	0.03
Testis	0.25	0.08	0.21	0.11

The focus was then directed to the injection techniques and a possibility of accumulation in the brain region. Intraperitoneal injection was then performed and biodistribution determined 2 and 5 hours post injection, Table 12. The biodistribution 2 hours post i.p. injections show an increase of uptake in the thyroid to 5.8% ID/g and after 5 hours to 13.1% ID/g and a decrease in the brain region from 0.02% ID/g to 0,01% ID/g.

Table 12: ^{123}I-1 biodistribution 2h and 5h post i.p injection

Organs	2h post i.p. %ID/g	SD±	5h post i.p. %ID/g	SD±
Blood	0.34	0.012	0.19	0.005
Urine	0.14	0.053	0.84	0.524
Bladder	0.32	0.094	0.26	0.087
Heart	0.15	0.026	0.08	0.005
Thyroid	5.79	1.957	13.14	1.809
Thymus	0.12	0.019	0.07	0.009
Saliv. Glands	0.13	0.009	0.08	0.005
Lungs	0.21	0.005	0.12	0.012
Pancreas	0.51	0.257	0.09	0.025
Spleen	0.16	0.022	0.09	0.005
Kidneys	0.18	0.005	0.11	0.005
Large I	0.20	0.054	0.35	0.323
Small I	1.49	0.947	0.20	0.109
Stomach	2.47	0.893	1.64	0.836
Feces	0.05	0.012	0.81	1.117
Brain	0.02	0.000	0.01	0.000
Bone	0.14	0.005	0.08	0.005
Liver	0.15	0.012	0.10	0.008
Muscle	0.06	0.005	0.03	0.005
Skin	0.26	0.042	0.18	0.040
Fat	0.07	0.042	0.14	0.189
Testis	0.13	0.000	0.10	0.005

Despite our predictions of the reactive nature of α-halogenated amides, compound **1** was stable sufficiently long for a validation of its *in vivo* effects. The compound was initially validated in saline, human and rat serum. The biodistribution study in rat compared with Na[123]I and the SPECT analysis did not show any statistical significant differences. Unfortunately, compound-1 did not show any uptake in the brain region despite the promising stability analyses and literature data. Compound-1 is therefore not suitable as a SPECT radiotracer. Further studies for similar compound with longer chain lengths are planned and our kinetics findings indicates far more robust compounds.[41]

6   CONCLUSIONS

We have synthesized a library of possible GnRH-R antagonists where several compounds were found to have good affinity for the GnRH-R. In addition, the thermodynamic solubility assay showed improved solubility. These compounds were designed to apply the late stage Cu-mediated Azide-Alkyne cycloaddition (CuAAC) mediated radiolabeling. In the second paper, the CuAAC was evaluated to include iodine. [123]I was used as a radionuclide and radiolabeling was performed in 76% and 11% analytical radiochemical yield for compound **4** and **5** in paper II (Scheme 3), respectively. Furthermore, a thorough mechanistic analysis of the anchimerically assisted Finkelstein reaction for the participation of amide neighboring group was disclosed. Compound **2a** from paper III (Scheme 4) was successfully radiolabeled using this method in 80% analytical radiochemical yield and 17% isolated radiochemical yield, respectively. *In vitro* evaluation of compound **3** and **4** from paper IV (Figure 15) were performed to evaluate these compounds prior to preclinical trials. Serum stability demonstrated stable compounds. A metabolic profiling (phase I) examined the metabolism performed by human and rat liver microsomes and found the compounds sufficient stable for imaging. In addition, autoradiography demonstrated binding of the compound to the rat brain. The two compounds (**3** and **4**) from paper IV (Figure 15) were found highly suitable for further preclinical evaluations. In addition, compound **1** from paper V (Figure 23) was evaluated *in vivo* and found not suitable as a radiotracer in the brain region partly due to its reactivity and inability to pass the blood brain barrier.

In light of these findings, several new GnRH-antagonists have been developed and have been found to have desirable characteristics as radiotracers radiolabeled with [123]I. The *in vitro* investigation showed promising results for further trials. As a concluding remark the work in this thesis indicated the high potential these GnRH-receptor antagonists have as radiotracers for pathophysiologic examination of AD and warrant further examination in preclinical trials which are expected to confirm their potential.

7   FURTHER PROSPECTS

Although several interesting molecules have been developed during this project, there are still several potentially interesting molecules to radiolabel and evaluate as possible radiotracers for the early detection of AD. In order to confirm the potential of these compounds more animal studies are strongly recommended. Moreover, the possibility of using ^{18}F, ^{124}I and ^{131}I should be closely evaluated.

8 REFERENCES

1. Hess, S.; Høilund-Carlsen, P. F.; Alavi, A., Historic Images in Nuclear Medicine: 1976 The First Issue of Clinical Nuclear Medicine and the First Human FDG Study. *Clinical Nuclear Medicine* **2014,** *39* (8), 701-703.

2. Alauddin, M. M., Positron emission tomography (PET) imaging with (18)F-based radiotracers. *American Journal of Nuclear Medicine and Molecular Imaging* **2012,** *2* (1), 55-76.

3. Nairne, J.; Iveson, P. B.; Meijer, A., Chapter Five - Imaging in Drug Development. In *Progress in Medicinal Chemistry*, Lawton, G.; Witty, D. R., Eds. Elsevier: 2015; Vol. 54, pp 231-280.

4. Noel, S.; Cadet, S.; Gras, E.; Hureau, C., The benzazole scaffold: a SWAT to combat Alzheimer's disease. *Chemical Society reviews* **2013,** *42* (19), 7747-7762.

5. Hicks, R. J.; Hofman, M. S., Is there still a role for SPECT–CT in oncology in the PET–CT era? *Nature Reviews Clinical Oncology* **2012,** *9*, 712.

6. Michel, C.; Ricard, M., 16. Quantification in SPECT/CT: Calibration, methodology during Q.Metrix software implementation. *Physica Medica* **2016,** *32*, 348-349.

7. Uribe, C. F.; Esquinas, P. L.; Tanguay, J.; Gonzalez, M.; Gaudin, E.; Beauregard, J.-M.; Celler, A., Accuracy of (177)Lu activity quantification in SPECT imaging: a phantom study. *EJNMMI Physics* **2017,** *4*, 2.

8. Association, W. N. Radioisotopes in Medicine. http://www.world-nuclear.org/information-library/non-power-nuclear-applications/radioisotopes-research/radioisotopes-in-medicine.aspx.

9. Silberstein, E. B., Radioiodine: The Classic Theranostic Agent. *Seminars in Nuclear Medicine* **2012,** *42* (3), 164-170.

10. Koehler, L.; Gagnon, K.; McQuarrie, S.; Wuest, F., Iodine-124: A Promising Positron Emitter for Organic PET Chemistry. *Molecules* **2010,** *15* (4).

11. Magill, J.; Pfennig, G.; Dreher, R.; Sóti, Z., Karlsruher nuklidkarte. Nucleonica GmbH 2012, licence from the European Atomic Energy Community: 2012.

12. Moldes-Anaya et al., unpublished data. Neurobiology Research Group, UIT, the Arctic university of Norway.

13. Samuel Kuttner, A. O., Elin Synnøve Hadler-Olsen.

14. Perrett, R. M.; McArdle, C. A., Molecular Mechanisms of Gonadotropin-Releasing Hormone Signaling: Integrating Cyclic Nucleotides into the Network. *Frontiers in Endocrinology* **2013,** *4*, 180.

15. Meethal, S. V.; Smith, M. A.; Bowen, R. L.; Atwood, C. S., The gonadotropin connection in Alzheimer's disease. *Endocr* **2005,** *26* (3), 317-326.

16. Tobin, V. A.; Millar, R. P.; Canny, B. J., Testosterone acts directly at the pituitary to regulate gonadotropin-releasing hormone-induced calcium signals in male rat gonadotropes. *Endocrinology* **1997,** *138* (8), 3314-3319.

17. Zhang, G.; Li, J.; Purkayastha, S.; Tang, Y.; Zhang, H.; Yin, Y.; Li, B.; Liu, G.; Cai, D., Hypothalamic programming of systemic ageing involving IKK-beta, NF-kappaB and GnRH. *Nature* **2013,** *497* (7448), 211-216.

18. Eisenegger, C.; Naef, M.; Snozzi, R.; Heinrichs, M.; Fehr, E., Prejudice and truth about the effect of testosterone on human bargaining behaviour. *Nature* **2010,** *463* (7279), 356-359.

19. Cheung, L. W. T.; Wong, A. S. T., Gonadotropin-releasing hormone: GnRH receptor signaling in extrapituitary tissues. *FEBS Journal* **2008,** *275* (22), 5479-5495.

20. Maggi, R., Physiology of Gonadotropin-Releasing Hormone (GnRH): Beyond the Control of Reproductive Functions. *MOJ Anat & Physiol* **2016,** *2* (5).

21. Hierowski, M. T.; Perla, A.; Redding, T. W.; Schally, A. V., The presence of LHRH-like receptors in Dunning R3327H prostate tumors. *FEBS Letters* **1983,** *154* (1), 92-96.

22. Emons, G.; Pahwa, G. S.; Brack, C.; Sturm, R.; Oberheuser, F.; Knuppen, R., Gonadotropin releasing hormone binding sites in human epithelial ovarian carcinomata. *European Journal of Cancer and Clinical Oncology* **1989,** *25* (2), 215-221.

23. Chien, C. H.; Chen, C. H.; Lee, C. Y.; Chang, T. C.; Chen, R. J.; Chow, S. N., Detection of gonadotropin-releasing hormone receptor and its mRNA in primary human epithelial ovarian cancers. *International journal of gynecological cancer : official journal of the International Gynecological Cancer Society* **2004,** *14* (3), 451-458.

24. Moriya, T.; Suzuki, T.; Pilichowska, M.; Ariga, N.; Kimura, N.; Ouchi, N.; Nagura, H.; Sasano, H., Immunohistochemical expression of gonadotropin releasing hormone receptor in human breast carcinoma. *Pathology International* **2001,** *51* (5), 333-337.

25. Skinner, D. C.; Albertson, A. J.; Navratil, A.; Smith, A.; Mignot, M.; Talbott, H.; Scanlan-Blake, N., GnRH Effects Outside the Hypothalamo-Pituitary-Reproductive Axis. *Journal of neuroendocrinology* **2009,** *21* (4), 282-292.

26. Prince, P. M.; Wimo, P. A.; Guerchet, D. M.; Ali, M. G.-C.; Wu, D. Y.-T.; Prina, D. M. *World Alzheimer report 2015*; 2015.

27. Mullard, A., Alzheimer amyloid hypothesis lives on. *Nature Reviews Drug Discovery* **2016,** *16*, 3.

28. Chien, D. T.; Bahri, S.; Szardenings, A. K.; Walsh, J. C.; Mu, F.; Su, M. Y.; Shankle, W. R.; Elizarov, A.; Kolb, H. C., Early Clinical PET Imaging Results with the Novel PHF-Tau Radioligand [F-18]-T807. *Journal of Alzheimer's Disease* **2013,** *34* (2), 457-468.

29. Kovacs, G. G., Invited review: Neuropathology of tauopathies: principles and practice. *Neuropathology and applied neurobiology* **2015,** *41* (1), 3-23.

30. Orr, M. E.; Sullivan, A. C.; Frost, B., A Brief Overview of Tauopathy: Causes, Consequences, and Therapeutic Strategies. *Trends in Pharmacological Sciences* **2017,** *38* (7), 637-648.

31. Webber, K. M.; Perry, G.; Smith, M. A.; Casadesus, G., The Contribution of Luteinizing Hormone to Alzheimer Disease Pathogenesis. *Clinical medicine and research* **2007,** *5* (3), 177–183.

32. Meethal, S.; Smith, M.; Bowen, R.; Atwood, C., The gonadotropin connection in Alzheimer's disease. *Endocr* **2005,** *26* (3), 317-325.

33. Hauze, D. B.; Chengalvala, M. V.; Cottom, J. E.; Feingold, I. B.; Garrick, L.; Green, D. M.; Huselton, C.; Kao, W.; Kees, K.; Lundquist Iv, J. T.; Mann, C. W.; Mehlmann, J. F.; Rogers, J. F.; Shanno, L.; Wrobel, J.; Pelletier, J. C., Small molecule antagonists of the gonadotropin-releasing hormone (GnRH) receptor: Structure–activity relationships of small heterocyclic groups appended to the 2-phenyl-4-piperazinyl-benzimidazole template. *Bioorganic & Medicinal Chemistry Letters* **2009,** *19* (7), 1986-1990.

34. Schottelius, M.; Berger, S.; Poethko, T.; Schwaiger, M.; Wester, H.-J., Development of Novel 68Ga- and 18F-Labeled GnRH-I Analogues with High GnRHR-Targeting Efficiency. *Bioconjugate Chemistry* **2008,** *19* (6), 1256-1268.

35. Guo, H.; Lu, J.; Hathaway, H.; Royce, M. E.; Prossnitz, E. R.; Miao, Y., Synthesis and Evaluation of Novel Gonadotropin-Releasing Hormone Receptor-Targeting Peptides. *Bioconjugate Chemistry* **2011,** *22* (8), 1682-1689.

36. Olberg, D. E.; Andressen, K. W.; Levy, F. O.; Klaveness, J.; Haraldsen, I.; Sutcliffe, J. L., Synthesis and in vitro evaluation of small-molecule [18F] labeled gonadotropin-releasing hormone (GnRH) receptor antagonists as potential PET imaging agents for GnRH receptor expression. *Bioorganic & Medicinal Chemistry Letters* **2014,** *24* (7), 1846-1850.

37. Olberg, D. E.; Bauer, N.; Andressen, K. W.; Hjørnevik, T.; Cumming, P.; Levy, F. O.; Klaveness, J.; Haraldsen, I.; Sutcliffe, J. L., Brain penetrant small molecule 18F-GnRH receptor (GnRH-R) antagonists: Synthesis and preliminary positron emission tomography imaging in rats. *Nuclear Medicine and Biology* **2016,** *43* (8), 478-489.

38. Cole, E. L.; Stewart, M. N.; Littich, R.; Hoareau, R.; Scott, P. J., Radiosyntheses using fluorine-18: the art and science of late stage fluorination. *Current topics in medicinal chemistry* **2014,** *14* (7), 875-900.

39. Firouzbakht, M. L.; Schyler, D. J.; Wolf, A. P., Effect of foil material on the apparent yield of the 124Xe(p, x)123I reaction. *International Journal of Radiation Applications and Instrumentation. Part A. Applied Radiation and Isotopes* **1992,** *43* (6), 741-745.

40. Mettler Jr, F. A.; Guiberteau, M. J., 4 - Thyroid, Parathyroid, and Salivary Glands. In *Essentials of Nuclear Medicine Imaging (Sixth Edition)*, W.B. Saunders: Philadelphia, 2012; pp 99-130.

41. Fjellaksel, R.; Dugalic, D.; Demissie, T. B.; Riss, P. J.; Hjelstuen, O.-K.; Sundset, R.; Hansen, J. H., An acylation-Finkelstein approach to radioiodination of bioactives: The role of amide group anchimeric assistance. *Journal of Physical Organic Chemistry* **2018**, e3835-n/a.

42.   Eisenhut, M.; Mier, W., Radioiodination Chemistry and Radioiodinated Compounds. In *Handbook of Nuclear Chemistry*, Vértes, A.; Nagy, S.; Klencsár, Z.; Lovas, R. G.; Rösch, F., Eds. Springer US: Boston, MA, 2011; pp 2121-2141.

43.   Olberg, D. E.; Hjelstuen, O. K.; Solbakken, M.; Arukwe, J.; Karlsen, H.; Cuthbertson, A., A Novel Prosthetic Group for Site-Selective Labeling of Peptides for Positron Emission Tomography. *Bioconjugate Chemistry* **2008,** *19* (6), 1301-1308.

44.   Meyer, J.-P.; Adumeau, P.; Lewis, J. S.; Zeglis, B. M., Click Chemistry and Radiochemistry: The First 10 Years. *Bioconjugate Chemistry* **2016,** *27* (12), 2791-2807.

45.   Worrell, B. T.; Malik, J. A.; Fokin, V. V., Direct Evidence of a Dinuclear Copper Intermediate in Cu(I)-Catalyzed Azide-Alkyne Cycloadditions. *Science* **2013,** *340* (6131), 457.

46.   Pelletier, J. C.; Chengalvala, M. V.; Cottom, J. E.; Feingold, I. B.; Green, D. M.; Hauze, D. B.; Huselton, C. A.; Jetter, J. W.; Kopf, G. S.; Lundquist, J. T.; Magolda, R. L.; Mann, C. W.; Mehlmann, J. F.; Rogers, J. F.; Shanno, L. K.; Adams, W. R.; Tio, C. O.; Wrobel, J. E., Discovery of 6-({4-[2-(4-tert-butylphenyl)-1H-benzimidazol-4-yl]piperazin-1-yl}methyl)quinoxal ine (WAY-207024): an orally active antagonist of the gonadotropin releasing hormone receptor (GnRH-R). *Journal of medicinal chemistry* **2009,** *52* (7), 2148-2152.

47.   Pelletier, J. C.; Chengalvala, M.; Cottom, J.; Feingold, I.; Garrick, L.; Green, D.; Hauze, D.; Huselton, C.; Jetter, J.; Kao, W.; Kopf, G. S.; Lundquist, J. T. t.; Mann, C.; Mehlmann, J.; Rogers, J.; Shanno, L.; Wrobel, J., 2-phenyl-4-piperazinylbenzimidazoles: orally active inhibitors of the gonadotropin releasing hormone (GnRH) receptor. *Bioorganic & medicinal chemistry* **2008,** *16* (13), 6617-6640.

48.   Egleton, R. D.; Davis, T. P., Development of Neuropeptide Drugs that Cross the Blood-Brain Barrier. *NeuroRx* **2005,** *2* (1), 44-53.

49.   Banerjee, A.; Maschauer, S.; Hübner, H.; Gmeiner, P.; Prante, O., Click chemistry based synthesis of dopamine D4 selective receptor ligands for the selection of potential PET tracers. *Bioorganic & Medicinal Chemistry Letters* **2013,** *23* (22), 6079-6082.

50.   Haubner, R.; Kuhnast, B.; Mang, C.; Weber, W. A.; Kessler, H.; Wester, H.-J.; Schwaiger, M., [18F]Galacto-RGD: Synthesis, Radiolabeling, Metabolic Stability, and Radiation Dose Estimates. *Bioconjugate Chemistry* **2004,** *15* (1), 61-69.

51.   Schottelius, M.; Rau, F.; Reubi, J. C.; Schwaiger, M.; Wester, H.-J., Modulation of Pharmacokinetics of Radioiodinated Sugar-Conjugated Somatostatin Analogues by Variation of Peptide Net Charge and Carbohydration Chemistry. *Bioconjugate Chemistry* **2005,** *16* (2), 429-437.

52.   Fjellaksel, R.; Boomgaren, M.; Sundset, R.; Haraldsen, I. H.; Hansen, J. H.; Riss, P. J., Small molecule piperazinyl-benzimidazole antagonists of the gonadotropin-releasing hormone (GnRH) receptor. *MedChemComm* **2017,** *8* (10), 1965-1969.

53.   Chebolu, R.; Kommi, D. N.; Kumar, D.; Bollineni, N.; Chakraborti, A. K., Hydrogen-Bond-Driven Electrophilic Activation for Selectivity Control: Scope and Limitations of Fluorous Alcohol-Promoted Selective Formation of 1,2-Disubstituted Benzimidazoles and Mechanistic Insight for Rationale of Selectivity. *The Journal of Organic Chemistry* **2012,** *77* (22), 10158-10167.

54.   Cheng, Y.-C.; Prusoff, W. H., Relationship between the inhibition constant (KI) and the concentration of inhibitor which causes 50 per cent inhibition (I50) of an enzymatic reaction. *Biochemical Pharmacology* **1973,** *22* (23), 3099-3108.

55.   Iatsimirskaia, E. A.; Gregory, M. L.; Anderes, K. L.; Castillo, R.; Milgram, K. E.; Luthin, D. R.; Pathak, V. P.; Christie, L. C.; Vazir, H.; Anderson, M. B.; May, J. M., Effect of testosterone suppression on the pharmacokinetics of a potent gnRH receptor antagonist. *Pharmaceutical research* **2002,** *19* (2), 202-208.

56.   Cho, N.; Harada, M.; Imaeda, T.; Imada, T.; Matsumoto, H.; Hayase, Y.; Sasaki, S.; Furuya, S.; Suzuki, N.; Okubo, S.; Ogi, K.; Endo, S.; Onda, H.; Fujino, M., Discovery of a novel, potent, and orally active nonpeptide antagonist of the human luteinizing hormone-releasing hormone (LHRH) receptor. *Journal of medicinal chemistry* **1998,** *41* (22), 4190-4195.

57.   van Oss, C. J., A review of: "Aqueous Solubility: Methods of Estimation for Organic Compounds" S.H. Yalkowsky and Sujit Banerjee, Marcel Dekker, New York, 1992. Hardbound, pp. vi + 263, $99.75. *Journal of Dispersion Science and Technology* **1992,** *13* (5), 583-583.

58.   Yan, R.; Sander, K.; Galante, E.; Rajkumar, V.; Badar, A.; Robson, M.; El-Emir, E.; Lythgoe, M. F.; Pedley, R. B.; Arstad, E., A one-pot three-component radiochemical reaction for rapid assembly of 125I-labeled molecular probes. *Journal of the American Chemical Society* **2013,** *135* (2), 703-709.

59.   Brotherton, W. S.; Clark, R. J.; Zhu, L., Synthesis of 5-Iodo-1,4-disubstituted-1,2,3-triazoles Mediated by in Situ Generated Copper(I) Catalyst and Electrophilic Triiodide Ion. *The Journal of Organic Chemistry* **2012,** *77* (15), 6443-6455.

60.   Smith, N. W.; Polenz, B. P.; Johnson, S. B.; Dzyuba, S. V., Base and concentration effects on the product distribution in copper-promoted alkyne–azide cycloaddition: additive-free route to 5-iodo-triazoles. *Tetrahedron Letters* **2010,** *51* (3), 550-553.

61.   Li, L.; Hao, G.; Zhu, A.; Liu, S.; Zhang, G., Three-component assembly of 5-halo-1,2,3-triazoles via aerobic oxidative halogenation. *Tetrahedron Letters* **2013,** *54* (45), 6057-6060.

62.   PAGE, M. I.; JENCKS, W. P., Entropic Contributions to Rate Accelerations in Enzymic and Intramolecular Reactions and the Chelate Effect. *Proc. Nat. Acad. Sci. USA 68* (8), 1978-1683.

63.   Bruice, T. C.; Lightstone, F. C., Ground State and Transition State Contributions to the Rates of Intramolecular and Enzymatic Reactions. *Accounts of Chemical Research* **1999,** *32* (2), 127-136.

64.   Lightstone, F. C.; Bruice, T. C., Ground state conformations and entropic and enthalpic factors in the efficiency of intramolecular and enzymatic reactions. 1. Cyclic anhydride formation by substituted

glutarates, succinate, and 3,6-endoxo-Δ4-tetrahydrophthalate monophenyl esters. *Journal of the American Chemical Society* **1996,** *118* (11), 2595-2605.

65.   Houk, K. N.; Tucker, J. A.; Dorigo, A. E., Quantitative modeling of proximity effects on organic reactivity. *Accounts of Chemical Research* **1990,** *23* (4), 107-113.

66.   Menger, F. M., On the source of intramolecular and enzymatic reactivity. *Accounts of Chemical Research* **1985,** *18* (5), 128-134.

67.   Bruice, T. C.; Pandit, U. K., The Effect of Geminal Substitution Ring Size and Rotamer Distribution on the Intramolecular Nucleophilic Catalysis of the Hydrolysis of Monophenyl Esters of Dibasic Acids and the Solvolysis of the Intermediate Anhydrides. *Journal of the American Chemical Society* **1960,** *82* (22), 5858-5865.

68.   Kirby, A. J.; Williams, N. H., Efficient intramolecular general acid catalysis of vinyl ether hydrolysis by the neighbouring carboxylic acid group. *Journal of the Chemical Society, Chemical Communications* **1991,** (22), 1643-1644.

69.   Cohen, T.; Lipowitz, J., A CASE OF INTRAMOLECULAR ASSISTANCE OF AMIDE HYDROLYSIS BY A NEIGHBORING AMIDE GROUP1. *Journal of the American Chemical Society* **1961,** *83* (23), 4866-4867.

70.   Calvaresi, M.; Rinaldi, S.; Arcelli, A.; Garavelli, M., Computational DFT Investigation of Vicinal Amide Group Anchimeric Assistance in Ether Cleavage. *The Journal of Organic Chemistry* **2008,** *73* (6), 2066-2073.

71.   Guiotto, A.; Canevari, M.; Pozzobon, M.; Moro, S.; Orsolini, P.; Veronese, F. M., Anchimeric assistance effect on regioselective hydrolysis of branched PEGs: a mechanistic investigation. *Bioorg. Med. Chem.* **2004,** *12* (19), 5031-5037.

72.   Chai, J.-D.; Head-Gordon, M., Long-range corrected hybrid density functionals with damped atom-atom dispersion corrections. *Phys. Chem. Chem. Phys.* **2008,** *10* (44), 6615-6620.

73.   Glukhovtsev, M. N.; Pross, A.; McGrath, M. P.; Radom, L., Extension of Gaussian-2 (G2) theory to bromine and iodine containing molecules: Use of effective core potentials. *J. Chem. Phys.* **1995,** *103* (5), 1878-1885.

74.   Krishnan, R.; Binkley, J. S.; Seeger, R.; Pople, J. A., Self‐consistent molecular orbital methods. XX. A basis set for correlated wave functions. *J. Chem. Phys.* **1980,** *72* (1), 650-654.

75.   Tomasi, J.; Mennucci, B.; Cammi, R., Quantum Mechanical Continuum Solvation Models. *Chem. Rev.* **2005,** *105* (8), 2999-3094.

76.   Médoc, M.; Sobrio, F., Nucleophilic Fluorination and Radiofluorination via Aziridinium Intermediates: N-Substituent Influence, Unexpected Regioselectivity, and Differences between Fluorine-19 and Fluorine-18. *The Journal of Organic Chemistry* **2015,** *80* (20), 10086-10097.

77.   Fjellaksel, R.; Sundset, R.; Hansen, J. H.; Riss, P. J., Copper mediated late-stage iodination and 123I-labeling of triazoles-benzimidazole bioactives. *Synlett, Accepted 16 March* **2018**.

78.   Legros, C.; Matthey, U.; Grelak, T.; Pedragona-Moreau, S.; Hassler, W.; Yous, S.; Thomas, E.; Suzenet, F.; Folleas, B.; Lefoulon, F.; Berthelot, P.; Caignard, D.-H.; Guillaumet, G.; Delagrange, P.; Brayer, J.-L.; Nosjean, O.; Boutin, A. J., New Radioligands for Describing the Molecular Pharmacology of MT1 and MT2 Melatonin Receptors. *International Journal of Molecular Sciences* **2013**, *14* (5).

79.   Legros, C.; Brasseur, C.; Delagrange, P.; Ducrot, P.; Nosjean, O.; Boutin, J. A., Alternative Radioligands for Investigating the Molecular Pharmacology of Melatonin Receptors. *Journal of Pharmacology and Experimental Therapeutics* **2016**, *356* (3), 681.

80.   Ghosh, A.; Raju, N.; Tweedle, M.; Kumar, K., In Vitro Mouse and Human Serum Stability of a Heterobivalent Dual-Target Probe That Has Strong Affinity to Gastrin-Releasing Peptide and Neuropeptide Y1 Receptors on Tumor Cells. *Cancer Biotherapy and Radiopharmaceuticals* **2017**, *32* (1), 24-32.

9 APPENDIX

PAPER I

Small molecule piperazinyl-benzimidazole antagonists of the gonadotropin-releasing hormone (GnRH) receptor

Richard Fjellaksel, Marc Boomgaren, Rune Sundset, Ira H. Haraldsen, Jørn H. Hansen and Patrick J. Riss.

MedChemComm

Check for updates

Small molecule piperazinyl-benzimidazole antagonists of the gonadotropin-releasing hormone (GnRH) receptor†

Richard Fjellaksel, [iD] *[abc] Marc Boomgaren,[c] Rune Sundset,[ad] Ira H. Haraldsen,[e] Jørn H. Hansen[c] and Patrick J. Riss[efg]

In this communication, we report the synthesis and characterization of a library of small molecule antagonists of the human gonadotropin releasing hormone receptor based upon the 2-(4-*tert*-butylphenyl)-4-piperazinyl-benzimidazole scaffold *via* Cu-catalysed azide alkyne cycloaddition. Our main purpose was to find a more soluble compound based on the WAY207024 lead with nanomolar potency to inhibit the GnRH receptor. A late stage diversification by the use of click chemistry was, furthermore developed to allow for expansion of the library in future optimisations. All compounds were tested in a functional assay to determine the individual potency of inhibiting stimulation of the receptor by the endogenous agonist GnRH. In conclusion, we found that compound **8a** showed improved solubility compared to WAY207024 and nanomolar affinity to GnRH receptor.

Gonadotropin-releasing hormone (GnRH) is a peptide hormone secreted from the hypothalamus into the hypophysial portal bloodstream. Once in circulation, the peptide acts as an endocrine signalling hormone mediating release of follicle stimulating hormone (FSH) and luteinizing hormone (LH) *via* gonadotropin-releasing hormone receptor (GnRHR) activation in the pituitary gland. LH and FSH directly regulate gender-specific production of androgens, estrogens, progesterone and inhibin in the gonads. The regulatory circuit is closed by the permeability of the blood–brain barrier to steroid hormones such as estrogen and testosterone, which form negative feedback loops. GnRH, LH and FSH are unlikely to permeate the blood–brain barrier, thus impeding any regulatory feedback on hormone balance, which substantiates the impact of testosterone and estrogen on neurochemical correlates of their respective effects on social behaviour, decision-making and ageing. The hypothalamic–pituitary–gonadal (HPG) signalling circuit is key to gender hormone homeostasis, which can lead to substantial implications in cognitive and behavioural traits.[1–4]

GnRH agonists are well-established pharmaceuticals used at low dose to stimulate hypofunctional GnRH in hypogonadism. At high dose, GnRH agonists deplete GnRH receptor function in the pituitary, limiting LH and FSH secretion and thereby the levels of androgens and estrogens in circulation and suppressing hormone production completely. GnRH receptor agonists play an important role in clinical care, *e.g.* in the treatment of hormone responsive cancer, reproductive diseases and for behavioral modification of sexual offenders *via* these mechanisms. However, GnRH agonists cannot address mild GnRH overfunction, which would require attenuation of the signaling circuit, rather than stimulation or depletion. To address this shortcoming, GnRH antagonists have attracted considerable attention in recent years specifically to treat diseases, which require some reduction of GnRH stimulation.[5–8]

We were interested in the development of a GnRH antagonist of moderate potency to address cognitive and behavioral correlates of GnRH-R attenuation. In our reasoning, a reversibly binding antagonist would reduce gonadal overstimulation by limiting the availability of binding sites by competition with the agonist. Thereby, the central effects of testosterone and estrogen would be buffered, while hormone homeostasis would be preserved. Small molecule antagonists of GnRHR are particularly interesting due to their

[a] Medical Imaging Group, Department of Clinical Medicine, UiT The Arctic University of Norway, 9037 Tromsø, Norway. E-mail: richard.fjellaksel@uit.no
[b] Drug Transport and Delivery Group, Department of Pharmacy, UiT The Arctic University of Norway, 9037 Tromsø, Norway
[c] Organic Chemistry Group, Department of Chemistry, UiT The Arctic University of Norway, 9037 Tromsø, Norway
[d] PET imaging center, division of diagnostics, UNN – University Hospital of North-Norway, 9038 Tromsø, Norway
[e] Department of neuropsychiatry and psychosomatic medicine, Oslo University Hospital, Oslo, Norway
[f] Realomics SFI, Department of Chemistry, University of Oslo, PO BOX 1033, Oslo 0371, Norway
[g] Norsk Medisinsk Syklotronsenter AS, Postboks 4950 Nydalen, 0424 Oslo, Norway
† Electronic supplementary information (ESI) available: Detailed experimental procedures and analytical characterisation of all compounds. See DOI: 10.1039/c7md00320j

direct, dose dependent inhibition of GnRH activity, lack of stimulatory side effects on the receptor and superior passive permeability into tissues relative to peptide agonists.

Several classes of small molecule antagonists have been developed previously. Pelletier and co-workers reported a 2-(4-*tert*-butylphenyl)-4-piperazinyl-benzimidazole-scaffold as a small molecule antagonist of the GnRHR with nanomolar inhibition potency, albeit low solubility was cited as a shortcoming by the authors.[9,10] Further optimization lead to the discovery of the slightly more soluble WAY 207024 compound as shown in Fig. 1.[11]

Based on these results, we have designed a novel library of potential antagonists addressing the following criteria:

a) A late stage diversification approach based on the 1,3-triazole motive to facilitate straightforward structural modification.

b) A moderate potency permitting competition of the ligand in circulation with endogenous GnRH for GnRHR binding sites, which would make GnRH activation subject to both GnRH concentration and the concentration of the inhibitor in tissue.

c) Improved solubility in aqueous media to improve bioavailability and pharmacokinetic profile of the lead.

Fig. 1 shows the title scaffold and some relevant properties discussed herein. As apparent from the high partitioning coefficient log P, the compound is highly lipophilic, which may hamper solubility in aqueous formulation as well as non-specific binding of the compound *in vivo*. In previous studies, it was found that the body of the scaffold (blue oval, A) is central to binding selectively the GnRH receptor, whereas structural modifications in the upper section of the lead (green oval, B) with planar, hydrogen bonding functional groups were found to be beneficial for modulating antagonist potency.

We surmised that the 1,3-functionalised triazole moiety would resemble well the planar geometry required for successful structural modification and simultaneously allow for introducing a broad spectrum of structural variations in the last synthetic stage using one robust reaction. Since the 1,3-functionalised triazole is obtained *via* the Cu-catalysed azide-

alkyne cycloaddition reaction, we opted for working with a building block based on A to obtain an alkyne substrate for the reaction.

The overall design strategy in this communication was to generate triazoles from different functionalized azides that would be beneficial for the potency to inhibit the GnRH receptor while improving the aqueous solubility. We incorporated a variety of azides *via* click chemistry, including sugar moieties, which have been thoroughly demonstrated to effect favourable solubility characteristics and are discussed extensively in the literature.[12–15] Furthermore, the reduced solubility of the alkyl and aromatic azides would also counteract our intention to improve aqueous solubility through reducing clog P (and hence, the bioavailability and pharmacokinetically desirable profile).

The desired intermediate (7) was synthesised in 19% overall yield over six steps on a multigram scale. In brief, 2,5-difluoronitrobenzene was converted to phenylene diamine 4 over three steps as described previously.[9] Contrary to the published method, we found that the oxidative conversion of 4 into imidazole 6 proceeded smoothly in absence of a transition metal catalyst with air as the oxidant. The observation of 6b as a minor by-product suggests a Cannizarro-like side reaction.[16] The route is shown in Scheme 1.

A further modification was made relative to literature to facilitate cleavage of the BOC protecting group. Substitution of the TFA used originally with HCl in dioxane gave a colourless solid instead of an oily product, which benefits the scalability of this route. Notably, compound 4 is fully converted into heterocyclic products, although the competing formation of 6b in about 8% yield limits the overall yield of 6a to 75% over two steps. Intermediate 7 was synthesized by
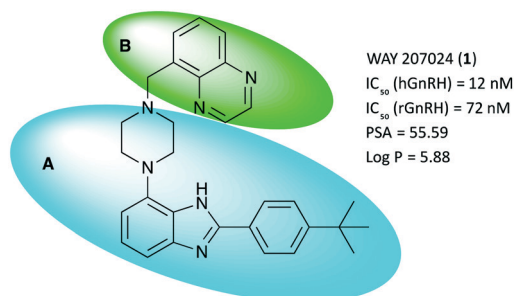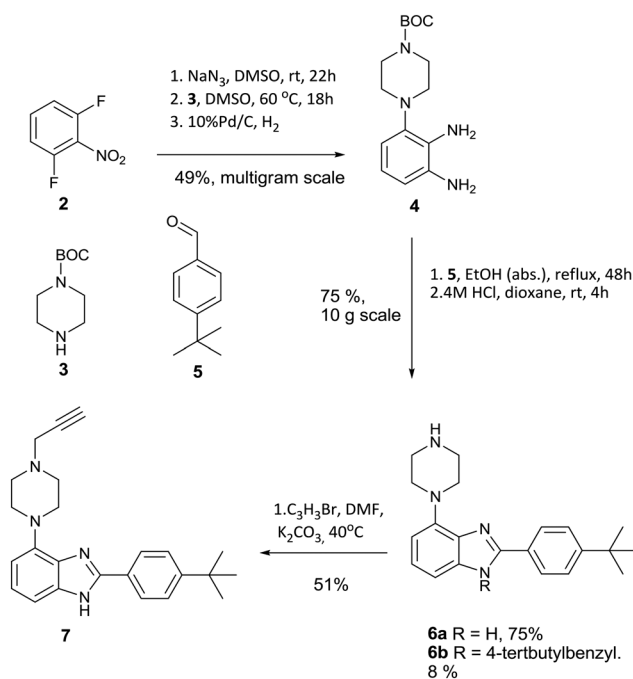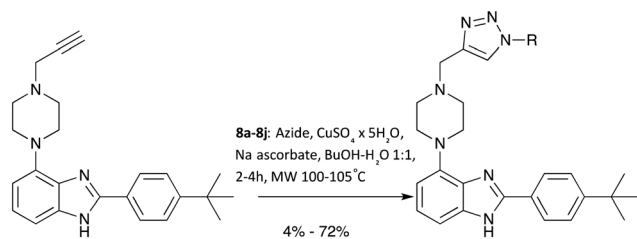

Fig. 1 Key properties and molecular structure of WAY 207024, the lead compound for GnRH antagonist development. A (blue oval) depicts the scaffold body; B (green oval) depicts the moiety of interest for further structural optimization. IC_{50} – concentration to inhibit GnRH binding to the receptor by 50%. hGnRH – human GnRH receptor. rGnRH – rat GnRH receptor. PSA – polar surface area in $Å^2$. cLog P – calculated octanol–water partitioning coefficient.

Scheme 1 Synthetic route to alkyne intermediate 7.

1966 | *Med. Chem. Commun.*, 2017, **8**, 1965–1969

This journal is © The Royal Society of Chemistry 2017

Scheme 2 Diversification of the scaffold body using CuAAC.

alkylation with propargyl bromide in dry DMF using potassium carbonate as base in 51% yield to furnish the desired substrate 7 for azide alkyne cycloaddition.

With a robust and high yielding route to gram amounts of 7 in hand, further diversification using the copper-catalysed azide-alkyne cycloaddition (CuAAC) reaction with a range of commercially available azide substrates became possible. See Scheme 2 for an overview.

Since products **8a**–**8j** were obtained in more than sufficient yields for biological testing following a published protocol, no attempts to optimise the reaction were made at this point.

Following synthesis and characterisation, inhibition of receptor activation by LHRH/GnRH was measured in division arrested cell lines from Multispan Inc. stably expressing functional hGnRH receptors. As described in the literature, the solubility of **1** and some of its derivatives is rather poor, which lead to a cut-off at 5×10^3 nM for the maximum concentration in the cell culture assay. Compounds insoluble in DMSO at 10 mM were dropped from testing. Nonetheless, concentration dependent competition studies were performed *in vitro* in presence of 5 nM LnRH antagonist with the remainder of derivatives. Compounds showing a $p\mathrm{IC}_{50} > 5$ were tested again over a wide range of concentrations (logarithmic, 0.1–10^3 nM). A one-site competitive inhibition model was found to work best for fitting of the data curves. To
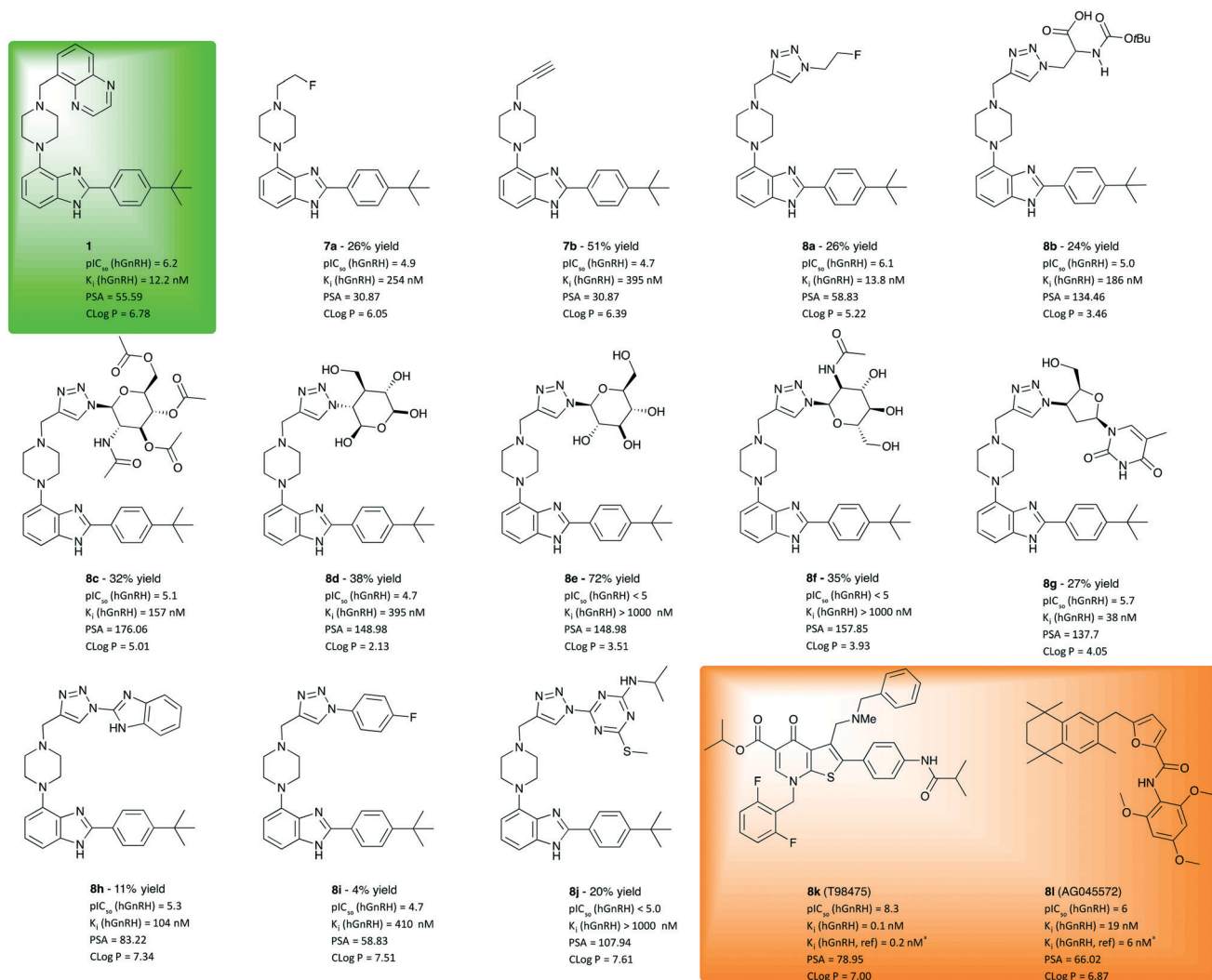
Fig. 2 Investigated molecular entities, isolated yields, inhibition potency, inhibition constant and properties computed for evaluation. For comparison, test results of lead **1** (green box) and positive controls **8k** and **8l** should be considered. [a]Reference value from literature.[17,18] IC$_{50}$ values are given as the geometric mean of two experiments, see ESI† for details. K$_i$ was calculated from mean value using the Cheng–Prusoff equation (Ki = IC$_{50}$/(1 + [L]/Kd)).[19] [c]Replicated twice with broader range of concentrations. [d]Based on single experiment.

evaluate the obtained inhibition potency values and to validate the assay, we included the well-described, commercially available GnRH antagonists T98475 (**8k**) and AG04557 (**8l**) as independent, positive controls and the metabolically stable peptide agonist buserelin as negative control. The lead compound WAY207024 (**1**) was included as a reference in the cell assay. All IC_{50} values obtained for each test compound in the concentration dependent screening were converted into K_i values using the equation of Cheng and Prusoff.[15]

As illustrated in Fig. 2, compounds derived from **1** using CuAAC were found to exhibit competitive antagonism against the endogeneous agonist GnRH. While alkyl piperazines **7a** and **7b** show only moderate potency, 21 and 43-fold lower than **1**, respectively, their clog P values are lower than that of **1**, which results in higher solubility (>100 nM). In line with our working hypothesis, the introduction of a planar triazole-core has a positive effect on potency. The 2-fluoroethyl triazole **8a** is equally potent as **1**, Interestingly the thermodynamic solubility assay showed that **8a** is 1.5 times more soluble than **1**, 3 μg ml^{-1} at pH 7.4 (phosphate buffered saline) and 2.098 mg mL^{-1} at pH 1.2 (simulated gastric fluid) which was indicated by the lower clog P-value. The introduction of an N-BOC-*Ala* functionalised triazole **8b** further improves polarity, albeit at the cost of a drop of one order of magnitude in potency. While these results may indicate that the triazole moiety is a useful pharmacophore, its vicinity was found to be much less tolerant to the introduction of pyranose moieties (**8c–f**), which was attempted to improve solubility. While these sugar derivatives lead to a major improvement of polarity as indicated by clog P values between 2 and 5, their potency to inhibit GnRH binding dropped out of the desired range. Masking the polyol as a tetraacetate (**8c**) helped with retaining potency, which does not bode well for making use of the solubility improvement by glycosylation. However, when varying the azide component to a synthetic glycoside to obtain **8g**, a viable compromise between solubility and inhibition potency was obtained. Derivative **8g** was measured to be soluble at pH 1.2, 1.2 mg ml^{-1} and <1 μg ml^{-1} at pH 7.4. With a potency of 38 nM, barely threefold lower than that of **1**, this hit may create an opening for further exploration using a library of diverse analogues of **8g**. Products **8h–j**, obtained from aromatic and heteroaromatic azides and **7**, did not lead to increased solubility or affinities compared to WAY207024.

In conclusion, 18 analogues were synthesized using an approach of late-stage diversification *via* CuAAC and evaluated for potency to inhibit hGnRHR activation. While molecular diversity can easily be introduced into the scaffold body *via* this route few compounds with hGnRH inhibition potency in the desired range were identified indicating limited tolerance for structural modification in the vicinity of the triazole. The pyranose derivatives did not give the desired inhibition to the GnRH receptors neither did the less soluble compounds **8h** and **8i**. Nonetheless, compounds **8a** and **8g** emerge as highly promising candidates for further investigation in behavioural animal models as a couple of GnRH modulating antagonists.

Conflicts of interest

The author declare no competing interests.

Acknowledgements

Notes and references

1 S. Meethal, M. Smith, R. Bowen and C. Atwood, *Endocrine*, 2005, **26**, 317–325.
2 V. A. Tobin, R. P. Millar and B. J. Canny, *Endocrinology*, 1997, **138**, 3314–3319.
3 G. Zhang, J. Li, S. Purkayastha, Y. Tang, H. Zhang, Y. Yin, B. Li, G. Liu and D. Cai, *Nature*, 2013, **497**, 211–216.
4 C. Eisenegger, M. Naef, R. Snozzi, M. Heinrichs and E. Fehr, *Nature*, 2010, **463**, 356–359.
5 H. van Poppel and S. Nilsson, *Urology*, 2008, **71**, 1001–1006.
6 R. L. Gustofson, J. H. Segars and F. W. Larsen, *Hum. Reprod.*, 2006, **21**, 2830–2837.
7 J. B. Engel and A. V. Schally, *Nat. Clin. Pract. Endocrinol. Metab.*, 2007, **3**, 157–167.
8 P. Briken, A. Hill and W. Berner, *J. Clin. Psychiatry*, 2003, **64**, 890–897.
9 J. C. Pelletier, M. Chengalvala, J. Cottom, I. Feingold, L. Garrick, D. Green, D. Hauze, C. Huselton, J. Jetter, W. Kao, G. S. Kopf, J. T. T. Lundquist, C. Mann, J. Mehlmann, J. Rogers, L. Shanno and J. Wrobel, *Bioorg. Med. Chem.*, 2008, **16**, 6617–6640.
10 D. B. Hauze, M. V. Chengalvala, J. E. Cottom, I. B. Feingold, L. Garrick, D. M. Green, C. Huselton, W. Kao, K. Kees, J. T. Lundquist Iv, C. W. Mann, J. F. Mehlmann, J. F. Rogers, L. Shanno, J. Wrobel and J. C. Pelletier, *Bioorg. Med. Chem. Lett.*, 2009, **19**, 1986–1990.
11 J. C. Pelletier, M. V. Chengalvala, J. E. Cottom, I. B. Feingold, D. M. Green, D. B. Hauze, C. A. Huselton, J. W. Jetter, G. S. Kopf, J. T. Lundquist, R. L. Magolda, C. W. Mann, J. F. Mehlmann, J. F. Rogers, L. K. Shanno, W. R. Adams, C. O. Tio and J. E. Wrobel, *J. Med. Chem.*, 2009, **52**, 2148–2152.
12 R. D. Egleton and T. P. Davis, *NeuroRx*, 2005, **2**, 44–53.
13 A. Banerjee, S. Maschauer, H. Hübner, P. Gmeiner and O. Prante, *Bioorg. Med. Chem. Lett.*, 2013, **23**, 6079–6082.
14 R. Haubner, B. Kuhnast, C. Mang, W. A. Weber, H. Kessler, H.-J. Wester and M. Schwaiger, *Bioconjugate Chem.*, 2004, **15**, 61–69.
15 M. Schottelius, F. Rau, J. C. Reubi, M. Schwaiger and H.-J. Wester, *Bioconjugate Chem.*, 2005, **16**, 429–437.
16 R. Chebolu, D. N. Kommi, D. Kumar, N. Bollineni and A. K. Chakraborti, *J. Org. Chem.*, 2012, **77**, 10158–10167.
17 E. A. Iatsimirskaia, M. L. Gregory, K. L. Anderes, R. Castillo, K. E. Milgram, D. R. Luthin, V. P. Pathak, L. C. Christie, H.

1968 | *Med. Chem. Commun.*, 2017, **8**, 1965–1969

This journal is © The Royal Society of Chemistry 2017

Vazir, M. B. Anderson and J. M. May, *Pharm. Res.*, 2002, **19**, 202–208.

18 N. Cho, M. Harada, T. Imaeda, T. Imada, H. Matsumoto, Y. Hayase, S. Sasaki, S. Furuya, N. Suzuki, S. Okubo, K. Ogi, S.

Endo, H. Onda and M. Fujino, *J. Med. Chem.*, 1998, **41**, 4190–4195.

19 Y.-C. Cheng and W. H. Prusoff, *Biochem. Pharmacol.*, 1973, **22**, 3099–3108.

PAPER II

Copper-mediated late-stage iodination and ^{123}I-labelling of triazole-benzimidazole bioactives.

Richard Fjellaksel, Rune Sundset, Jørn H. Hansen, Patrick J. Riss.

PAPER III

An Acylation-Finkelstein Approach to Radioiodination of Bioactives: The role of amide group anchimeric assistance.

Richard Fjellaksel, Damir Dugalic, Taye B. Demissie, Patrick J. Riss, Ole-Kristian Hjelstuen, Rune Sundset, and Jørn H. Hansen.

RESEARCH ARTICLE

WILEY *Journal of* Physical Organic Chemistry

An acylation-Finkelstein approach to radioiodination of bioactives: The role of amide group anchimeric assistance

Richard Fjellaksel[1,2,3] | Damir Dugalic[2,3] | Taye B. Demissie[3,4] | Patrick J. Riss[5,6,7] |
Ole-Kristian Hjelstuen[2] | Rune Sundset[1,8] | Jørn H. Hansen[3]

[1] Medical Imaging Group, Department of Clinical Medicine, UiT The Arctic University of Norway, Tromsø, Norway

[2] Drug Transport and Delivery Group, Department of Pharmacy, UiT The Arctic University of Norway, Tromsø, Norway

[3] Organic Chemistry Group, Department of Chemistry, UiT The Arctic University of Norway, Tromsø, Norway

[4] Hylleraas Centre for Quantum Molecular Sciences, Department of Chemistry, UiT The Arctic University of Norway, Tromsø, Norway

[5] Department of neuropsychiatry and psychosomatic medicine, Oslo University Hospital, Oslo, Norway

[6] Realomics SFI, Department of Chemistry, University of Oslo, Oslo, Norway

[7] Norsk Medisinsk Syklotronsenter AS, Oslo, Norway

[8] PET Imaging Center, Division of Diagnostics, University Hospital of North Norway, Tromsø, Norway

Correspondence
Jørn H. Hansen, Organic Chemistry Group, Department of Chemistry, UiT The Arctic University of Norway, 9037 Tromsø, Norway.
Email: jorn.h.hansen@uit.no

Funding information
Department of Chemistry, UiT The Arctic University of Norway; Helse Nord, Grant/Award Numbers: SFP1196-14, SFP1196-14; NOTUR, Grant/Award Number: nn4654k; Department of Chemistry at UiT The Arctic University of Norway

Abstract

Herein, we report a straightforward sequential acylation-Finkelstein approach to achieve iodination of amine containing bioactives. The utility was demonstrated by successful radiolabelling with ^{123}I in high radiochemical yield. Moreover, microwave-assisted Finkelstein reaction can be employed to enhance conversion and reaction rates to obtain the desired iodides. The method is of interest for radioiodination of amine-containing bioactives. The mechanistic details of the iodination process were studied by kinetics and density functional theory calculations, which revealed the mechanistic complexity of the reaction involving amide group anchimeric assistance. We disclose a number of fundamental aspects of amide group anchimeric assistance in substitution reactions.

KEYWORDS

amide anchimeric assistance, bioactives, DFT mechanism, Finkelstein, radioiodination

1 | INTRODUCTION

Continued advances in medical imaging require effective and versatile radiolabeling methods. Imaging techniques, such as single photon emission computed tomography and positron emission tomography, increasingly employ radiolabeled bioactive organic molecules as radiotracers. Important criteria for production of clinical radiotracers are rapid radiolabeling reaction rates, high radiochemical yield (RCY), and high specific activity [1]. Herein, we disclose a straightforward radioiodination protocol for bioactives based on a sequential acylation-Finkelstein approach. However, the mechanistic complexity of the

substitution process requires careful consideration before this strategy can be applied, and, as such, we have conducted in-depth mechanistic analyses to reveal the detailed nature of the processes involved.

The intramolecular nucleophilic participation of functional groups adjacent to reactive centers, commonly known as anchimeric assistance, has been widely studied by the physical organic chemistry community over the past 60 years or so [2–8]. However, anchimeric assistance by amide groups has only been sparsely reported [9] despite recent studies indicating its importance in biological systems, such as catalytic enzyme glycoside bond breakage in O-GlcNAcases and B-hexosaminidases [10–14]. A study

by Garavelli and co-workers [15] reported experimental and computational evidence for amide group anchimeric assistance in acid-catalyzed ether cleavage reactions. A thorough general understanding of the thermodynamic and kinetic details of anchimeric assistance provided by amide groups is lacking and would be a valuable addition to the reaction design toolkit and to the enhanced understanding of the role of amide groups in biological systems.

The use of anchimeric assistance by adjacent amino groups as a strategy to enhance introduction of radioactive fluoride was recently described by Médoc and co-workers, in which radiosubstitution via activated aziridinium intermediates was shown to successfully lead to ^{18}F-labelling (Scheme 1A) [16]. Inspired by the previous works, and the need to enhance fundamental understanding of amide group anchimeric assistance, we decided to explore a straightforward acylation-Finkelstein strategy (Scheme 1B) for iodide incorporation. Despite the weak bond strength of the C—I bond relative to the C—Cl bond, the Finkelstein reaction is driven forward by the precipitation of sodium chloride in the solvent (typically acetone), thereby rendering the chloride displacement irreversible [17,18]. At certain chain lengths ($n = 2$–7), one might expect the adjacent amide group to engage in anchimeric assistance in the displacement of the chloride ion—in competition with direct bimolecular substitution. The effects of this mechanistic complication are a major topic of this paper.

In this paper, we aim to (1) disclose our studies of the acylation-Finkelstein approach to iodination and radioiodination of bioactive model molecules and (2) unravel the mechanistic complexity involved in the substitution processes—in particular, the influence of amide group anchimeric assistance. We have explicitly studied the latter using combined experimental and computational techniques. We have compared relative rates of substitution depending on carbon chain lengths and the ring size of the activated intermediate electrophile.
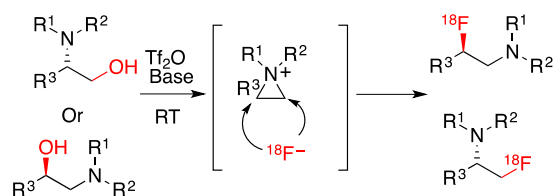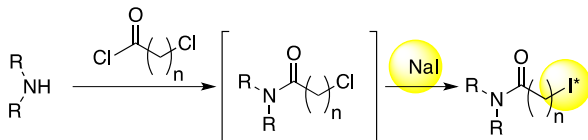
Because amide groups have not been extensively studied for their ability to effect anchimeric assistance, we have conducted a detailed computational study of the mechanistic details of such processes using density functional theory (DFT) calculations. These studies are necessary to guide future applications of this iodination strategy to other bioactives, and they provide a fundamental insight into the details of amide group anchimeric assistance. To validate our approach for radioiodination, we have demonstrated that an acylated analogue of a bioactive molecule can be effectively radiolabelled.

2 | EXPERIMENTAL DETAILS

2.1 | General experimental details

All solvents and reagents were obtained from Sigma Aldrich (Sigma-Aldrich Norway AS) except Na[123]I. Na[123]I was obtained from GE Healthcare, Netherlands. Instruments used: Microwave Anton Parr Monowave 300®, Biotage SP1 Flash Chromatography systems®, HRMS: Thermo scientific LTQ Orbitrap XL + Electrospray ion source (ION-MAX)—the instrument was made at Thermo's factory in Bremen, Germany, IR: Varian 7000e FT-IR spectrometer, Pike miracle ATR. NMR: 400-MHz Bruker Avance III HD equipped with a 5-mm SmartProbe BB/1 h (BB = 19F, 31p-15N), HPLC systems: Waters 2545 HPLC pump. Waters 2998 PDA detector, 200 to 500 nm. Waters 2767 sample manager. XBridge® prep C18 5-μm OBD[tm] 19 × 250 mm column. UPLC systems: Acquity UPLC H class. Acquity column manager. Acquity PDA detector. Acquity UPLC® BEH C18 1.7 μm. 2,1x50nm column, Determination of purity by UPLC: Column at 50°C, the same method used for all analyses. Method: 0.6 mL/minute initial % H_2O 0.1% trifluoroacetic acid (TFA), 5% acetonitrile (ACN) 0.1% TFA. Then, linear change during 10 minutes to 50% H_2O 0.1% TFA, 50% ACN 0.1% TFA. Semi-preparative HPLC for radiochemistry: DIONEX HPLC system, HPLC pump P680, automated sample injector ASI-100, PDA-detector PDA-100 with XBridge® prep C18 5-μm OBD[tm] 19 × 250 mm column, analytical XBridge® C18 3 μm 2.1 × 150 mm column and "Radioactivity flow detector for HPLC LB 509" (BERTHOLD TECHNOLOGIES). All experiments were repeated at least twice.

(A) *Anchimerically assisted radiofluorination by Médoc et al.*

(B) *Acylation-Finkelstein approach to radioiodination*

SCHEME 1 Use of anchimerically assisted radiofluorination by Médoc et al [16] (A) versus acylation/Finkelstein approach (B, current work)

2.2 | Chemical synthesis protocols and characterization

2.2.1 | 2-(4-tert-Butylphenyl)-4-(piperazin-1-yl)-1H-benzo [d]imidazole (1)

Compound **1** was obtained as previously described [19], as a white powder (489 mg, 96% yield). **Purity** 97.2%

^{1}**H-NMR** (400 MHz DMSO-d6), δ in ppm = 9.67 (Br s, 1H), 8.49 (d, 8.0 Hz, 2H), 7.71(d, 8.0 Hz, 2H), 7.53(d, 8.0 Hz, 1H), 7.48 (t, 1H), 7.13 (d, 8.0 Hz, 1H), 3.45 to 3.37(m, 8H), 1.34 (s, 9H). ^{13}**C-NMR** (101 MHz DMSO-d6), δ in ppm = 156.5, 148.9, 139.5, 132.9, 129.2, 126.7, 126.1, 125.4, 120.2, 114.0, 108.4, 47.8, 42.7, 35.1, 30.8. **HRMS (ESI)** [M + H]$^+$ for $C_{21}H_{27}N_4$ m/z Found 335.2236, Calculated: 335.2236. **IR (Neat)** 2955, 2689, 2466, 1622, 1459, 1383.

2.2.2 | 1-(4-(2-(4-tert-butylphenyl)-1H-benzo[d]imidazol-4-yl) piperazin-1-yl)-2-chloroethanone (2a)

To a solution containing 12-mL DMF (anhydrous) and 0.31 mL (1.86 mmol, 3 equiv.) diisopropyl ethylamine (DIPEA), 0.2 g (0.6 mmol) of 2-(4-tert-Butylphenyl)-4-(piperazin-1-yl)-1H-benzo[d]imidazole (**1**) was added. The solution was cooled down to 0°C in an ice bath under inert conditions, and 0.15-mL (1.86 mmol, 3 equiv.) chloroacetyl chloride was added at 0°C. The solution was stirred for 1 hour and then warmed to 27°C. The reaction was monitored by TLC. DMF was then evaporated on a rotavap. The reaction mixture was chromatographed on biotage SP1 flash chromatography systems by a Biotage snap ultra C18rp 12 g column. 15 mL/minute. At 20 minutes, there was a linear change to 100% ACN. Fractions were collected, and the solvents were removed by evaporation to provide a white powder (166 mg, 67% yield). **Purity** 97.21% ^{1}**H NMR** (400 MHz, Methanol-d_4) δ 8.02 (d, J = 8.4 Hz, 2H), 7.57 (d, J = 8.4 Hz, 2H), 7.22 (d, J = 7.9 Hz, 1H), 7.16 (t, J = 7.8 Hz, 1H), 6.74 (d, J = 7.5 Hz, 1H), 4.31 (s, 2H), 3.85 (dt, J = 16.1, 5.2 Hz, 2H), 3.40 (t, J = 5.0 Hz, 2H), 3.37 to 3.32 (m, 2H), 1.36 (s, 9H). ^{13}**C NMR** (101 MHz, Methanol-d_4) δ 167.7, 155.0, 152.0, 142.9, 138.8, 134.8, 127.9, 127.8, 127.0, 125.0, 110.8, 108.3, 52.1, 51.6, 47.4, 43.4, 42.0, 35.8, 31.6. **HRMS (ESI)** [M + H]$^+$ for $C_{23}H_{28}ON_4Cl$ m/z Found 411.1955. Calculated 411.1946 **IR (Neat)** 2961, 1644, 1437, 1234, 1015, 842, 788, 738.

2.2.3 | 1-(4-(2-(4-Tert-butylphenyl)-1H-benzo[d]imidazol-4-yl)piperazin-1-yl)-2-iodoethanone (4a)

Fifty-eight milligrams (0.15 mmol) of compound **2a** was added to a solution of 5-mL acetone and 500-mg (3.3 mmol, 25 equiv.) NaI. The reaction was stirred for 1 hour. The reaction mixture was filtered and then chromatographed on Biotage SP1 flash chromatography systems using a Biotage snap ultra C18rp 12-g column. 15 mL/minute. At 20 minutes, there was a linear change to 100% ACN. Fractions were collected, and the solvents

were removed by evaporation to provide a white powder (23 mg, 32% yield). **Purity** 95.38%. ^{1}**H NMR** (400 MHz, Acetone-d_6) δ 8.15 (d, J = 8.3 Hz, 2H), 7.57 (d, J = 8.3 Hz, 2H), 7.19 to 7.00 (m, 2H), 6.63 (d, J = 7.1 Hz, 1H), 3.97 (s, 2H), 3.78 (s, 4H), 3.72 (s, 2H), 3.54 (s, 2H), 1.36 (s, 9H). ^{13}**C NMR** (101 MHz, Acetone-d_6) δ 166.9, 153.6, 149.9, 143.2, 138.1, 136.0, 128.6, 127.2, 126.6, 124.2, 108.3, 105.9, 50.5, 50.2, 47.9, 42.7, 35.4, 31.5, 2.3 **HRMS (ESI)** [M + H]$^+$ for $C_{23}H_{28}ON_4I$ m/z Found 503.1300. Calculated 503.1308 **IR (Neat)** 2961, 1637, 1437, 1015, 841, 788, 737.

2.2.4 | 1-(4-(2-(4-Tert-butylphenyl)-1H-benzo[d]imidazol-4 yl)piperazin-1-yl)-3-chloropropan-1-one (2)

To a solution containing 5-mL DMF (anhydrous) and 0.26 mL (1.62 mmol, 3 equiv.) DIPEA, 0.2 g (0.54 mmol) **1** was added. The solution was cooled to 0°C with an ice bath under inert conditions, and 0.14 mL (1.62 mmol, 3 equiv.) chloropropinoyl chloride **3b** was added at 0°C. The solution was warmed to room temperature and stirred for 18 hours. The solvents were evaporated by a rotavapor. The reaction mixture was then diluted with DCM and chromatographed on Biotage SP1 flash chromatography systems using a Biotage snap ultra C18rp 12 g column. 15 mL/minute. At 20 minutes, there was linear change to 100% ACN. The solvents were removed by evaporation to provide a white powder (99 mg, 46.7% yield). **Purity** 97.97% ^{1}**H NMR** (400 MHz, Acetone-d_6) δ 8.15 (t, J = 9.0, 7.3 Hz, 2H), 7.55 (d, J = 7.1 Hz, 2H), 7.17 to 7.03 (m, 2H), 6.60 (d, J = 6.5 Hz, 1H), 3.85 (t, J = 7.7, 7.3 Hz, 2H), 3.78 (dd, J = 35.9, 8.7 Hz, 4H), 3.64 (s, 2H), 3.53 (d, J = 4.7 Hz, 2H), 2.93 (d, J = 6.7 Hz, 2H), 1.35 (s, 9H). ^{13}**C NMR** (101 MHz, Acetone-d_6) δ 168.55, 153.51, 149.87, 143.29, 138.08, 136.03, 128.65, 127.17, 126.53, 124.20, 108.26, 105.86, 50.94, 50.41, 46.07, 42.28, 41.06, 36.50, 35.33, 31.48 **HRMS (ESI)** [M + H]$^+$ for $C_{24}H_{30}ON_4Cl$ m/z Found 425.2099. Calculated 425.2108 **IR (Neat)** 2964, 1629, 1465, 1438, 1197, 1130, 1014.

2.2.5 | 1-(4-(2-(4-Tert-butylphenyl)-1H-benzo[d]imidazol-4-yl)piperazin-1-yl)-3-iodopropan-1-one (4b)

To a solution containing 3-mL acetone and 0.1-g (0.66 mmol, 5.0 equiv.) NaI, 0.047 g (0.11 mmol) of 1-(4-(2-(4-tert-butylphenyl)-1H-benzo[d]imidazol-4-yl) piperazin-1-yl)-3-chloropropan-1-one (compound **4a**) was added. The solution was heated to 55°C under reflux and stirred for 16 hours. Then, the solution was filtered and transferred to a vial for HPLC. Method for HPLC

separation: 25 mL/minute initial 95% H_2O, 5% ACN and 0.1% TFA. At 15 minutes, there was linear change to 5% H_2O, 95% ACN 0.1% TFA. The product fractions were collected and lyophilized to give a white powder (23 mg, 37% yield). **Purity** 95.38%. **^{1}H NMR** (400 MHz, Acetone-d_6) δ 8.22 (d, $J = 8.7$ Hz, 2H), 7.66 (d, $J = 8.7$ Hz, 2H), 7.45 (d, $J = 8.1$ Hz, 1H), 7.38 to 7.30 (m, 1H), 6.98 (d, $J = 7.8$ Hz, 1H), 3.81 (s, 4H), 3.50 to 3.34 (m, 4H), 3.29 (s, 2H), 3.09 (t, $J = 7.3$ Hz, 2H), 1.37 (s, 9H). **^{13}C NMR** (101 MHz, Acetone-d_6) δ 169.5, 156.6, 150.1, 141.7, 141.6, 135.5, 129.6, 128.7, 127.1, 126.7, 126.6, 123.5, 113.2, 108.6, 52.1, 51.6, 45.8, 42.2, 37.7, 35.7, 31.3, −0.5. **HRMS (ESI)** $[M + H]^+$ for $C_{24}H_{30}ON_4I$ m/z Found 517.1462. Calculated 517.1459. **IR (Neat)** 3232, 2961, 1710, 1616, 1476, 1360, 1235, 1022.

2.2.6 | 1-(4-(2-(4-Tert-butylphenyl)-1H-benzo[d]imidazol-4-yl)piperazin-1-yl)-4-chlorobutan-1-one (2c)

To a solution containing 5-mL DMF (anhydrous) and 0.28-mL (1.62 mmol 3 equiv.) DIPEA, 0.2 g (0.54 mmol) 2-(4-tert-butylphenyl)-4-(piperazin-1-yl)-1H-benzo[d] imidazole (**1**) was added. The solution was cooled down to 0°C in an ice bath under inert conditions, and 0.9 mL (1.6 mmol, 3 equiv.) chlorobutanoyl chloride **3c** was added at 0°C. The solution was warmed to room temperature and stirred for 2 hours. The reaction was monitored by TLC. The reaction mixture was transferred to a separatory funnel. First, 0.2-mL 1 M HCl was added, then 40 mL of water followed by 1 M NaOH to give a pH 7 to 8. The solution was washed with 3 × 40 mL DCM. The organic phase was dried over sodium sulfate and filtered. Then, the residue was dissolved in DCM and chromatographed on biotage SP1 flash chromatography systems using a Biotage snap ultra C18rp 12-g column. Flow rate: 15 mL/minute; at 20 minutes, there was linear change to 100% ACN. Fractions were collected, and the solvents were removed by evaporation to provide a white powder (105 mg, 44% yield). **Purity** 95.83%. **^{1}H NMR** (400 MHz, Acetone-d_6) δ 11.87 (s, 1H), 8.14 (ddt, $J = 25.2, 12.5, 8.2, 6.4$ Hz, 2H), 7.66 to 7.37 (m, 3H), 7.25 to 6.86 (m, 2H), 6.58 (dd, $J = 6.8, 2.0$ Hz, 1H), 3.80 (q, $J = 4.6$ Hz, 4H), 3.71 (t, $J = 6.5$ Hz, 4H), 3.59 (d, $J = 5.6$ Hz, 2H), 2.61 (t, $J = 7.0$ Hz, 2H), 2.11 (q, $J = 6.8$ Hz, 2H), 1.37 (s, 9H). **^{13}C NMR** (101 MHz, Acetone-d_6) δ 170.4, 153.5, 149.5, 143.9, 137.3, 137.0, 128.9, 127.0, 126.6, 124.3, 107.6, 104.7, 50.8, 50.3, 46.1, 45.6, 42.2, 35.4, 31.5. **HRMS (ESI)** $[M + H]^+$ for $C_{25}H_{32}ON_4Cl$ m/z Found 439.2257. Calculated 439.2259. **IR (Neat)** 2962, 1592, 1463, 1269, 1017, 842.

2.2.7 | 2-(4-Tert-butylphenyl)-6-iodo-4-(piperazin-1-yl)-1H-benzo[d]imidazole (5)

To a solution containing 1.22-g NaI (8.1 mmol, 10 equiv.) and 10 mL of acetone, 0.36-g 1-(4-(2-(4-tert-butylphenyl)-1H-benzo[d]imidazol-4-yl)piperazin-1-yl)-4-chlorobutan-1-one (0.81 mmol, 1 equiv.) was added. The solution was heated to 55°C under reflux and stirred for 16 hours. Then, the solution was filtered and transferred to a vial for HPLC. Method for HPLC separation; flow rate 25 mL/minute initial 95% H_2O 0.1% TFA, 5% ACN. At 15 minutes, there was linear change to 5% H_2O, 95% ACN 0.1% TFA. The product fractions were collected and lyophilized to give white powder (73.5 mg, 20%). **Purity** 95.21%. **^{1}H NMR** (400 MHz, DMSO-d_6) δ 9.32 (s, 1H), 8.22 (d, $J = 8.4, 1.8$ Hz, 1H), 7.57 (d, 1H), 7.49 (d, $J = 8.2$ Hz, 1H), 6.56 (d, $J = 7.8$ Hz, 1H), 3.35 (s, 8H), 1.34 (d, $J = 1.7$ Hz, 9H). **^{13}C NMR** (101 MHz, DMSO-d_6) δ 152.8, 131.8, 127.3, 126.8, 125.4, 99.5, 68.3, 60.2, 46.6, 42.7, 34.6, 31.0, 27.4, 21.8. **HRMS (ESI)** $[M + H]^+$ for $C_{21}H_{26}N_4I$ m/z Found 461.1205. Calculated 461.1197 **IR (Neat)**: 2963, 2839, 1619, 1489, 1273, 1023.

2.2.8 | 1-(4-(2-(4-Tert-butylphenyl)-1H-benzo[d]imidazol-4-yl) piperazin-1-yl)-5-chloropentan-1-one (2d)

To a solution containing 5-mL DMF (anhydrous) and 0.21-mL (1.2 mmol, 3 equiv.) DIPEA, 0.15-g (0.405 mmol) 2-(4-tert-butylphenyl)-4-(piperazin-1-yl)-1H-benzo[d] imidazole (**1**) was added. The solution was cooled down to 0°C in ice bath, under inert conditions, and 0.16-mL (1.2 mmol, 3 equiv.) chlorovaleroryl chloride **3d** was added at 0°C. The solution was then warmed to room temperature and stirred for 18 hours. The solvent was evaporated on a rotavapor. The residue was then dissolved in DCM and chromatographed on Biotage SP1 flash chromatography systems by a Biotage snap ultra C18rp 12 g column. Flow rate: 15 mL/minute. At 20 minutes, there was linear change to 100% ACN. ^{1}H NMR was obtained, but the compound showed impurities. The compound was then further purified on HPLC. Method for HPLC separation, 25 mL/minute initial 95% H_2O 0.1% TFA, 5% ACN 0.1% TFA. At 15 minutes, there was linear change to 5% H_2O 0.1% TFA, 95% ACN 0.1% TFA. Fractions were collected, and solvents were removed by evaporation to provide a white powder. (44 mg, 24% yield). **Purity** 99.46%. **^{1}H NMR** (400 MHz, Acetone-d_6) δ 11.92 (s, 1H), 8.34 to 8.01 (m, 2H), 7.68 to 7.46 (m, 2H), 7.17 to 7.03 (m, 2H), 6.58 (s, 1H), 3.78 (d, $J = 14.9$ Hz, 4H), 3.68 to 3.55 (m, 6H), 2.47 (t, 2H), 1.90 to 1.80 (m, 2H), 1.80 to 1.70 (m, 2H), 1.36 (s, 9H). **^{13}C NMR** (101 MHz, Acetone-d_6) δ 171.2,

153.4, 149.6, 143.9, 137.3, 137.0, 128.8, 127.1, 126.5, 126.5, 124.2, 107.6, 104.7, 50.9, 50.3, 46.2, 45.6, 45.6, 42.2, 35.3, 33.1, 32.6, 31.5, 23.3. **HRMS (ESI)** [M + H]$^+$ for $C_{26}H_{34}ON_4Cl$ m/z Found 453.2413. Calculated 453.2416. **IR (neat)** 2966, 1631, 1465, 1438, 1198, 1131, 1015.

2.2.9 | 1-(4-(2-(4-Tert-butylphenyl)-1H-benzo[d]imidazol-4-yl) piperazin-1-yl)-5-iodopentan-1-one (4d)

To a solution containing 2 mL of acetone and 66 mg (0.44 mmol, 10 equiv.) NaI, 0.02-g (0.044 mmol) 1-(4-(2-(4-tert-butylphenyl)-1H-benzo[d]imidazol-4-yl)piperazin-1-yl)-5-chloropentan-1 one (**2d**) was added. The solution was heated to 160°C in the microwave for 5 minutes. The reaction mixture was filtered and separated by HPLC. HPLC method used for separation; 25 mL/minute initial 95% H_2O 0.1% TFA, 5% ACN 0.1% TFA. At 15 minutes, there was linear change to 5% H_2O 0.1% TFA, 95% ACN 0.1% TFA. After HPLC purification, the compound was lyophilized to provide a white powder (6.2 mg, 26% yield). **Purity** 99.14%. **^{1}H NMR** (400 MHz, Acetone-d_6) δ 8.25 (d, $J = 8.5$ Hz, 2H), 7.67 (d, $J = 8.4$ Hz, 2H), 7.49 (d, $J = 8.1$ Hz, 1H), 7.36 (t, $J = 8.0$ Hz, 1H), 7.01 (d, $J = 7.8$ Hz, 1H), 3.84 to 3.67 (m, 4H), 3.38 to 3.21 (m, 6H), 2.48 (t, $J = 7.3$ Hz, 2H), 1.96 to 1.82 (m, 2H), 1.77 to 1.67 (m, 2H), 1.37 (s, 9H). **^{13}C NMR** (101 MHz, Acetone-d_6) δ 171.2, 156.7, 150.1, 141.6, 135.3, 129.3, 128.9, 127.1, 126.8, 123.3, 113.5, 108.7, 52.2, 51.8, 48.3, 46.0, 44.5, 42.0, 35.7, 34.0, 32.2, 31.3, 26.8, 7.5. **HRMS (ESI)** [M + H]$^+$ for $C_{26}H_{34}ON_4I$ m/z Found 545.1765. Calculated 545.1772. **IR (neat)** 2961, 2923, 1712, 1609, 1361, 1258, 1235, 1012.

2.2.10 | 1-(4-(2-(4-Tert-butylphenyl)-1H-benzo[d]imidazol-4-yl) piperazin-1-yl)-6-chlorohexan-1-one (2e)

To a solution containing 5-mL DMF (anhydrous) and 0.01-mL (0.69 mmol, 3 equiv.) DIPEA, 0.089-g (0.23 mmol) 2-(4-tert-Butylphenyl)-4-(piperazin-1-yl)-1H-benzo[d]imidazole (**1**) was added. The solution was cooled down to 0°C in an ice bath under inert conditions, and 0.08-mL (0.69 mmol, 3 equiv.) chlorohexanoyl chloride **3e** was added at 0°C. The solution was warmed to room temperature and stirred for 18 hours. The solvent was evaporated on a rotavapor. The residue was then dissolved in DCM and chromatographed on Biotage SP1 flash chromatography systems by a Biotage snap ultra C18rp 12-g column. Flow rate: 15 mL/minute. At 20 minutes, there was linear change to 100% ACN. The solvents were removed by evaporation to provide a white powder (104 mg, 65% yield). **Purity** 99.17%. **^{1}H NMR** (400 MHz, Acetone-d_6) δ 11.91 (s, 1H), 8.16 (dd, $J = 8.3, 3.0$ Hz, 2H), 7.58 (dd, $J = 8.4, 2.8$ Hz, 2H), 7.10 (d, $J = 6.6$ Hz, 2H), 6.59 (t, $J = 4.1$ Hz, 1H), 3.80 (s, 4H), 3.71 (s, 2H), 3.61 (dt, $J = 18.9, 5.6$ Hz, 4H), 2.46 (d, $J = 7.9$ Hz, 2H), 1.86 to 1.78 (m, 2H), 1.67 to 1.65 (m, 2H), 1.58 to 1.49 (m, 2H), 1.38 (m, 9H). **^{13}C NMR** (101 MHz, Acetone-d_6) δ 171.3, 153.4, 149.5, 143.9, 137.3, 137.0, 128.9, 127.0, 126.6, 124.2, 107.6, 104.7, 50.9, 50.3, 46.3, 45.7, 42.2, 35.4, 33.3, 33.3, 31.5, 27.4, 25.3. **HRMS (ESI)** [M + H]$^+$ for $C_{27}H_{36}ON_4Cl$ m/z Found 467.2566. Calculated 467.2572 **IR (Neat)** 3197, 2981, 1619, 1479, 1433, 1233, 1019.

2.2.11 | 1-(4-(2-(4-Tert-butylphenyl)-1H-benzo[d]imidazol-4-yl) piperazin-1-yl)-6-iodohexan-1-one (4e)

To a solution containing 3 mL of acetone and 124 mg (0.83 mmol, 5 equiv.) NaI, 0.077 g (0.165 mmol) of 1-(4-(2-(4-tert-butylphenyl)-1H-benzo[d]imidazol-4-yl) piperazin-1-yl)-6-iodohexan-1-one (**2e**) was added. The solution was heated to 55°C under reflux and stirred for 16 hours. Then, it was filtered to and transferred to a vial for HPLC. Method for HPLC separation; 25 mL/minute initial 95% H_2O 0.1% TFA, 5% ACN 0.1% TFA. At 13 minutes, there was linear change to 5% H_2O 0.1% TFA, 95% ACN 0.1% TFA. Product fractions were collected and lyophilized to provide white powder (10 mg, 11% yield). **Purity** 98.22%. **^{1}H NMR** (400 MHz, Acetone-d_6) δ 8.32 to 8.17 (m, 2H), 7.69 (d, $J = 8.6$ Hz, 1H), 7.45 (d, $J = 8.1$ Hz, 1H), 7.36 (t, $J = 8.0$ Hz, 1H), 6.98 (d, $J = 7.9$ Hz, 1H), 3.83 (t, $J = 5.1$ Hz, 4H), 3.43 (t, $J = 5.0$ Hz, 2H), 3.37 to 3.25 (m, 4H), 2.48 (t, $J = 7.4$ Hz, 2H), 1.89 to 1.85 (m, 2H), 1.74 to 1.59 (m, 2H), 1.55 to 1.49 (m, 2H), 1.40 (s, 9H). **^{13}C NMR** (101 MHz, Acetone-d_6) δ 171.4, 156.3, 150.2, 141.9, 135.9, 130.3, 128.6, 127.1, 126.4, 124.1, 112.7, 108.3, 52.1, 51.6, 46.1, 42.0, 35.7, 34.3, 33.2, 31.3, 31.0, 24.9, 7.7. **HRMS (ESI)** [M + H]$^+$ for $C_{27}H_{36}ON_4I$ m/z Found: 559.1935 Calculated: 559.1928. **IR (neat)** 2964, 2868, 1629, 1464, 1437, 1197, 1129.

2.3 | Kinetics experiments

Compounds **2** (1 equiv.) were added to a solution of acetone-d6 (0.60 mL) and NaI (10 equiv.) in an NMR tube. The reaction was monitored by ^{1}H-NMR, following the disappearance of **2** and appearance of **4** by acquisition of a spectrum every 10 minutes over 12 hours unless otherwise specified. For each compound, the CH_2-Cl peak was identified, and the rate of the reaction was monitored by the disappearance of the integral. ***Reaction of 2a to form 4a:*** 10 mg (0.024 mmol, 1 equiv.) of **2a** and 36 mg (0.24 mmol, 10 equiv.) NaI. ***Reaction of 2b to form 4b:*** 10-mg (0.024 mmol, 1 equiv.) **2b** and 35-mg (0.24 mmol, 10 equiv.) NaI heated to 60°C. The reaction

monitored by ^{1}H-NMR at 1, 2, 5, 8, and 11 hours. ***Reaction of 2c to form 4c:*** 10-mg (0.022 mmol, 1 equiv.) **2c** and 33-mg (0.22 mmol, 10 equiv.) NaI, heated to 60°C. The reaction was monitored by ^{1}H-NMR at 1, 2, 5, 8, and 11 hours. ***Reaction of 2e to form 4e:*** 10-mg (0.021 mmol, 1 equiv.) **2e** and 32-mg (0.21 mmol, 10 equiv.) NaI heated to 60°C. The reaction was monitored by ^{1}H-NMR at 1, 2, 5, 8, and 11 hours.

2.4 | Radiolabeling of 4a non-carrier added

Ten milliliters of Na^{123}I in water (37 MBq/mL at 99.9% purity at calibration time, specific activity 4.2 pmol/mL 123I-Iodine) was obtained from GE Healthcare. Water was removed from Na^{123}I by evaporation overnight by a gentle stream of nitrogen gas. Then, 40 mg (0.1 mmol) of **2a** was dissolved in 2 mL of acetone and added 370 MBq (decay corrected to calibration time) Na^{123}I at the start of the reaction. The solution was capped in a vial (Biotage microwave reaction glass vial 2-5 mL), heated to 60°C, and stirred for 1 hour. The product was then purified by radio-HPLC with the HPLC method; 10 mL/minute initial 95% H$_2$O, 0.1% TFA, 5% ACN 0.1% TFA, then there was linear change over 3 minutes to 40% H$_2$O 0.1% TFA, 60% ACN 0.1% TFA, then there was linear change over 7 minutes to 5% H$_2$O 0.1% TFA, 95% ACN 0.1% TFA. Each fraction was collected and solvents were evaporated, then dissolved in PEG 400:water (4:6). An aliquot was then analyzed by analytical radio-HPLC: 0.5 mL/minute initial 95% H$_2$O 0.1% TFA, 5% ACN 0.1% TFA, then there was linear change over 20 minutes to 5% H$_2$O 0.1% TFA, 95% ACN 0.1% TFA.

2.5 | Microwave reactions

Reaction of 2b to 4b: 10 mg (0.024 mmol, 1 equiv.) of 2b was added to a solution of 2 mL of acetone and 35 mg (0.24 mmol, 10 equiv.) of NaI. The solution was heated to 160°C in a microwave reactor for 5 minutes, then filtered and analyzed by ^{1}H-NMR. **Reaction of 2d to 4d:** 20 mg (0.044 mmol, 1 equiv.) of 2b was added to a solution of 2-mL acetone and 66 mg (0.44 mmol, 10 equiv.) of NaI. The solution was heated to 160°C in a microwave reactor for 5 minutes, then filtered and analyzed by ^{1}H-NMR. **Reaction of 2e to 4e:** 20-mg (0.043 mmol, 1 equiv.) **2e** was added to a solution of 2 mL acetone and 32 mg (0.21 mmol, 5 equiv.) of NaI. The solution was heated to 160°C in a microwave reactor for 5 minutes, then filtered and analyzed by ^{1}H-NMR.

2.6 | Computational details

All the DFT calculations were performed using the Gaussian 09 program package [20]. The ωB97XD functional [21], and 6-311G(d,p) basis sets [22,23] were used for all the calculation of the results used in the main paper. Solvent effects were corrected by using the polarizable continuum model (PCM) [24] in its integral equation formalism (IEFPCM) [25,26], together with acetone as a solvent. For the sake of validating the approach, we performed additional calculations using PBE [27,28], CAM-B3LYP [29] and M06-L [30] functionals (see the ESI). The optimized geometries were confirmed to be real minima on the potential energy surface with no imaginary frequencies by performing a normal-mode vibrational analysis at the same level of theory. The transition state calculations were confirmed by the presence of an appropriate and a single imaginary vibrational frequency. The Gibbs free energies were calculated at the standard conditions and reported as kcal/mol.

3 | RESULTS AND DISCUSSION

3.1 | Synthesis of test substrates

The key bioactive intermediate **1** was synthesized according to previously published procedures in 37% overall yield from 2,6-difluoronitrobenzene (Scheme 2) [19]. This template has been shown to effect binding to the GnRH receptor while maintaining acceptable blood-brain barrier penetration properties [19]. Moreover, our approach relies on the presence of an N—H moiety amenable to acylation chemistry which makes compound **1** an ideal test substrate.

Acylated chlorides **2a to e** were generated as shown in Scheme 3. Treatment of **1** with chloroacyl chlorides **3a to e** in the presence of excess DIPEA in DMF afforded products **2a to e** in 24% to 67% yields (Scheme 3).

The halogen exchange reactions on **2a to e** were conducted using excess NaI in acetone until full conversion of the starting materials was observed (Scheme 4). In general, the isolated chemical yields were poor (11%–37%). **2a** proceeded readily at ambient temperature in 67% yield, whereas the other analogues required heating to 55°C to achieve reasonable conversion rates. The low chemical yields can also be coupled to incomplete precipitation of sodium chloride, which is a central driving force for the Finkelstein reaction. In an attempt to boost yields and shorten reaction times, we
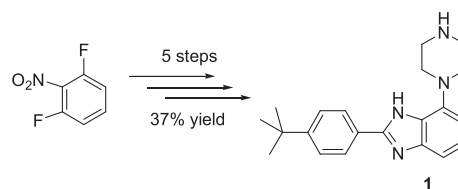
SCHEME 2 Synthesis of key intermediate **1** [19]
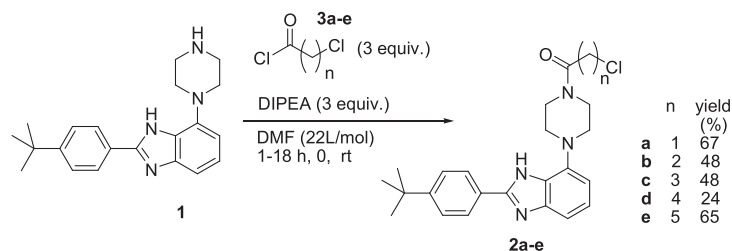
SCHEME 3   Acylation of intermediate **1**
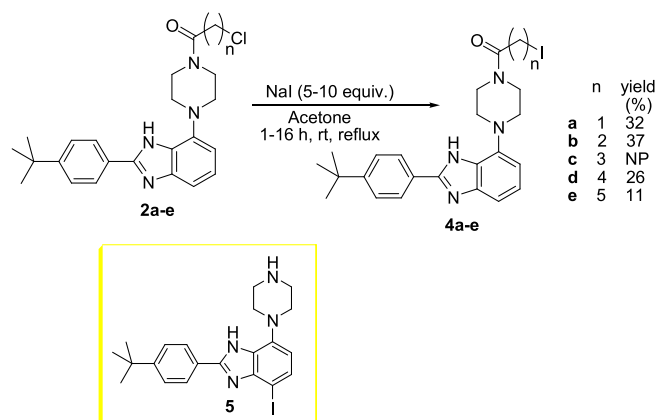
SCHEME 4   Finkelstein reactions on chloroamides **2a to e**, and the identified compound **5** from the reaction of **2c**

decided to try a microwave-assisted approach for compound **2d** ($n = 4$). Treatment of compound **2d** with 10 equivalents of sodium iodide in acetone for 5 minutes at 160°C in microwave afforded the desired product **4d** in 26% yield. In ^{1}H-NMR, we observed full conversion of all substrates, so the poor isolated yields were likely due to instability issues in the work-up and isolation steps. Interestingly, we were unable to isolate the expected product **4c** ($n = 3$). The major isolated compound was **5** in which the acyl chain was completely gone and an iodide had been substituted on the benzimidazole core. An explanation for these observations will be discussed in the mechanism section.

3.2 | Reaction rates

In order to get a quantitative handle on the relative rates of halide substitution in the various substrates, the reaction progress for the iodination reactions was monitored by ^{1}H-NMR. Semi-logarithmic plots of the CH$_2$-Cl peak integral versus reaction time would indicate whether the reactions display the expected pseudo-first order kinetics. The corresponding CH$_2$-I peak signal was also monitored to ensure conversion occurred to the desired product compounds. The iodinations were performed in an NMR tube in deuterated acetone in which a proton NMR spectrum was acquired every 10 minutes. The reaction rate of **2a** was very high, and formation of **4a** was complete before

10 minutes had passed. The other reactions were conducted at 60°C. Compounds **2b**, **2d**, and **2e** displayed clear pseudo-first order kinetics, and the corresponding observed rate constants (moduli of the slopes) are summarized in Figure 1. The rates are remarkably similar, but the conversion of **2e** (0.061 h^{-1}) appeared to be the most rapid after **2a**. The experimentally observed rate constants (k_{obs}) for initial disappearance of the starting acyl chloride must be understood in terms of contribution from 2 mechanistic pathways as shown in Equation 1 and Scheme 5.

$$k_{obs} = (k_{SN2}[I^-] + k_{Anchimeric}) \quad (Eq1)$$

where k_{SN2} is the bimolecular rate constant from direct S$_N$2-substitution and $k_{Anchimeric}$ is the unimolecular rate constant from cyclization of the amide. The similarity of the rates could suggest significant contributions from both
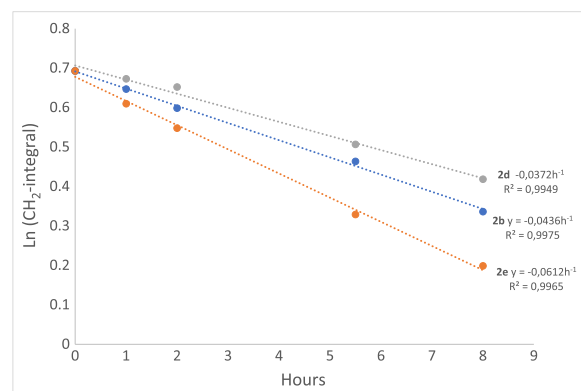
FIGURE 1   Semi-logarithmic plots for the disappearance of **2b**, **2d**, and **2e** with corresponding linear regression analyses
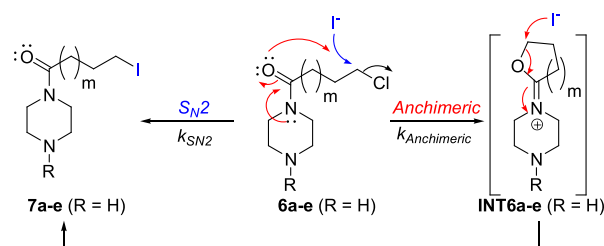
SCHEME 5   Mechanistic pathways in the conversion of **6a to e** ($m = 0–3$) model systems to products

terms in the 3 cases. A detailed computational analysis was conducted to obtain a deeper understanding of the data.

3.3 | Mechanistic analysis

A hypothesis in this work was that the anchimeric effect of the amide group could be employed as a modulating element for the substitution reaction rate. Because amide group anchimeric assistance is sparsely described in the literature [15,31] and would be of great interest to the physical organic chemistry community, we decided to pursue a deep mechanistic understanding of this phenomenon in our system using DFT calculations. We have assessed anchimerically assisted pathways in addition to the direct S_N2 substitution mechanisms for all our model chain lengths using ωB97XD/6-311G(d,p)/PCM/acetone (see the Electronic Supporting Information (ESI) for a discussion about the influence of different DFT methods). In the calculations, we have employed simplified molecules **6a to e** (Scheme 5, R = H) as models for **2a to e**, where only an acylated piperidine ring has been considered. As the remainder of the molecule is likely to not affect the reactive center to a large extent, this model system was deemed representative. The computed barriers were compared with experimental and computed free energies of activation reported for an amide cyclization and Finkelstein reactions by Arcelli et al [32] and Zaczek et al [33], respectively. Our computed barriers are in excellent agreement with these reports.

In order to gauge the experimental rates with our computational study and attempt to explain our experimental observations, we computed free energy barriers for direct S_N2 substitutions on the 5 model substrates **6a to e** based on the potential energy surfaces in Figure 2. Qualitatively, the predicted barriers follow the observed experimental rate trend **6a > 6e > 6d**. The observed rates for **2d** and **2b** are not very different, so these are hard to distinguish experimentally without more sophisticated experiments. Comparing the faster **2e** with **2d**, we see an experimental reaction rate ratio of 1.65, corresponding to a free energy barrier difference of 0.3 kcal/mol. This is remarkably consistent with the computed free energy barrier difference of 0.4 kcal/mol for the 2 S_N2 reactions, particularly considering error bars for DFT calculations [34]. Because our rate study was conducted with 10-fold excess of iodide to ensure pseudo-first order kinetics, the results likely represent direct S_N2 substitution reactions of our chloride substrates, which is consistent with the computational study.

Conversion of substrate **6a** to the iodinated product clearly follows a classical S_N2 pathway owing to the stabilizing interaction the adjacent pi-orbital has on the
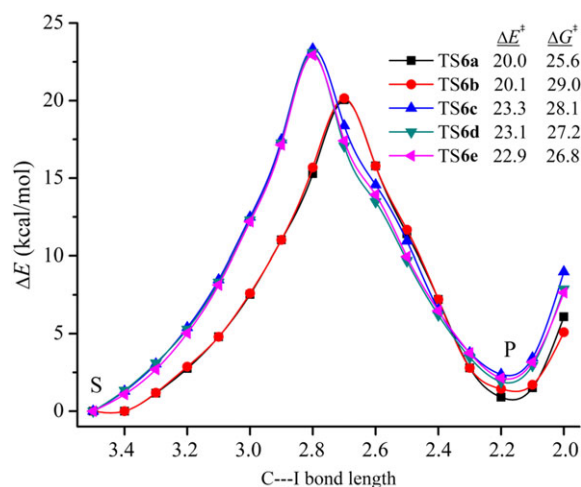

FIGURE 2 Potential energy surface (PES) for the S_N2 reactions of **6a to e** calculated using ωB97XD/6-311G(d,p)/PCM/acetone

transition state and the lack of stability due to ring strain in the hypothetical 3-membered intermediate in an anchimerically assisted pathway. This was confirmed by scanning the potential energy surface as shown in Figure 3, which shows a classical S_N2 trajectory.

For substrate **6b**, the situation becomes more complex (Figure 4). Here, the S_N2 pathway has a 29.0 kcal/mol barrier versus the alternative anchimerically assisted pathway, in which the amide group expels chloride first, followed by iodide substitution. The latter pathway has a 28.4 kcal/mol barrier for chloride extrusion, followed by rapid iodide attack on the intermediate product **INT6b** with a barrier of only 14.8 kcal/mol. Although the anchimerically assisted pathway is slightly faster, there
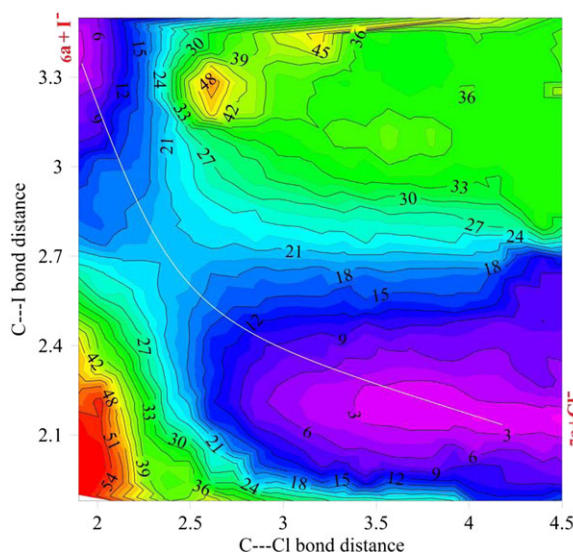

FIGURE 3 Potential energy surface (PES) for the conversion of **6a** to **7a** calculated using ωB97XD/6-311G(d,p)/PCM/acetone. The conversion of **6a** to **7a** follows an S_N2 reaction pathway (see the white line)
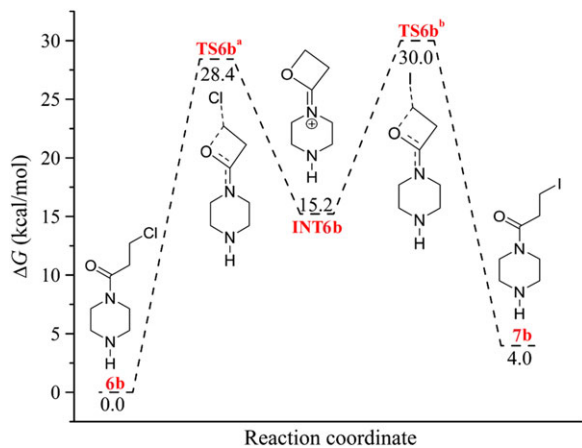
FIGURE 4 Energy diagram for the anchimerically assisted halogen exchange reaction mechanism in substrate **6b**

is contribution from the direct S$_N$2 pathway as it has a barrier of only 0.6 kcal/mol higher than the former. Moreover, at high iodide concentrations, the direct substitution could predominate. The similarity of rate contributions from both mechanisms could explain why **2b** appears to be slightly faster than substrate **2d** in our rate study.

Although we did not observe the desired product in case of substrate **2c**, we computed free energy surfaces for both anchimerically assisted and direct S$_N$2 pathways for the model compound **6c** also (Figure 5). Here, the anchimerically assisted pathway is predominant because of the 7.2 kcal/mol lower free energy barrier. Furthermore, the calculations reveal why this substrate behaves significantly different from the others. In this case, the cyclic intermediate is considerably more stable than the substrate **6c** by 3.6 kcal/mol, making **INT6c** a predominant reactive species in the solution. The high concentration of **INT6c**, as well as the relatively high barrier for its iodide substitution (31.4 kcal/mol), would render it more
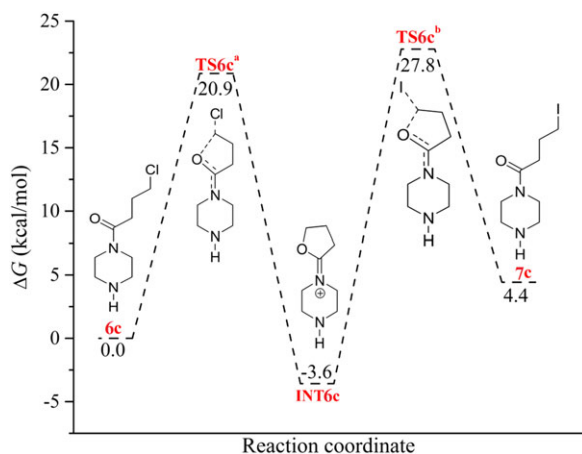
susceptible to hydrolysis and other side reactions, which would explain the observation of hydrolyzed by-product **5** lacking the acyl group and none of the desired iodinated product.

The anchimeric pathway with **6d** is favored as the cyclization barrier is 22.5 kcal/mol, approximately 5 kcal/mol smaller than the direct S$_N$2 pathway (Figure 6). The cationic intermediate **INT6d** is 6.5 kcal/mol less stable than the reactants but can rapidly react with iodide ions to form the corresponding product **7d** with a barrier of only 17.4 kcal/mol. At low iodide concentrations, this is certainly the predominant pathway. Unsurprisingly, the cyclization barrier goes up when moving to the 7-membered ring cyclization of **6e** with a 25.3 kcal/mol barrier (Figure 7). Otherwise, the situation is similar to that of the pathway for **6d**.

The Finkelstein reaction depends on coupling with the precipitation of sodium chloride to provide a driving
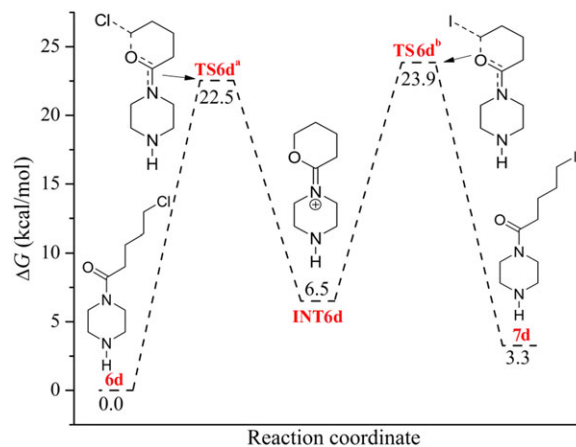

FIGURE 6 Energy diagram for the halogen exchange reaction mechanism in substrate **6d**

FIGURE 5 Energy diagram for the halogen exchange reaction mechanism in substrate **6c**
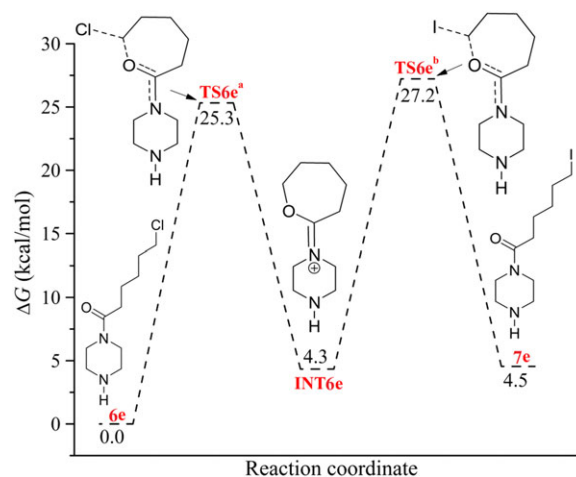

FIGURE 7 Energy diagram for the halogen exchange reaction mechanism in substrate **6e**

force for the reaction. Our computational study demonstrates the endergonic nature of these reactions in the absence of considering the precipitation process. The precipitation of sodium chloride will render the chloride expulsion step irreversible.

3.4 | Radiolabelling studies

Although our mechanistic analysis of the reactions earlier revealed that anchimeric assistance modulation of substitution rates is not straightforward, we decided to attempt radiolabelling of **2a** to demonstrate the validity of the acylation-Finkelstein approach for radioiodination. Compound **2a** readily undergoes substitution and was chosen based on the rapid substitution rate compared to the higher chain analogues. In an attempt to maximize the RCY, water in the commercially delivered Na^{123}I solution was evaporated in a concentration step before the reaction. The reaction of **2a** was subsequently analyzed by Radio-HPLC after 1-hour reaction time at 60°C. The radiochromatogram of labeled ^{123}I-**4a** and HPLC-UV trace of cold **4a** are shown in Figure 8. These chromatograms confirm that the radiolabel is effectively incorporated into **4a**.

A non-carrier added approach to the radiolabeling was attempted as shown in Scheme 6 and produced radiolabeled compound ^{123}I-**4a**. The RCY was determined by comparing the product peak in the HPLC radiochromatogram relative to Na^{123}I and other impurities. The RCYs were not corrected for activity lost in the HPLC; however, we did not observe major losses when the column was screened for residual radioactivity. The RCY
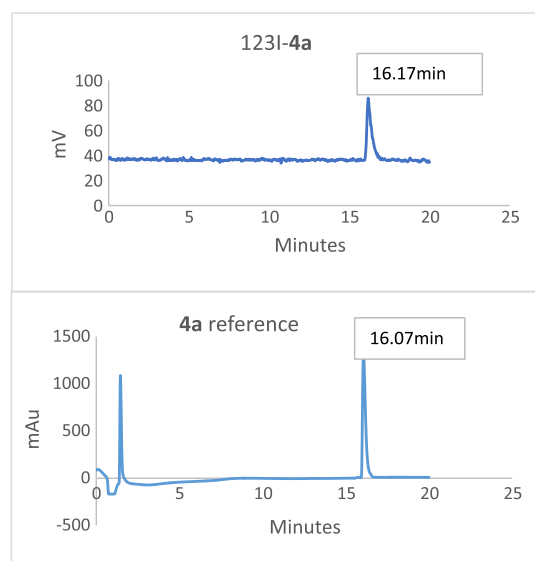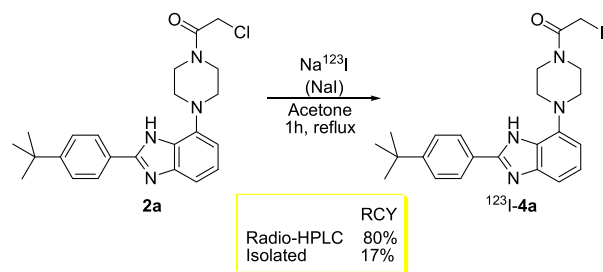

SCHEME 6 Radiochemical yields (RCYs) observed for ^{123}I-**4a**

determined from radio-HPLC was found to be 80%, whereas decay-corrected RCY for isolated ^{123}I-**4a** was found to be 17%.

Effective radiolabelling reactions must have a reasonable reaction rate in order to be of practical use. In our study, only compound **2a** underwent radioiodination at a high rate. However, a weakness with the α-iodo substrate is that it is quite reactive, and this will cause loss of the radiolabel in physiological settings. As such, the longer chain analogues may be more interesting in order to retain the label longer in the bioactive molecule. However, the substitution rates are rather slow, as is supported by the computed barriers and our kinetic study, even at 60°C, and the conversions were less than 50% after 11-hour reaction time. A possible solution would be to increase the substitution efficiency by employing microwave irradiation. We tested this hypothesis by conducting the reactions at 160°C in a microwave reactor and, to our delight, observed full conversion of all substrates **2b**, **2d**, and **2e** to the corresponding iodides by NMR after only 5 minutes of reaction time (see ESI). This approach allows us to employ the different chain lengths as desired, and we can expect to achieve radiolabelling in minutes. Moreover, we have shown that the longer chains display relatively slow substitution rates at ambient temperatures, which could render them more interesting for imaging applications as they would retain the radiolabel longer in physiological settings.

4 | CONCLUSIONS

We have demonstrated a straightforward acylation-Finkelstein approach to iodination and radioiodination of amine-containing bioactives by using a recently developed GnRH antagonist scaffold as a model system. The approach implies the use of anchimeric assistance by amide groups to modulate radiosubstitution rates, which has been studied in molecular detail using chemical synthesis, kinetics, high-level DFT-calculations, and radiolabelling studies. The mechanistic studies have revealed a complex interplay between competing

FIGURE 8 Analytical radiochromatogram of compound ^{123}I-**4a** compared to HPLC-UV (214 nm) trace of cold **4a** reference

mechanistic pathways and solvent effects and show several fundamental aspects of amide group anchimeric assistance that have previously not been reported. Amide group anchimeric assistance only appears to potentially increase substitution reaction rates when 5-membered and 6-membered ring intermediates are involved. In the 5-membered ring intermediate, its stability rendered it susceptible to side reactions.

Despite limitations, we have successfully conducted iodination in several systems, and our study shows that this strategy is most promising with the use of 2, 3, 5, and 6-carbon chloroacyl groups. Radioiodination was demonstrated on the C2 system in very high analytical RCY of 80%. A major conclusion is also that iodination could be effected rapidly under microwave conditions for the slower 3-carbon, 5-carbon, and 6-carbon systems, while they remain substitutionally stable at physiological temperature—a potential major advantage for in vivo activity and further studies in this area are underway.

ACKNOWLEDGEMENTS

ORCID

Richard Fjellaksel 🄳 http://orcid.org/0000-0002-6783-5198
Jørn H. Hansen 🄳 http://orcid.org/0000-0002-3888-5217

REFERENCES

[1] G. B. Saha, *Fundamentals of Nuclear Pharmacy*, Springer New York, New York, NY **1992** 80.

[2] M. I. Page, W. P. Jencks, *Proc. Natl. Acad. Sci. U. S. A.* **1971**, *68*, 1678.

[3] T. C. Bruice, F. C. Lightstone, *Acc. Chem. Res.* **1999**, *32*, 127.

[4] F. C. Lightstone, T. C. Bruice, *J. Am. Chem. Soc.* **1996**, *118*, 2595.

[5] K. N. Houk, J. A. Tucker, A. E. Dorigo, *Acc. Chem. Res.* **1990**, *23*, 107.

[6] F. M. Menger, *Acc. Chem. Res.* **1985**, *18*, 128.

[7] T. C. Bruice, U. K. Pandit, *J. Am. Chem. Soc.* **1960**, *82*, 5858.

[8] A. J. Kirby, N. H. Williams, *J. Chem. Soc. Chem. Commun.* **1991**, 1643.

[9] (a) T. Cohen, J. Lipowitz, *J. Am. Chem. Soc.* **1964**, *86*, 5611; (b) J. Suh, S. S. Yoon, E. Oh, C. Kang, E. Lee, *Bioorg. Chem.* **1988**, *16*, 245. and references therein

[10] M. S. Macauley, G. E. Whitworth, A. W. Debowski, D. Chin, D. J. Vocadlo, *J. Biol. Chem.* **2005**, *280*, 25313.

[11] N. Çetinbaş, M. S. Macauley, K. A. Stubbs, R. Drapala, D. J. Vocadlo, *Biochemistry* **2006**, *45*, 3835.

[12] R. J. Dennis, E. J. Taylor, M. S. Macauley, K. A. Stubbs, J. P. Turkenburg, S. J. Hart, G. N. Black, D. J. Vocadlo, G. J. Davies, *Nat. Struct. Mol. Biol.* **2006**, *13*, 365.

[13] B. L. Mark, D. J. Vocadlo, S. Knapp, B. L. Triggs-Raine, S. G. Withers, M. N. G. James, *J. Biol. Chem.* **2001**, *276*, 10330.

[14] S. Knapp, D. Vocadlo, Z. Gao, B. Kirk, J. Lou, S. G. Withers, *J. Am. Chem. Soc.* **1996**, *118*, 6804.

[15] M. Calvaresi, S. Rinaldi, A. Arcelli, M. Garavelli, *J. Org. Chem.* **2008**, *73*, 2066.

[16] M. Médoc, F. Sobrio, *J. Org. Chem.* **2015**, *80*, 10086.

[17] H. Finkelstein, *Ber. Dtsch. Chem. Ges.* **1910**, *43*, 1528.

[18] R. D. Pace, Y. Regmi, *J. Chem. Educ.* **2006**, *83*, 1344.

[19] R. Fjellaksel, M. Boomgaren, R. Sundset, I. H. Haraldsen, J. H. Hansen, P. J. Riss, *Med. Chem. Commun.* **2017**, *8*, 1965.

[20] M. J. Frisch, G. W. Trucks, H. B. Schlegel, G. E. Scuseria, M. A. Robb, J. R. Cheeseman, G. Scalmani, V. Barone, B. Mennucci, G. A. Petersson, H. Nakatsuji, M. Caricato, X. Li, H. P. Hratchian, A. F. Izmaylov, J. Bloino, G. Zheng, J. L. Sonnenberg, M. Hada, M. Ehara, K. Toyota, R. Fukuda, J. Hasegawa, M. Ishida, T. Nakajima, Y. Honda, O. Kitao, H. Nakai, T. Vreven, J. A. Montgomery Jr., J. E. Peralta, F. Ogliaro, M. Bearpark, J. J. Heyd, E. Brothers, K. N. Kudin, V. N. Staroverov, R. Kobayashi, J. Normand, K. Raghavachari, A. Rendell, J. C. Burant, S. S. Iyengar, J. Tomasi, M. Cossi, N. Rega, J. M. Millam, M. Klene, J. E. Knox, J. B. Cross, V. Bakken, C. Adamo, J. Jaramillo, R. Gomperts, R. E. Stratmann, O. Yazyev, A. J. Austin, R. Cammi, C. Pomelli, J. W. Ochterski, R. L. Martin, K. Morokuma, V. G. Zakrzewski, G. A. Voth, P. Salvador, J. J. Dannenberg, S. Dapprich, A. D. Daniels, O. Farkas, J. B. Foresman, J. V. Ortiz, J. Cioslowski, D. J. Fox, *Gaussian 09*, Revision D01, Gaussian, Inc., Wallingford CT, USA **2009**.

[21] J.-D. Chai, M. Head-Gordon, *Phys. Chem. Chem. Phys.* **2008**, *10*, 6615.

[22] M. N. Glukhovtsev, A. Pross, M. P. McGrath, L. Radom, *J. Chem. Phys.* **1995**, *103*, 1878.

[23] R. Krishnan, J. S. Binkley, R. Seeger, J. A. Pople, *J. Chem. Phys.* **1980**, *72*, 650.

[24] J. Tomasi, B. Mennucci, R. Cammi, *Chem. Rev.* **2005**, *105*, 2999.

[25] E. Cancès, B. Mennucci, J. Tomasi, *J. Chem. Phys.* **1997**, *107*, 3032.

[26] B. Mennucci, J. Tomasi, *J. Chem. Phys.* **1997**, *106*, 5151.

[27] J. P. Perdew, K. Burke, M. Ernzerhof, *Phys. Rev. Lett.* **1997**, *78*, 1396.

[28] J. P. Perdew, K. Burke, M. Ernzerhof, *Phys. Rev. Lett.* **1996**, *77*, 3865.

[29] T. Yanai, D. P. Tew, N. C. Handy, *Chem. Phys. Lett.* **2004**, *393*, 51.

[30] Y. Zhao, D. G. Truhlar, *Theor. Chem. Acc.* **2008**, *120*, 215.

[31] A. Guiotto, M. Canevari, M. Pozzobon, S. Moro, P. Orsolini, F. M. Veronese, *Bioorg. Med. Chem.* **2004**, *12*, 5031.

[32] A. Arcelli, G. Porzi, S. Rinaldi, S. Sandri, *J. Phys. Org. Chem.* **2004**, *17*, 289.

[33] S. Zaczek, F. Gelman, A. Dybala-Defratyka, *J. Phys. Chem. A* **2017**, *121*, 2311.

[34] S. E. Wheeler, A. Moran, S. N. Pieniazek, K. N. Houk, *J. Phys. Chem. A* **2009**, *113*, 10376.

SUPPORTING INFORMATION

Additional Supporting Information may be found online in the supporting information tab for this article.

How to cite this article: Fjellaksel R, Dugalic D, Demissie TB, et al. An acylation-Finkelstein approach to radioiodination of bioactives: The role of amide group anchimeric assistance. *J Phys Org Chem.* 2018;e3835. https://doi.org/10.1002/poc.3835

PAPER IV

In vitro evaluation of two promising bioactive triazole-benzimidazole GnRH Receptor-antagonists as possible candidates for SPECT imaging.

Richard Fjellaksel, Angel Moldes-Anaya, Ana Oteiza, Montserrat Martin-Armas, Terje Vasskog, Patrick J. Riss, Ole K. Hjelstuen, Jørn H. Hansen and Rune Sundset.

Manuscript

In vitro evaluation two promising bioactive triazole-benzimidazole GnRH Receptor-antagonists as possible SPECT radiotracers

Richard Fjellaksel,[a-e] Angel Moldes-Anaya,[e] Ana Oteiza,[d,e] Montserrat Martin-Armas,[d,e] Terje Vasskog,[f] Patrick J. Riss,[g-i] Ole-Kristian Hjelstuen,[b] Jørn H. Hansen,[c] and Rune Sundset [a,d,e]

[a]*Medical Imaging Research Group, Department of Clinical Medicine, UiT The Arctic University of Norway, 9037 Tromsø, Norway.*

[b]*Drug Transport and Delivery Research Group, Department of Pharmacy, UiT The Arctic University of Norway, 9037 Tromsø, Norway.*

[c]*Organic Chemistry Research Group, Department of Chemistry, UiT The Arctic University of Norway, 9037 Tromsø, Norway.*

[d]*Preclinical PET/SPECT/CT, Department of Clinical Medicine, Department of Pharmacy, UiT The Arctic University of Norway, 9037*

[e]*Research and Development unit, PET imaging center, UNN – University Hospital of North-Norway, 9037 Tromsø, Norway.*

[f]*Natural Products and Medicinal Chemistry Research group, UiT The Arctic University of Norway, 9037 Tromsø, Norway.*

[g]*Department of neuropsychiatry and psychosomatic medicine, Oslo University Hospital, Oslo, Norway.*

[h]*Realomics SFI, Department of Chemistry, University of Oslo, PO BOX 1033, Oslo 0371, Norway.*

[i]*Norsk Medisinsk Syklotronsenter AS, Postboks 4950   Nydalen,   0424 Oslo*

ABSTRACT

The discovery of two promising compounds suitable for imaging were disclosed recently. The compounds have previously shown nanomolar potential to inhibit the gonadotropin releasing hormone (GnRH) receptor in a competitive binding assay. In this study, further evaluation of the compounds ability for preclinical trials were performed. *In vitro* evaluation became necessary and serum stability, metabolic profile and autoradiography were performed. The serum stability analysis showed stable compounds where more than 84 % of the compounds remained after 22 hours incubated in human serum. The metabolic profile (phase 1 metabolism) identified and quantified the formation rate for these metabolites. The investigated compounds showed good stability against liver microsome metabolism. As a final step of the *in vitro* evaluation, autoradiography of rat brain sections was performed. The compounds were exposed for the brain sections in competition to [125]I-[D-Trp6]-LHRH. The decrease in the signalling show the competitive antagonistic compounds ability to bind to rat brain sections. In addition, one compound where directly labelled with ^{123}I and incubated on rat brain sections where it showed binding to the rat brain sections. The two promising bioactive triazole-benzimidazole GnRH receptor antagonists are highly suitable for further preclinical evaluation.

INTRODUCTION

In medicine, more radiotracers are needed to be able to cure diseases, to monitor diseases and to develop a deeper understanding of human physiology and pathophysiology. However, the development of radiotracers is a complex field and requires translational cooperation of expert's spanning from organic chemistry, radiochemistry, pharmacology, computer aided chemistry and

biology, radiopharmacy, cell biology, physics, image analysis, preclinical evaluation and clinical evaluation. Millions are spent on the development of new radiotracers and the ability to discard a radiotracer candidate at an early phase of the development is of high importance. The *in vitro* evaluation is an essential step towards a successfully developed radiotracer.[1]

The discovery of promising Gonadotropin releasing hormone receptor (GnRH-R) antagonist candidates based upon a benzimidazole –piperazine scaffold suitable for imaging was recently disclosed, figure 1.[2, 3] Further diversification from the initial study led to the discovery of two highly promising [^{123}I]-labelled triazole-benzimidazole GnRH-R antagonists, figure 1.[4] In the present paper we evaluate the potential for the two promising triazole-benzimidazole GnRH-R antagonists as SPECT radiotracers. The GnRH-R is located in the hypothalamus-pituitary-gonadal axis (HPG axis) together with GnRH where it has its main function as in reproductive physiology. The GnRH and GnRH-R is also located outside the HPG axis and are involved in a wide range of biological processes like reproductive functions, sex behavior, cognition and several diseases such as cancer and neurodegeneration.[5-10] The GnRH is known as luteinizing-hormone releasing hormone (LHRH) which is a neurohormone that consists of 10 amino acids. It is produced in hypothalamus and released in a pulsatile manner into the hypophysial portal bloodstream. When it reaches the pituitary gland it binds to its own G-protein coupled receptor (GnRH-R) then it stimulates the production of two gonadotropins in the anterior pituitary gland – Luteinizing hormone (LH) and Follicle stimulation hormone (FSH). The release of gonadotropins acts in the gonads to produce androgens and estrogens. The release of gonadotropins is controlled by the pulsatile release of GnRH in the hypophysial portal blood stream and by the feedback mechanism of androgens and estrogens.
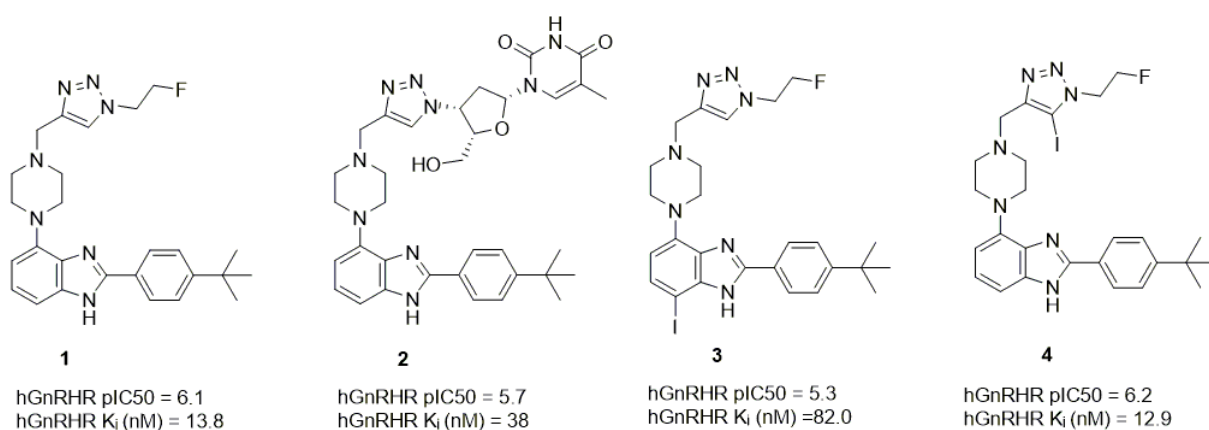

1
hGnRHR pIC50 = 6.1
hGnRHR K_i (nM) = 13.8

2
hGnRHR pIC50 = 5.7
hGnRHR K_i (nM) = 38

3
hGnRHR pIC50 = 5.3
hGnRHR K_i (nM) =82.0

4
hGnRHR pIC50 = 6.2
hGnRHR K_i (nM) = 12.9

Figure 1: Previously disclosed compounds. Compound 1 and 2 from the initial study.[2] Compound 3 and 4 were developed in the continuation of the initial study.[4]

As a continuation of the discovery of compound **3** and **4**, further *in vitro* evaluation became necessary. Serum stability and metabolic activity have been sparsely reported previously for similar structures were **WAY207024** have a reported half-life of 14 minutes for rat liver microsomes.[11] In this study; serum stability, metabolic phase I activity and autoradiography was evaluated to assess the imaging potential for these candidates.

EXPERIMENTAL

Reagents

Acetonitrile and trifluoroacetic acid were obtained from Sigma Aldrich (Sigma-Aldrich, St. Louis, MO, USA). Silica gel 60 TLC plates with fluorescence indicator (F254) from Merck (Darmstadt, Germany) were used. All reactions were conducted multiple times. Anhydrous conditions were conducted only if mentioned. Rat serum was purchased from Sigma Aldrich. Human serum was a kind gift from the Vascular Biology research group at UiT - The Arctic university of Norway. Rat and human liver microsomes were purchased from Thermo Fisher Scientific, Waltham, MA, USA. MilliQ water rinsing system with rinsing from Millipore was used. β-nicotinamide adenine dinucleotide phosphate sodium salt (NADP), β -nicotinamide adenine dinucleotide phosphate reduced tetrasodium salt (NADPH), D-glucose-6-phosphate, D-glucose-6-phosphate dehydrogenase were also purchased from Sigma Aldrich. [125]I-[D-Trp6]-LHRH where bought from Perkin-Elmer, Oslo. Compounds **3** and **4** were synthesised as previously described.[4]

Evaluation of compounds 3 and 4 in human and rat serum

The stability of compounds **3** and **4** was investigated in human and rat serum. In assay, compounds **3** and **4** (50 ul 4 mM) were dissolved in a mixture of 5 % ethanol, 5 % Polysorbate 80 and 90 % water for injection. The compounds were then incubated with 400 μl human and 300 μl rat serum at 37 °C. An aliquot (40-50 μl) from previous mixtures was subsequently extracted with ice-cold acetonitrile at 0, 10, 30, 60, 120, 240 and 1320 minutes post-incubation. Samples were centrifuged at 13.000 *g* for 5 minutes. The supernatants were analysed by LC-MS. Serum experiments were performed in triplicate.

Incubation with rat and human liver microsomes

Incubations were performed by following the protocol presented by Moldes-Anaya et al., 2009.[12] In brief, stock solutions (2 mM) of the substrates were prepared by dissolving compounds **3** and **4** in acetonitrile: water (*v/v*, 75:25). The compounds were incubated in a total volume of 1 ml in Pyrex® test tubes at 37°C in an shaking water bath (Heto-Holten, Allerod, Denmark) with commercially available

rat and human liver microsomes (Thermo Fisher Scientific, Waltham, MA, USA). Human liver microsomes consisted on a mixed gender pool of 15 donors (20 mg/ml protein), whereas rat liver microsomes consisted of an undetermined number of male donors at 20 mg/ml protein. The incubation was performed in NADPH regeneration system in HEPES buffer (pH 7.4) containing (19.4 mM glucose-6-phosphate, 0.91 mM NADPH, 0.84 mM NADP and 5.72 units of glucose-6-phosphate dehydrogenase according to previously published literature. At 0, 2, 5, 15, 30, 60, 120, 180 minutes 0.1 ml aliquots were taken and transferred to Eppendorf tubes containing ice-cold 0.1 ml acetonitrile and 100 ng/ml internal standard to quench the reaction. The samples were centrifuged at 21.000 *g* (Eppendord,…). The supernatant were collected and transferred to HPLC insert-vials for further analysis on the LC –MS system. Positive and negative controls were included in each incubation mixture in order to validate the experimental setup. As a positive control, lidocaine was used. Lidocaine has a well-known metabolic profile and, in addition, structural similarities with the substrates to be studied in the present study.[13, 14] As negative control incubations, a mixture containing all the components of the experiments except the substrates and an incubation containing the substrates without the microsomes were included.

Semi quantitative analysis of compounds 3 and 4 and screening for metabolites

Semi-quantitative analysis of compounds **3** and **4** was performed by using LC-MS. Assuming similar analytical response for parent compounds and metabolic products, signal response areas relative to an internal standard were registered as a function of the parent compound. 2-(4-(*tert*-Butylphenyl)-4-(4-(2-fluoroethyl)piperazin-1-yl)-1H-benzo[d]imidazole was used as an internal standard at a concentration of 100 μg/ml. Calibration curves were constructed for the parent compounds (**3** and **4**) in a concentration range from 0.5 μg/ml to 8 μg/ml. Calibration standards were made in matrix and showed appropriate linearity in the range of concentrations studied, experiments were performed at least three times, with at least three injection each time. The linearity for compound **3** was calculated by the method of least square and found to be $R^2 = 0,9731$, y = 0,1929x + 0,1354, for compound **4** the linearity was calculated by the method of least square and found to be $R^2 = 0,9608$, y = 0,2072x + 0,1426.

HPLC-MS/MS

The rate of metabolism and metabolite identification were performed on a Waters (Millford, MA, USA) Xevo G2 Q-ToF mass spectrometer connected to a Waters Acquity UPLC I-class separation module. The separation was done on a Waters Acquity BEH C18 2.1x100 mm column with 1.7 μm particle size. The mobile phases consisted of A: water with 0.1% formic acid and B: acetonitrile with 0.1% formic acid.

The analysis was performed with gradient elution starting with 2% B with a linear increase to 95% B after 10 minutes. The flow rate was set to 0.6 ml/min, the injection volume was 5 μl, and the column temperature was set to 65 °C. For full scan analysis of all compounds the mass spectrometer had a capillary voltage of 600 V, the cone voltage was set to 30 V, the cone gas flow was set to 10 l/h and 130 °C and the desolvation gas flow was set to 800 l/h and 450 °C. Nitrogen from a Genius NM32LA nitrogen generator (Peak Scientific, Incinnan, Great Britain) was used as both cone and desolvation gas. The mass range was set to m/z 105 – m/z 1200 and the analysis was performed with positive electrospray ionization. Leucine-enkephaline with an m/z of 556.2771 was used as lockspray for increased mass accuracy. For MS/MS experiments for identification similar settings were used, but instead of full scan analysis the protonated molecular ion of each compound was set as precursor ion for fragmentation. The fragmentation was done by collision induced fragmentation with argon (Aga, Oslo, Norway) as collision gas, and a collision energy ramp of 20 to 40 eV was used for all compounds. Fragments were detected in the mass range m/z 50 – m/z 650. Identification of metabolites was done manually by considering normal phase 1 metabolism and by the software Metabolynx by Waters set to identification of phase 1 metabolites.

Autoradiography

Male Wistar Han IGS rats were purchased from Charles River (Germany). Rats were anesthetised using isoflurane (Induction 4%, Maintenance 2% in oxygen) and euthanized while still under anaesthesia with an overdose of pentobarbital (100 ml/kg) administered intraperitoneally. Whole brains of male Wistar rats were rapidly removed embedded in O.C.T. Tissuetek® (Sakura-Finetek, USA) and frozen by immersion in isopentane and liquid nitrogen. Organs were stored at -80°C until use. Coronal brain sections (−20°C, 20 μm thick) were prepared on a cryostat and thaw-mounted on Superfrost ® Plus glass slides (Carl Roth GmbH & Co. KG, Karlsruhe, Germany). Sections were allowed to thaw and dry at room temperature for 30 minutes. A DAKO DAB pen was used to delineate the area for drop incubation. The samples were pre-incubated with TMSA buffer (25mM Tris, 5mM $MgCl_2$, 32mM sucrose, 1% BSA, pH 7.4) for 30 minutes before incubation with compound 3 and 4 in different concentrations, ranging from 0 to 2mM for 60 minutes at room temperature in TMSA buffer (pH 7.4); washed once with TMSA buffer; and [125]I-[D-Trp6]-LHRH (0.1 nM) added in a drop fashion for further incubation (60 minutes at room temperature). The sections were then washed 4 times with ice cold TA buffer (25mM Tris, 1% BSA pH 7.4) and once in milliQ water. The samples were dried and exposed to a phosphor screen for 7 days at -20oC. The screens were scanned with Fujifilm BAS-5000 from FUJIFILM Life Science and analysed with Image J software.

RESULT AND DISCUSSION

Previously reported literature disclose the synthesis, radiolabelling and biological competitive binding assay for compound **1**, **2**, **3** and **4**.[2, 4] In brief, compounds **3** and **4** were synthesised in a 6 step synthesis with an overall yield of 1% for 3 and 7% for 4. As previously published [^{123}I]-3 gave 76% analytical radiochemical yield and [^{123}I]-4 11% analytical radiochemical yield. Serum stability of compound **3** and **4** was analysed by LC-MS, Table 1. The compounds were found to be stable, more than 84 % of the compounds remained after 120 minutes. After 22 hours more than 70% of the compounds remained, which indicates good stability in human and rat serum.

Table 1: Serum stability of 3 and 4 in human and rat serum.

Minutes	Compound 3 human serum[a]	Compound 4 Human serum[a]	Compound 3 Rat serum[a]	Compound 4 Rat serum[a]
0	100	100	100	100
30	97	109	101	98
60	107	99	94	92
120	103	106	98	81
1320	84	91	86	70

[a]Stability given as the mean of two experiments.

In addition to the serum stability analysis, a metabolic profile for compounds **3** and **4** (paper IV). MS/MS fragment ions of compounds **3** and **4** were identified by LC-MS/MS and are shown in Figure 2. The fragmentation of the metabolites was then identified based on the fragmentation of the parent compounds, and the structures were partly determined. MS/MS spectra with structural information of metabolites can be found in the supporting information. Molecular ions and main fragment ions of the metabolites are given in Table 2 and Table 3.
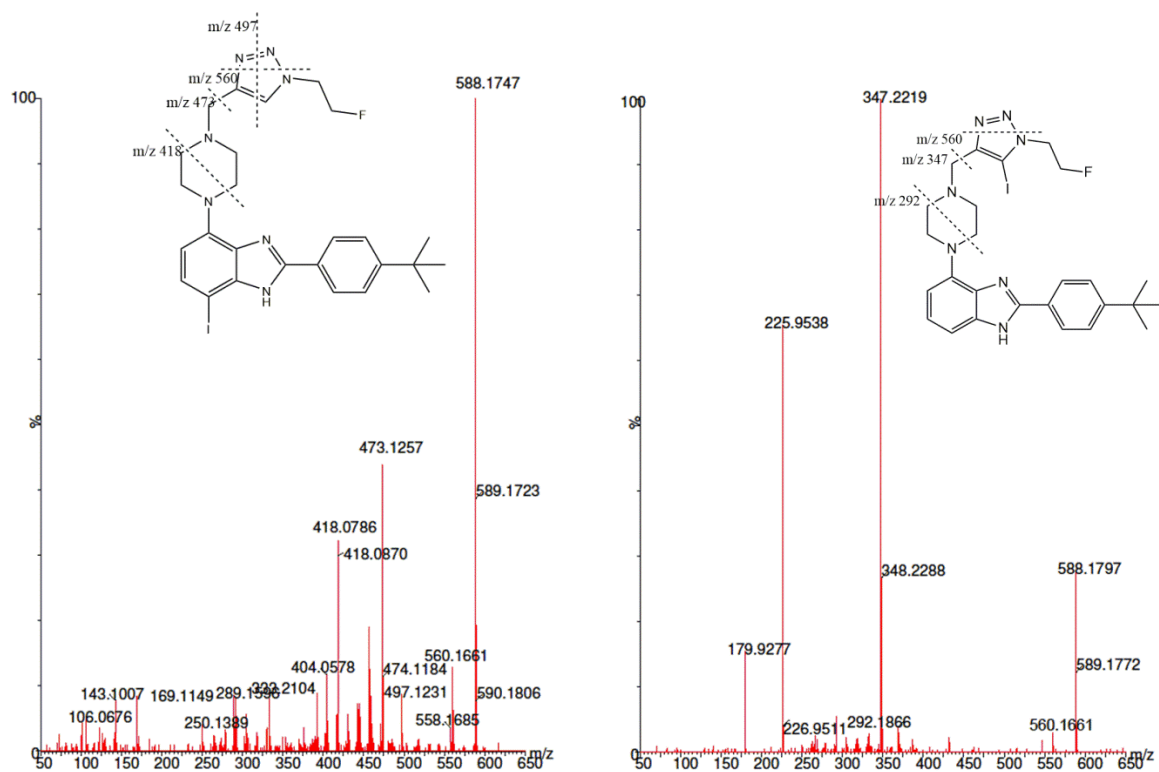
*Figure 2: Structural information obtained by LC-MS/MS. MS/MS spectrum of compound **3** to the left and compound **4** to the right. Major product ions are shown in the structures as mass to charge ratio (m/z).*

Major fragment ions for compound **3** were identified as *m/z* 560, 497, 473 and 418. The fragment ion *m/z* 560 is a loss of two nitrogen's, most likely from the triazole-ring. The *m/z* 497 fragment is probably due to a fragmentation of the triazole-ring where the fluoroethyl group in addition is lost, while the fragment m/z 473 is most likely loss of the entire triazole-ring including the fluoroethyl group. Signal m/z 418 is probably a fragmentation of the piperazine.

The metabolites from compound **3** were identified as M1 m/z 604 (hydroxylation), M2 m/z 578 (hydration and two demethylations), M3 m/z 584 (two sequential desaturations), M4 m/z 461 (loss of the fluoroethyl-group) and M5 m/z 477 (hydroxylation and loss of the fluoroethyl-group) as shown in Table 9.

M1 (m/z 604) shows a typical difference of 16 amu compared to compound **3** at m/z 588, which presumably is a hydroxylation. The MS/MS spectrum shows a fragment signal at m/z 576, equal to fragment m/z 560 of compound 3. The signal at m/z 489 and m/z 434 is equal to the signal at m/z 473 and m/z 418 of compound **3**. M2 (m/z 578) is 10 amu lower than for compound **3 at** m/z 588, most likely due to hydration and two demethylations. The fragment signals at m/z 461 and m/z and 434 is equal to m/z 473 and m/z 418 for compound **3**. The signal m/z 307 is equal to m/z 418 for compound 3, but with an additional loss of iodine on the benzimidazole. The signal at m/z 295 is equal to the

fragment m/z 418 for compound 3, however most likely with the additional loss iodine and 12 amu, which is probably a loss of a carbon nearby the nitrogen in the piperazine. Identification of the metabolites M3, M4 and M5 were identified by LC-MS analysis of the parent and fragment ions and additionally by the Metabolynx software (Waters).

Table 2: Compound 3 incubated with human liver microsomes. Structural information obtained by LC-MS and LC-MS/MS of metabolites.

Identity	Rt	[M+H]$^+$	Metabolite description	Major fragment ions (m/z)[a]
3	4.01	588	Parent	560, 497, **473,** 418,
M1	3.05	604	3 [+OH]	576, **489,** 434
M2	2.91	578	3 [+H_2O, -CH_2, -CH_2]	461, 434, 307, **295**
M3	3.82	584	3 [two sequential desaturations]	*
M4	3.79	461	3 [-$C_5H_6N_3F$]	*
M5	2.82	477	3 [+OH-$C_5H_6N_3F$]	*

*Unable to obtain reliable MS/MS data due to too low concentration. [a]In bold, diagnostic fragment ions.

There is a remarkable similarity between metabolism by rat and human liver microsomes for compound **3**, as shown in Figure 3. Notably, compound **3** is metabolised at a lower rate in human liver microsomes compared to rat liver microsomes. The maximum amount of M1 is produced within 15-30 minutes. In addition, M2 is produced at a lower rate in human- than in rat- liver microsomes. The metabolites M3-M5 are produced in minor amounts (Figure 3). Additionally, the half-life of compound **3** incubated in human liver microsomes was found to be 43 minutes and for rat liver microsomes 59 minutes.
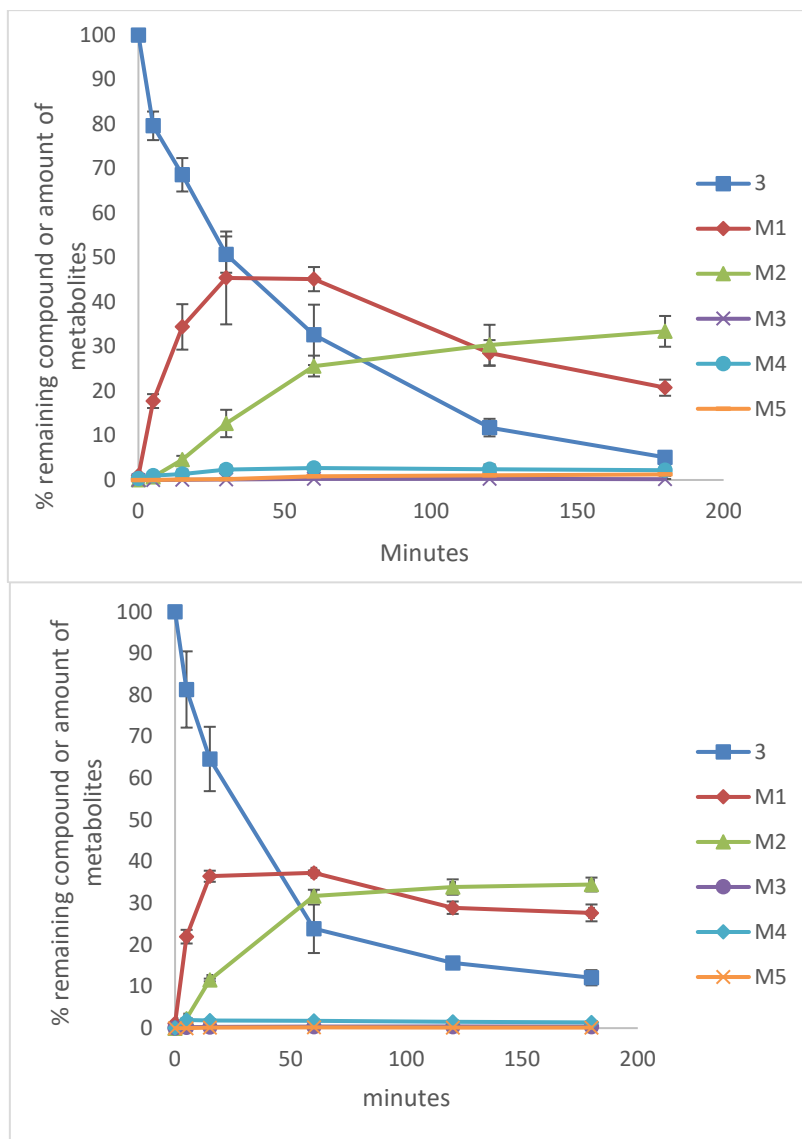
*Figure 3: Metabolic transformation of compound **3** with metabolites. Upper graph presents the compound incubated with human liver microsomes and the lower graph with rat liver microsomes. The experiment was performed as two independent experiments with four injections on LC MS-MS.*

The ion chromatograms for compound **3** and the metabolites M1-M6 are shown in Figure 4. The increase of the metabolites is seen at the selected time points 15 and 180 minutes for compound **3**.
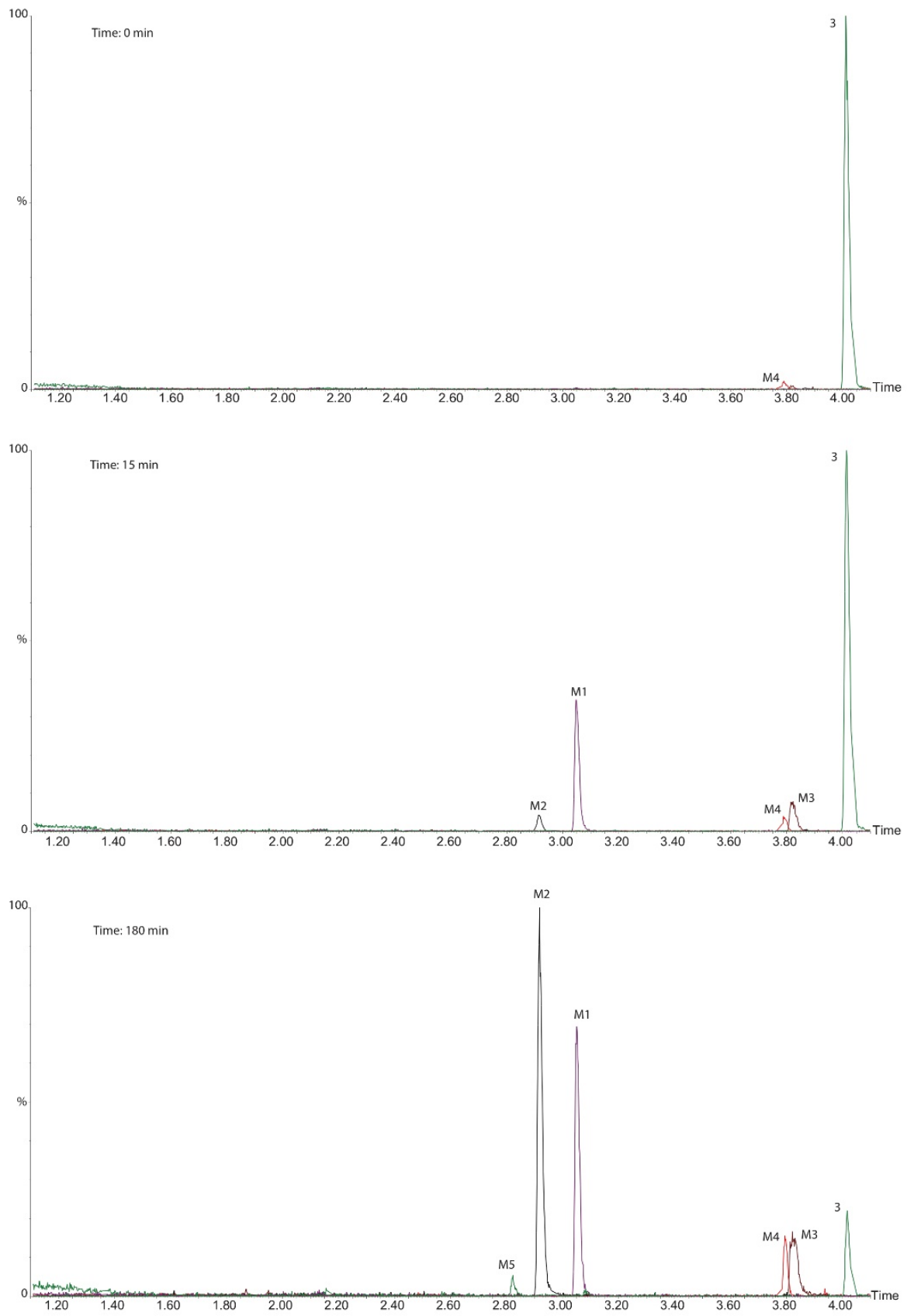
*Figure 4: Ion chromatograms for compound **3** and metabolites incubated with human liver microsomes at time points 0, 15 and 180 minutes.*

For compound **4** the fragmentation by LC-MS/MS revealed the major fragment ions as m/z 560, 347, 292, 226 and 180. Similarly as for compound **3**, the loss of two nitrogen's probably resulted in the fragment signal of m/z 560 from compound **4**. The m/z 347 fragment ion is most likely a loss of triazole with the fluoroethyl group in addition to the loss of iodine. The signal m/z 292 is possibly due to a cleavage of the piperazine. The m/z of 226 and 180 is most likely a fragmentation in the triazole, where the signal at m/z 226 indicates that the fluoroethyl group is still present.

The metabolites from compound **4** were identified as M1 m/z 604 (hydroxylation), M2 m/z 478 (hydroxylation and deiodination), M3 m/z 335 (loss of the triazole with the fluoroethyl group and iodine), M4 m/z 558 (hydroxylation and loss of the fluoroethyl group), M5 m/z 578 (hydration and demethylation), see Table 3.

M1 (m/z 604) shows a difference of 16 amu compared to compound **4**, which most likely is hydroxylation. Furthermore, fragment ions of M1 (m/z 604) corresponds to a large degree to the fragments of compound **4** (fragment m/z 363 corresponds to m/z 347, fragment m/z 308 corresponds to m/z 292, fragment m/z 226 corresponds to m/z 226 and fragment m/z 180 corresponds to m/z 180). M2 (m/z 478) is probably hydroxylated in addition to a deiodination. The fragment ions of M2 corresponds to a large degree on the fragments of compound **4** (fragment m/z 363 corresponds to m/z 347, fragment m/z 308 corresponds to m/z 292). In addition, signals m/z 226 and m/z 180 are missing, which most likely makes iodine on the triazole important for the fragmentation, and when the iodine is missing these fragments are also missing. M3 (m/z 335) is most likely the loss of the triazole with the fluoroethyl group and the iodine. The fragment ions for M3 also corresponds to a large degree to the fragments for compound **4** (fragment m/z 292 corresponds to m/z 292, fragment m/z 277 and m/z 262 corresponds to m/z 292, most likely due to the loss of one CH_2-group and subsequently another CH_2-group. In addition the signals m/z 226 and m/z 180 is missing here as well, again indicating the importance of the iodine on the triazole for the fragmentation. M4 (m/z 558) is probably a hydroxylation with the loss of the fluoroethyl group at the triazole. Additionally, the fragment ions for M4 (m/z 558) corresponds to a large degree on the fragments for compound **4** (Fragment m/z 402 corresponds to m/z 560 for compound **4** with the additional loss of iodine, fragment m/z 351 corresponds to 347, however with the additional loss of a carbon, m/z 308 corresponds to m/z 292, fragment m/z 277 corresponds to m/z 292, most likely due to the loss of one CH_2-group). The signal for M5 (m/z 578) is most likely hydration and two demethylations. As for the other metabolites the fragment ions for M5 (m/z 578) corresponds to a large degree to the fragment ions for compound 4 (signal m/z 337 corresponds m/z 347, m/z 308 corresponds to m/z 292, m/z 226 corresponds to m/z 226 and m/z 180 corresponds to m/z 180). M6 (m/z 542 is probably a fragmentation of the fluoroethyl group. The fragment ions for this metabolite also corresponds to a large degree to the fragment ions

for compound **4** (The m/z 386 is probably the loss of iodine and two nitrogen's. The m/z 335 corresponds to m/z 347 with the additional loss of a carbon, signal m/z 292 corresponds to m/z 292. The m/z 278 and m/z 266 corresponds to m/z 292 (difference of 12 amu) is most likely due to a fragmentation on the piperazine where only a nitrogen is left for m/z 266).

Table 3: Compound 4 incubated with human liver microsomes. Structural information obtained by LC-MS and LC-MS/MS of metabolites in human microsomes.

Identity	Rt	[M+H]$^+$	Metabolite description	Major fragment ions (m/z)[a]
4	3.17	588	Parent	560, **347,** 292, 226, 180
M1	2.26	604	4 [+OH]	**363**, 308, 226, 180
M2	1.98	478	4 [+OH-I+H]	363, **308,**
M3	2.52	335	4 [-C$_5$H$_5$N$_3$FI]	**292**, 277, 262,
M4	2.16	558	4 [+OH-C$_2$H$_3$F]	**402**, 351, 308, 277
M5	2.08	578	4 [+H$_2$O-CH$_2$-CH$_2$]	**337**, 308, 226, 180
M6	3.07	542	4 [-C$_2$H$_3$F]	386, **335**, 292, 278, 266

[a]In bold, diagnostic fragment ions

The metabolism is slower in rat liver microsomes than in humans liver microsomes for compound **4,** Figure 5. The main metabolites are M1, M2 and M4. More M1 is formed than M2 and M4 in human liver microsomes. The minor metabolites in human microsomes were M3, M5 and M6. In rat liver microsomes more M1 is formed compared to M2. The minor metabolites in rat liver microsomes are M3-M6. Additionally, the half-life for compound **4** incubated in human liver microsomes was found to be 64 minutes and for rat liver microsomes 224 minutes.
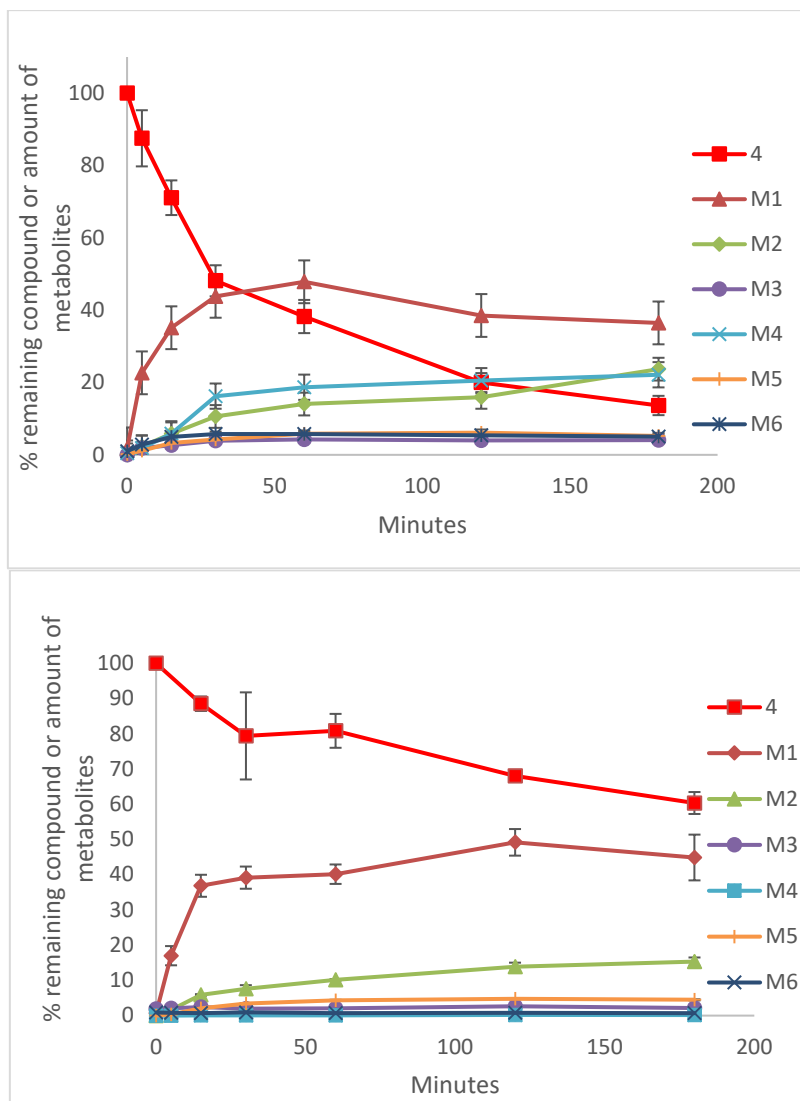
Figure 5: Metabolic transformation of compounds *3* and *4* *incubated with rat liver microsomes. The results are from two different experiments with four injections on LC MS-MS.*

The ion chromatograms for compound **4** and the metabolites M1-M6 are shown in Figure 6. The increase in the metabolites are seen at the selected time points 15 and 180 minutes for compound **4**.
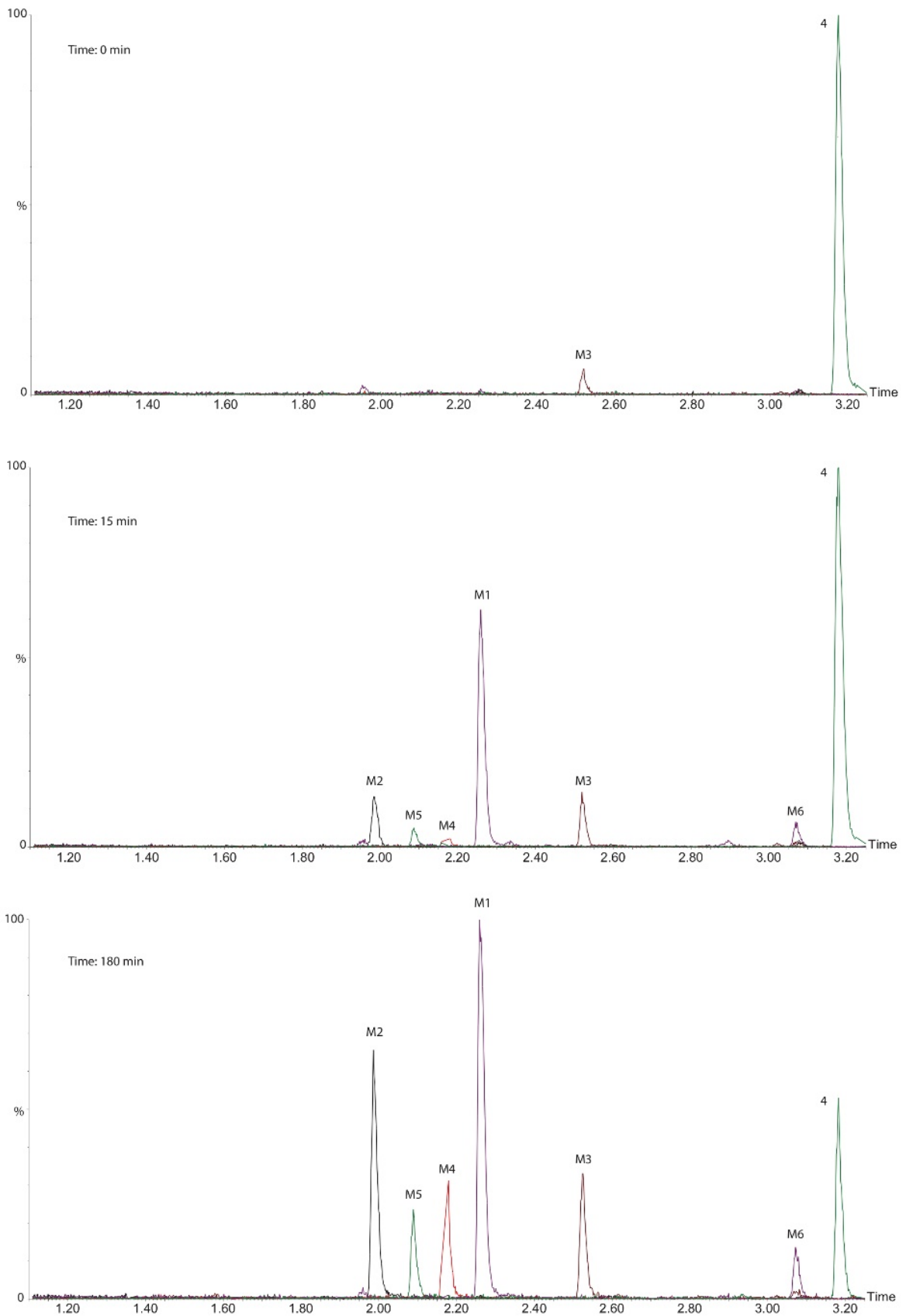
*Figure 6: Ion chromatogram for compound **4** incubated with human liver microsomes at time points 0, 15 and 180 minutes.*

The metabolic profile identified five metabolites for compound **3** and six metabolites for compound **4**. In the light of the metabolic profile, the metabolism for compounds **3** and **4** both in rat- and human-liver microsomes were found suitable as imaging agent in human and rat. The metabolic half-life were found to be 43 minutes (human liver microsomes) and 59 minutes (rat liver microsomes) for compound 3. The half-life for compound **4** incubated in human liver microsomes was found to be 64 minutes and for rat liver microsomes 224 minutes. For compound **3** and **4**, the half-life is more than sufficient enough for imaging agents.

Additionally, the potential for compounds **3** and **4** to bind to GnRH-R in rat brains were performed in paper IV. Initially, we designed an indirect autoradiography study of binding to rat brain sections. Which means that the competitive agonist [^{125}I]-[D-Trp6]-LH-RH were incubated with the GnRH-R first and then compounds **3** and **4** were incubated with the GnRH-R so that they could compete for the binding to the GnRH-R. The images show the bound [^{125}I]-[D-Trp6]-LH-RH in competition with compounds **3** and **4**. Compound **3** showed a decrease in signalling when increasing amounts (from 0.1 nM to 100 mM) of compound **3** were added, Figure 7. There is a clear diminution of the activity; not even at concentration of 100 mM compound **3** is able to inhibit totally the binding of the hormone. Compound **4** shows a decrease in signalling when increasing amounts of compound **4** were added. Compound **4** shows a stronger inhibition of the binding of the hormone to the brain sections already at a concentration of 1 nM of and almost no activity when in competition with 10 mM. This is in consistency with our competitive binding assay where compound **3** have a K_i of 82 nM and compound 4 a K_i of 12.9 nM.
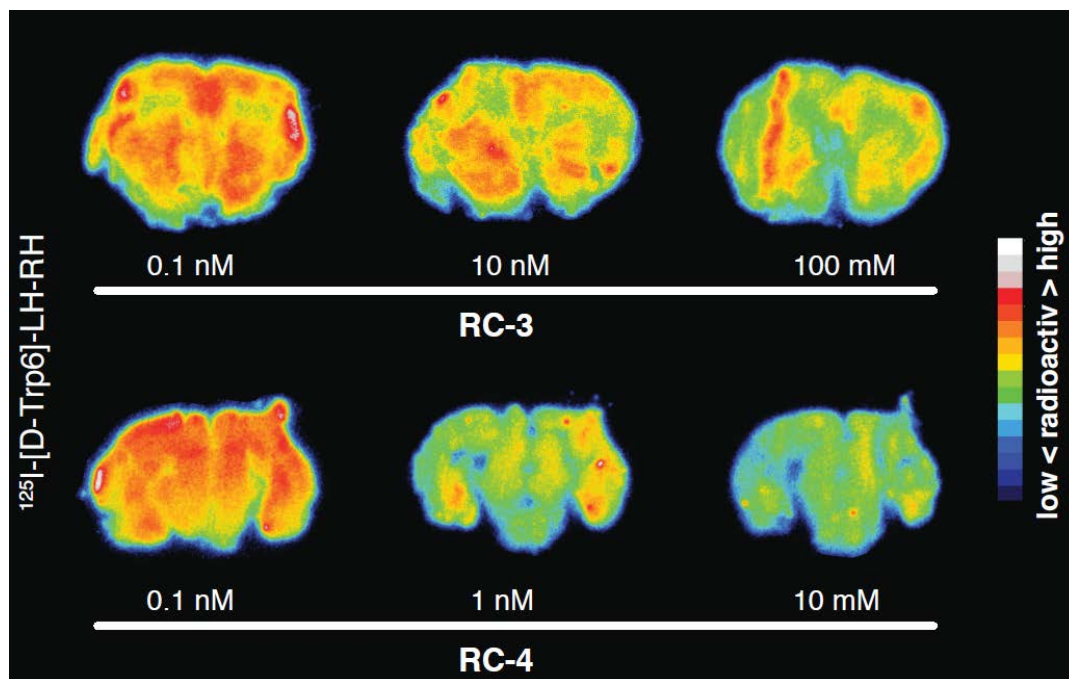
Figure 7: Example of initial autoradiography showing the competition of compounds 3 and 4 against the competitive agonist ^{125}I[D-Trp6]-LH-RH, n=3.

To confirm our results in the indirect autoradiography study of compounds **3** and **4** we radiolabeled compound **4** with ^{123}I as previously described (paper II) and performed an direct autoradiography study in rat brain sections, Figure 8. By directly labelling the **4** with ^{123}I we were able to visualize the binding in the rat brain region.
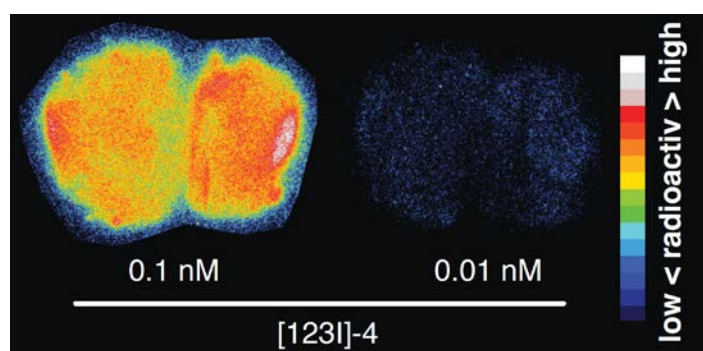

Figure 8: Autoradiography of [123I-1 in rat brain, n=1.

CONCLUSIONS

Compounds **3** and **4** were evaluated *in vitro* for assessment into preclinical studies. The serum stability in rat and human serum showed stable compounds. More than 70 % of the compounds remained in rat- and human- serum for 22 hours. The thoroughly analysis of the phase 1 metabolism for **3** and **4** showed a metabolic half-life more than sufficient enough for the use as imaging agents**,** which is in compliance with the serum stability analysis. In addition, five metabolites were identified and quantified for compound 3 and six metabolites were identified and quantified for compound 4. Additionally we have performed autoradiography indirect and direct to prove our concept where **3** and **4** shows binding to rat GnRH-R in brain regions. *In vivo* characterization by SPECT imaging, pharmacokinetics and biodistribution studies are underway. Furthermore, ^{18}F labeling are in progress in our laboratory.

CONFLICT OF INTEREST

The authors declare no conflict of interest

SUPPORTING INFORMATION

Supporting information is available as electronic supporting information

REFERENCE

1.	R. Sharma and E. Aboagye, *British Journal of Pharmacology*, 2011, **163**, 1565-1585.
2.	R. Fjellaksel, M. Boomgaren, R. Sundset, I. H. Haraldsen, J. H. Hansen and P. J. Riss, *MedChemComm*, 2017, **8**, 1965-1969.
3.	R. Fjellaksel, D. Dugalic, T. B. Demissie, P. J. Riss, O.-K. Hjelstuen, R. Sundset and J. H. Hansen, *Journal of Physical Organic Chemistry*, 2018, DOI: 10.1002/poc.3835, e3835-n/a.
4.	R. Fjellaksel, R. Sundset, J. H. Hansen and P. J. Riss, *Synlett, Accepted 16 March* 2018.
5.	R. Maggi, *MOJ Anat & Physiol*, 2016, **2**.
6.	M. T. Hierowski, A. Perla, T. W. Redding and A. V. Schally, *FEBS Letters*, 1983, **154**, 92-96.
7.	G. Emons, G. S. Pahwa, C. Brack, R. Sturm, F. Oberheuser and R. Knuppen, *European Journal of Cancer and Clinical Oncology*, 1989, **25**, 215-221.

8.   C. H. Chien, C. H. Chen, C. Y. Lee, T. C. Chang, R. J. Chen and S. N. Chow, *International journal of gynecological cancer : official journal of the International Gynecological Cancer Society*, 2004, **14**, 451-458.

9.   T. Moriya, T. Suzuki, M. Pilichowska, N. Ariga, N. Kimura, N. Ouchi, H. Nagura and H. Sasano, *Pathology International*, 2001, **51**, 333-337.

10.   D. C. Skinner, A. J. Albertson, A. Navratil, A. Smith, M. Mignot, H. Talbott and N. Scanlan-Blake, *Journal of neuroendocrinology*, 2009, **21**, 282-292.

11.   J. C. Pelletier, M. V. Chengalvala, J. E. Cottom, I. B. Feingold, D. M. Green, D. B. Hauze, C. A. Huselton, J. W. Jetter, G. S. Kopf, J. T. Lundquist, R. L. Magolda, C. W. Mann, J. F. Mehlmann, J. F. Rogers, L. K. Shanno, W. R. Adams, C. O. Tio and J. E. Wrobel, *Journal of medicinal chemistry*, 2009, **52**, 2148-2152.

12.   A. Moldes-Anaya, A. L. Wilkins, T. Rundberget and C. K. Fæste, *Drug and Chemical Toxicology*, 2009, **32**, 26-37.

13.   T. Hansen, M. K. Moe, T. Anderssen and M. B. Strøm, *European Journal of Drug Metabolism and Pharmacokinetics*, 2012, **37**, 191-201.

14.   J. Hermansson, H. Glaumann, B. Karlén and C. von Bahr, *Acta Pharmacologica et Toxicologica*, 1980, **47**, 49-52.

Supporting information

In vitro evaluation two promising bioactive triazole-benzimidazole GnRH Receptor-antagonists as possible SPECT radiotracers

Richard Fjellaksel,[a-e] Angel Moldes-Anaya,[e] Ana Oteiza,[d,e] Montserrat Martin-Armas,[d,e] Terje Vasskog,[f] Patrick J. Riss,[g-i] Ole-Kristian Hjelstuen,[b] Jørn H. Hansen,[c] and Rune Sundset [a,d,e]

[a]*Medical Imaging Research Group, Department of Clinical Medicine, UiT The Arctic University of Norway, 9037 Tromsø, Norway.*

[b]*Drug Transport and Delivery Research Group, Department of Pharmacy, UiT The Arctic University of Norway, 9037 Tromsø, Norway.*

[c]*Organic Chemistry Research Group, Department of Chemistry, UiT The Arctic University of Norway, 9037 Tromsø, Norway.*

[d]*Preclinical PET/SPECT/CT, Department of Clinical Medicine, Department of Pharmacy, UiT The Arctic University of Norway, 9037*

[e]*Research and Development unit, PET imaging center, UNN – University Hospital of North-Norway, 9037 Tromsø, Norway.*

[f]*Natural Products and Medicinal Chemistry Research group, UiT The Arctic University of Norway, 9037 Tromsø, Norway.*

[g]*Department of neuropsychiatry and psychosomatic medicine, Oslo University Hospital, Oslo, Norway.*

[h]*Realomics SFI, Department of Chemistry, University of Oslo, PO BOX 1033, Oslo 0371, Norway.*

[i]*Norsk Medisinsk Syklotronsenter AS, Postboks 4950   Nydalen,   0424 Oslo*

Serum stability analysis by LC-MS

Injection volume 2.0ml. Program

A: 0.1% formic acid in water
B: 0.1% formic acid in acetonitrile
Flow 500 ul/min

Time	%A	%B
0.00	95	5
0.50	95	5
7.00	5	95
8.00	5	95
8.01	95	5
10.00	95	5

MS:
Full scan, positive mode m/z 400-620. Resolution 15000. Microscans 1. Max inject time 250 ms. Sheath gas. Flow 70. Aux gas Flow 10. Sweep Gas Flow 10. Spray Voltage 4.50 kV. Capillary Temp 330°C. Capillary voltage. 37 V. Tube Lens 80V

Figure S1: 588 compound 3

Figure S1: M1

3
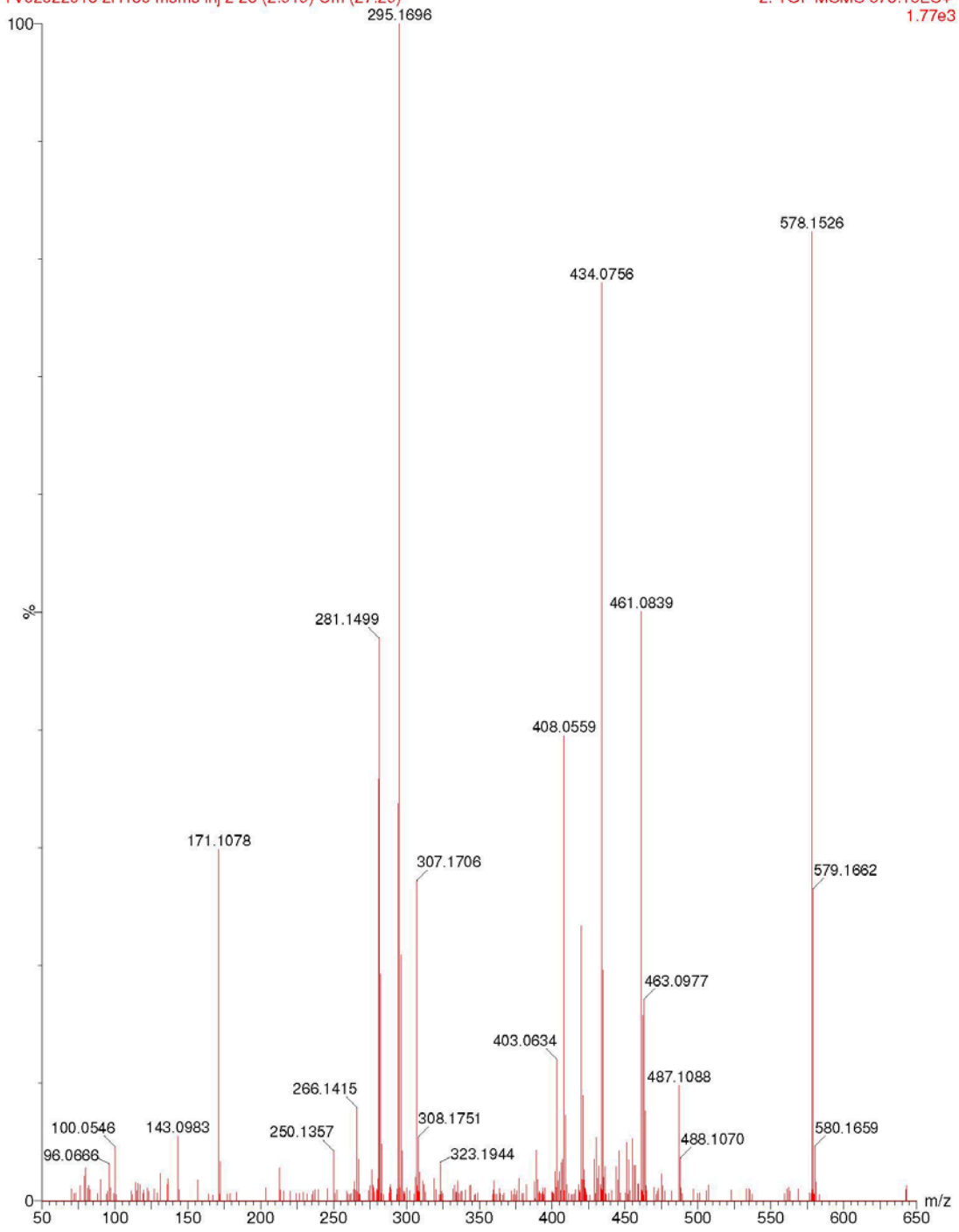
Figure S1: M2

Figure S1: M3

Figure S1: M4

Figure S1: M5

Figure S1: m/z 588 compound 4
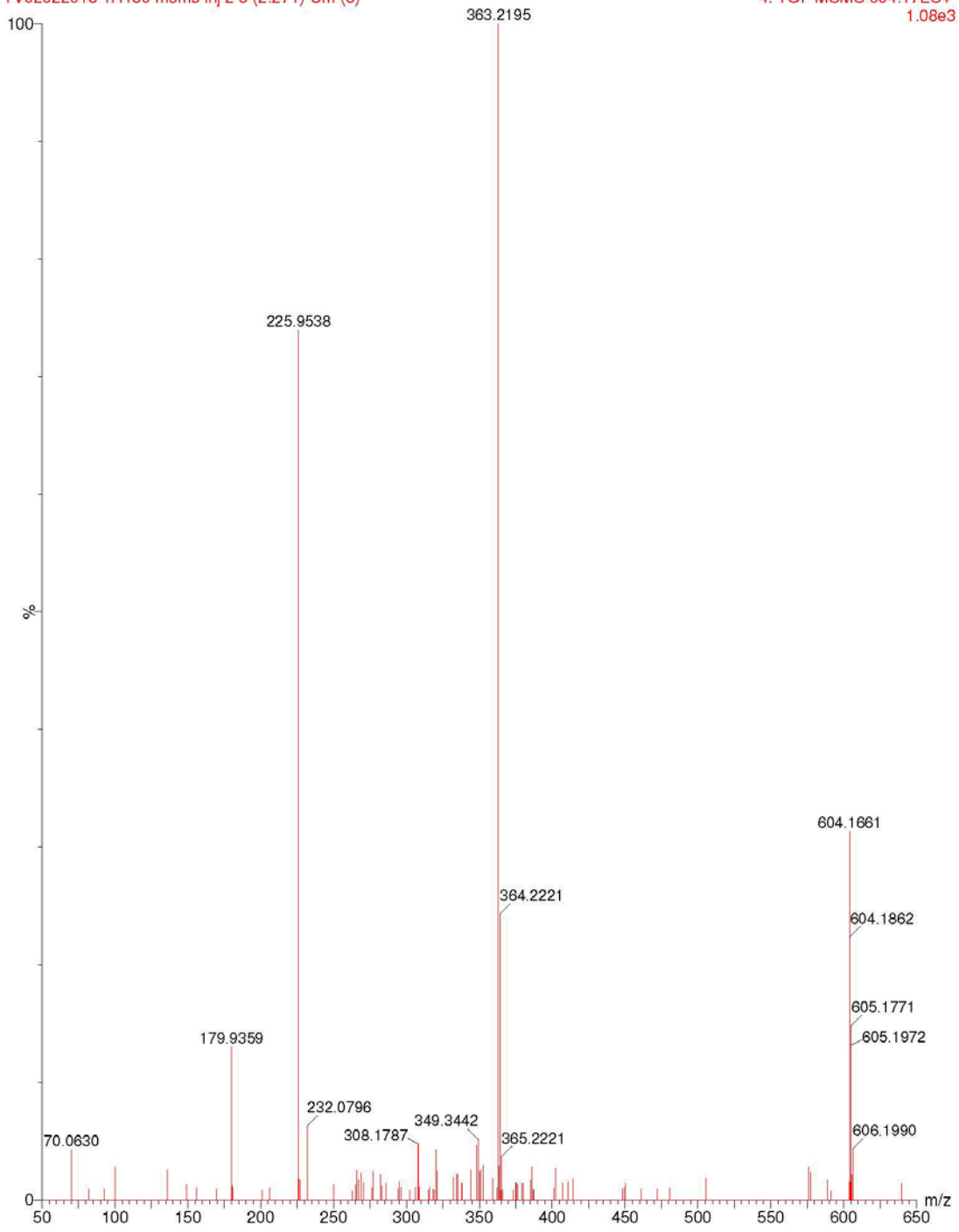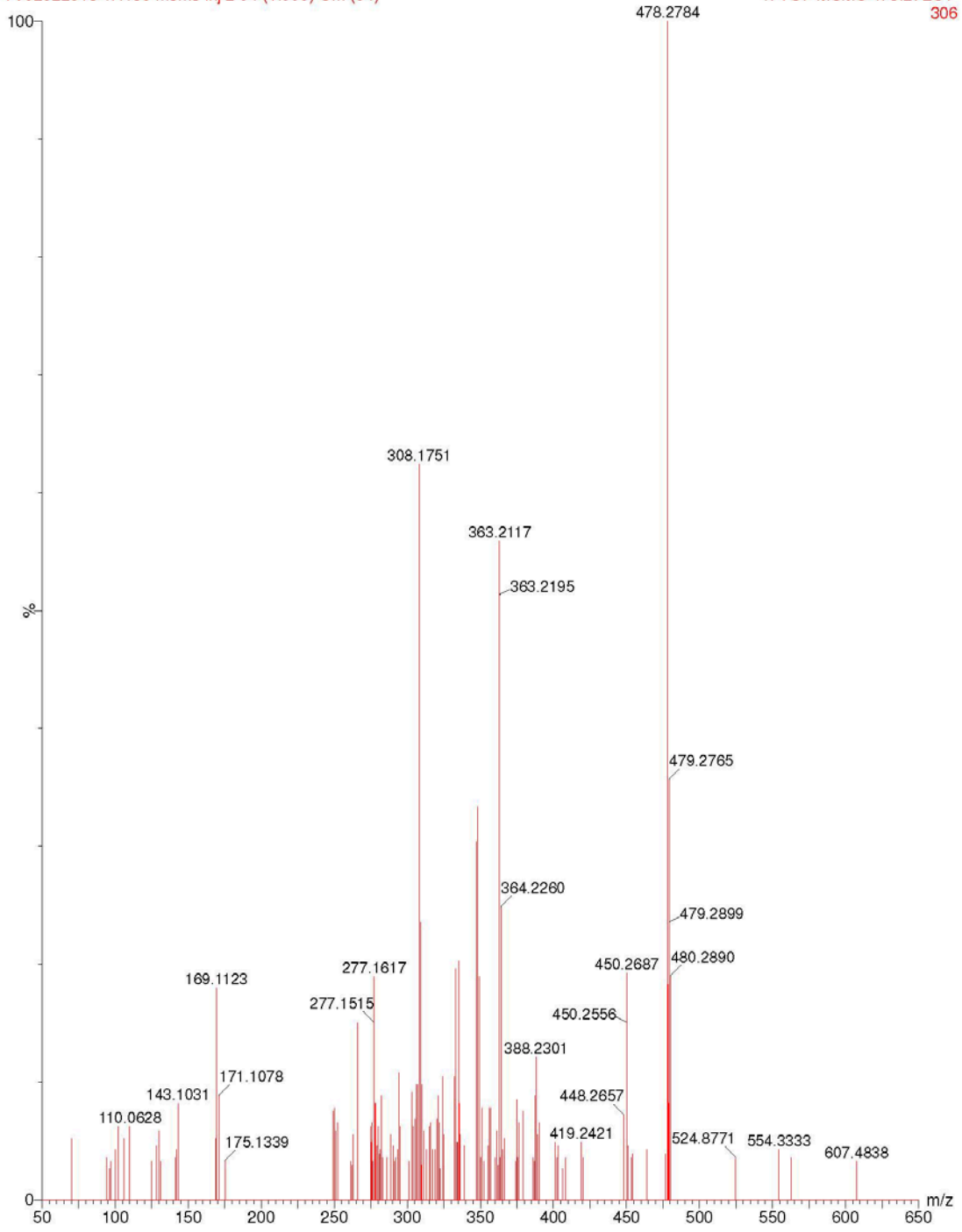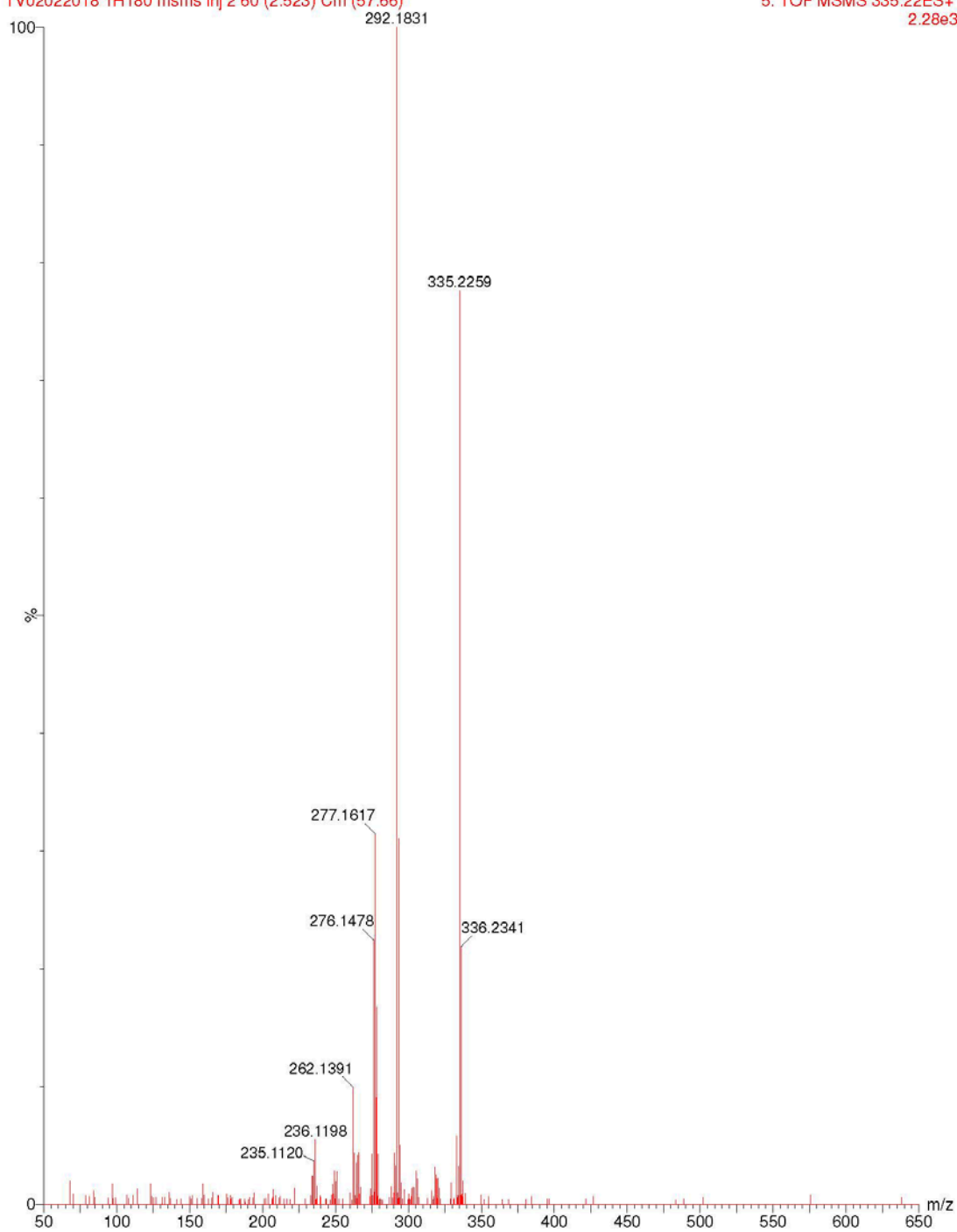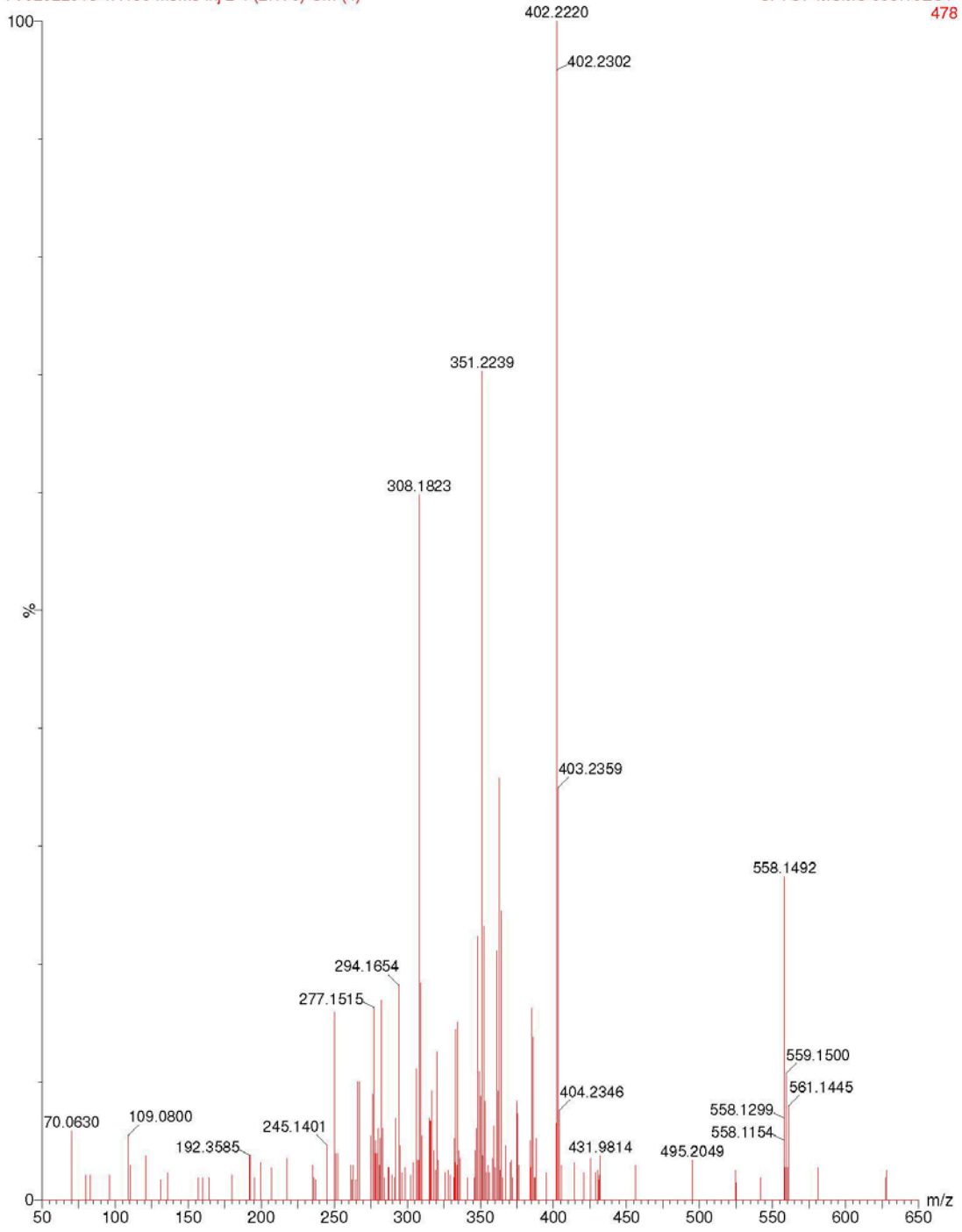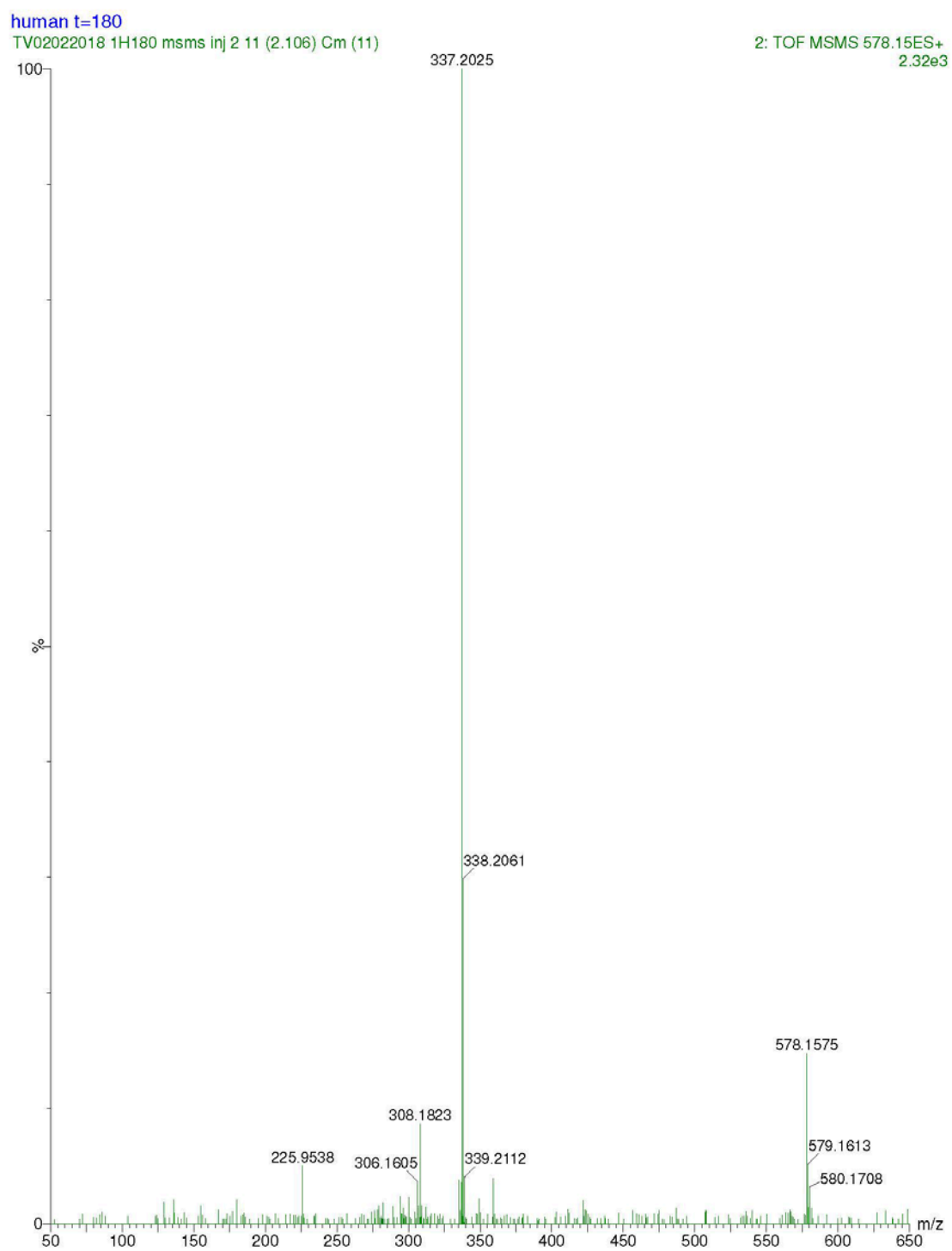
Figure S1: M1

Figure S1: M2

Figure S1: M3

Figure S1: M4
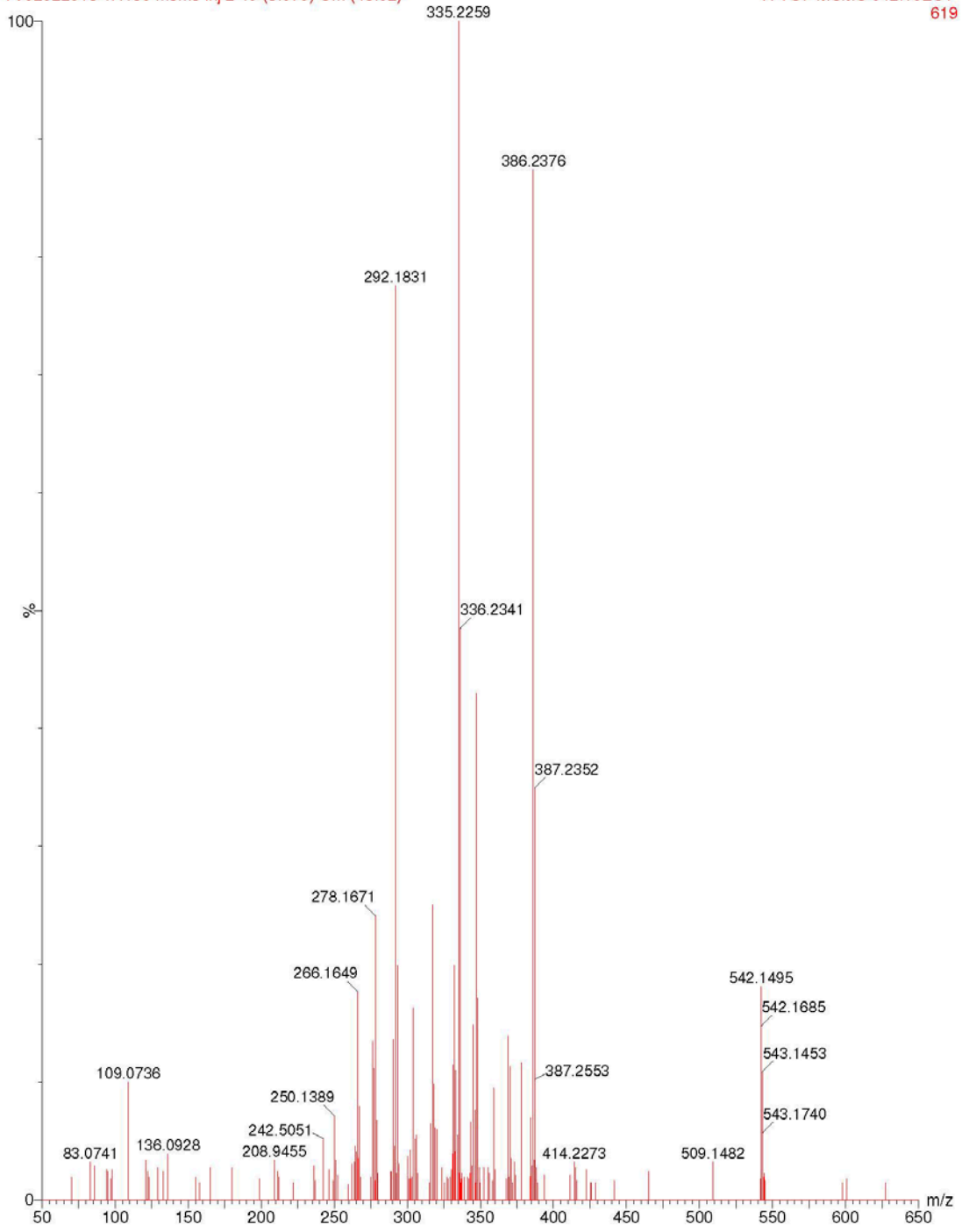
Figure S1: M5

Figure S1: M6

The metabolism of lidocaine used as a positive control (rat liver microsome)
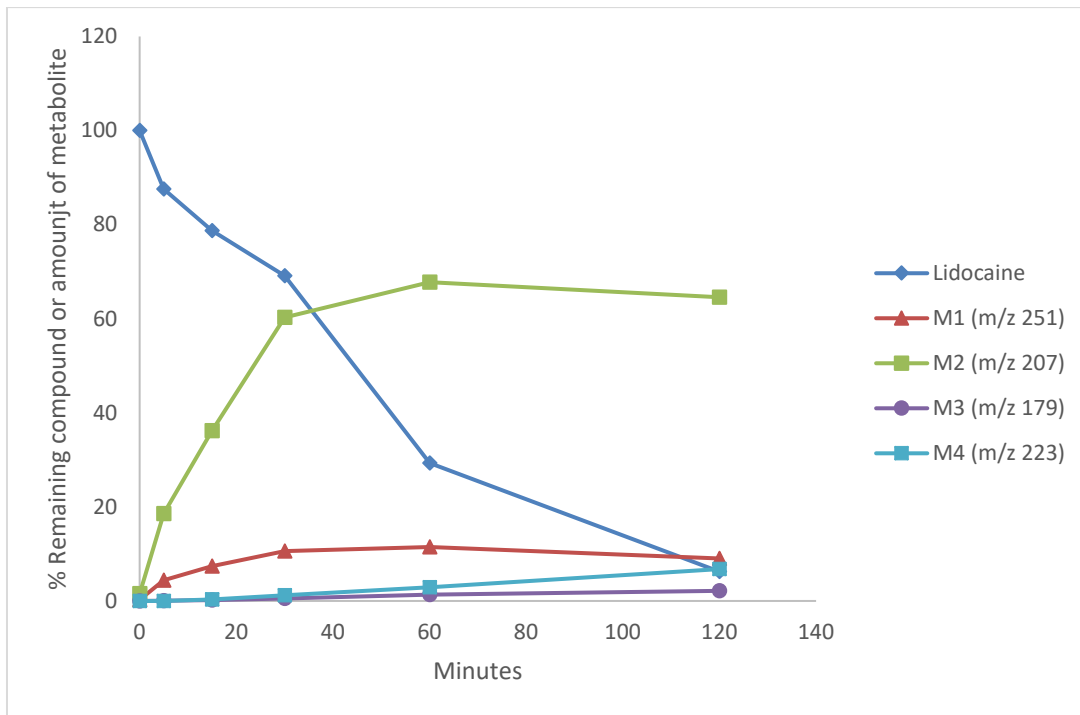
PAPER V

First *in vivo* evaluation of a potential SPECT brain radiotracer for the gonadotropin releasing hormone receptor based upon the piperazinyl-benzimidazole class of compounds.

Richard Fjellaksel, Ana Oteiza, Montserrat Martin-Armas, Patrick J. Riss, Ole K. Hjelstuen, Samuel Kuttner, Jørn H. Hansen and Rune Sundset.

Manuscript

First *in vivo* evaluation of a potential SPECT brain radiotracer for the gonadotropin releasing hormone receptor based upon the chemical piperazinyl-bemzimidazole class of compounds.

Richard Fjellaksel,[a-e] Ana Oteiza,[d,e] Montserrat Martin-Armas,[d,e] Patrick J. Riss,[f-h] Ole Kristian Hjelstuen,[b] Samuel Kuttner,[a,e] Jørn H. Hansen[c] and Rune Sundset [a,d,e]

[a]*Medical Imaging Research Group, Department of Clinical Medicine, UiT The Arctic University of Norway, 9037 Tromsø, Norway.*

[b]*Drug Transport and Delivery Research Group, Department of Pharmacy, UiT The Arctic University of Norway, 9037 Tromsø, Norway.*

[c]*Organic Chemistry Research Group, Department of Chemistry, UiT The Arctic University of Norway, 9037 Tromsø, Norway.*

[d]*Preclinical PET core facility, Department of Clinical Medicine, UiT The Arctic University of Norway, 9037 Tromsø, Norway.*

[e]*Research and Development unit, PET imaging center, University Hospital of North-Norway, 9038 Tromsø, Norway.*

[f]*Department of neuropsychiatry and psychosomatic medicine, Oslo University Hospital, Oslo, Norway.*

[g]*Realomics SFI, Department of Chemistry, University of Oslo, PO BOX 1033, Oslo 0371, Norway.*

[h]*Norsk Medisinsk Syklotronsenter AS, Postboks 4950 Nydalen, 0424 Oslo*

ABSTRACT

We have used a simple, robust high yielding radiolabeling procedure to radiolabel the α-halogenated compound 1-(4-(2-(4-tert-butylphenyl)-1H-benzo[d]imidazol-4-yl) piperazin-1-yl)-2-iodoethanone. The compound was selected because of its high radiochemical yield. Initially, this reactive compound was considered to be too unstable in physiologic conditions and was not evaluated for *in vitro* and *in vivo* testing. However, literature findings showed similar α-halogenated compounds suitable for *in vivo* evaluations. Furthermore, LC-MS analysis in saline, human and rat serum resulted in 46%, 52% and 44% stability after incubation for 1 hour respectively. The stability and literature findings made further *in vivo* investigations necessary. The compound were found to possess nM affinity for the GnRH-R in a competition dependent inhibition study. In addition rat brain single photon emission tomography imaging and biodistribution studies gave further insight in the nature of the compound as a radiotracer.

INTRODUCTION

Disturbance of gonadotropin releasing hormone (GnRH) signaling is implied in a variety of human diseases spanning from reproductive diseases, hormone dependent oncological diseases and neurodegenerative diseases. GnRH receptors (GnRH-R) play a central role in this context and have consequently attracted considerable interest as therapeutic targets[1-2].

The neurohormone GnRH has its main action in the hypothalamic-pituitary-gonadal axis (HPG-axis). GnRH is released in a pulsatile manner stimulating two other gonadotropins in the anterior pituitary gland, follicle stimulation hormone and luteinizing hormone. The release of these gonadotropins acts in the gonads to produce androgens and estrogens.[3] In addition, the GnRH-R localization in mammals outside the HPG-axis is well documented. Several areas of the central nervous system (CNS) have been shown to express GnRH-R: Retina, olfactory bulb, cortex (especially piriform cortex), lateral septum, preoptic area, arcuate nucleus, hippocampus, amygdala, central grey, cerebellum and spinal cord.[4] Besides the CNS, the GnRH-R is also expressed in other sites, such as: kidney, liver and heart.[4]

Novel single photon emission computed tomography (SPECT) and positron emission tomography (PET) radiotracers for imaging are of high importance in diagnostic medicine. This is linked to the necessity of advances in radiochemistry and radiobiology development.[5] The aim of the present study was to develop a GnRH-R SPECT radiotracer to allow for non-invasive quantification of GnRH-R in brain *in vivo*.

We have previously disclosed the discovery of gonadotropin releasing hormone (GnRH) receptor antagonists and a thorough mechanistic analysis of halogen exchange by the use of anchimeric assistance for amide groups. In addition, 1-(4-(2-(4-tert-butylphenyl)-1H-benzo[d]imidazol-4-yl) piperazin-1-yl)-2-iodoethanone (compound 1) has been radiolabeled in high radiochemical yield (figure 1).[6-7] Consequently, compound 1 was selected for further evaluation. α-halogenated molecules are widely used in organic chemistry, medicinal chemistry and radiochemistry as prosthetic groups and for further diversification of lead molecules.[8-9] However, little is published for α-halogenated amides as possible radiotracers. A possible explanation may be due to the natural high reactivity of α-halogenated amides.[10] Nevertheless, Legros et al investigated the molecular pharmacology of melatonin receptors with alpha halogenated amides. The reported compounds SD6 and S70254 contain an α-iodide next to an amide group. SD6 and S70254 were ^{125}I-labeled and their receptor specificity evaluated by cell membrane binding assays, tissue membrane saturation assays and *in vitro* autoradiography of

brain and retina from rat and sheep. [^{125}I]- S70254 can be used with both cells and tissue in addition to autoradiography. Legros et al describes for the first time radiolabeled tools that are specific for one of the melatonin receptors (MT$_2$). These tools are amenable to binding experiments and to autoradiography using sheep and rat tissues. Furthermore, these specific tools will permit better understanding of the role and implication in physiophatologic processes of the melatonin receptors.[11-12]

In light of this promising literature reference, our focus turned to a further evaluation of compound 1 as a potential candidate for *in vivo* imaging studies despite its α-halogenated properties. ^{123}I-labeling was achieved for compound 1 in 80% analytical radiochemical yield.[6] However, compound 1 stability in rat and human serum is a prerequisite for further investigation. To evaluate the biological properties, the compound biodistribution in rat was studied. Furthermore, SPECT analyses were performed for evaluation of the imaging abilities of [^{123}I]-compound-1.

MATERIALS AND METHODS

Reagents and materials

All solvents and reagents were obtained from Sigma Aldrich (Sigma-Aldrich Norway AS) except Na^{123}I (GE Healthcare, Netherland). Rat and human serum were kindly donated by the Vascular Biology research group at UiT Arctic university of Norway. The semi-preparative radio-HPLC consists of a DIONEX HPLC system, HPLC pump P680 with a PDA.detector (PDA-100) with XBridge® prep C18 5µm OBD^{tm} 19x250nm column and a radioactivity flow detector for HPLC LB 509 (Berthold technologies, Germany). The LC-MS is a Thermo, scientific LTQ Orbitrap XL, ESI-ionmax (Germany).

Animals

Male Wistar Han IGS rats of 6-9 weeks age were purchased from Charles River (Germany). The animals were housed in the Department of Comparative Medicine at UiT- The Artic University of Norway. The animals were fed standard chow (Scanbur, BK, Nyttedal, Norway) *ad libitum*. All experimental protocols were approved by The Norwegian Food Safety Authority and conducted in accordance to the Norwegian law, FOR-2017-04-05-451.

Chemical synthesis and ^{123}I labeling

The key intermediate 1a and compound 1 was prepared according to literature procedures (figure 1).[6-7] In brief, Na^{123}I (specific activity of 4.2 pmol ^{123}I-Iodide per ml) was prepared in a concentration step over 4 hours evaporating the solvent. Na^{123}I reacted with 1a in acetone for 1 hours in reflux. The fractions were collected and the solvents evaporated. Products was confirmed by radio-HPLC. The radiolabelling experiments where repeated in n>6 times.

Saline and serum stability

The stability of compound 1 was initially investigated in saline. Compound 1 (50 ul, 4 mM) was dissolved in ethanol:Polysorbate 80:water (5:5:90) then incubated with 300µl 0.9% NaCl at ambient temperature. Aliquots were taken at 0, 60, 120 and 1560 minutes, then analysed by LC-MS. Furthermore, compound 1 was investigated in human and rat serum. Compound 1 (50 ul 4 mM) in ethanol:Polysorbate 80:water (5:5:90) was incubated with 400 µl human and 300 µl rat serum at 37ºC. An aliquot (40-50 µl) from previous mixtures was extracted with ice-cold acetonitrile at 0, 10, 30, 60, 120, 240 and 1320 minutes post-incubation. Samples were centrifuged at 13000 rpm for 5 minutes. The supernatants were analysed by LC-MS. Serum experiments were performed in triplicate.

Competitive binding studies

HEK293T (a division arrested cell line, Multispan Inc, USA) cells stably expressing GnRH receptors were used to measure the inhibition of competitive binding for LHRH/GnRH by a fluorescence based FLIPR assay.[13] Compound 1 was tested in concentrations from 50 µM to 0.5 nM with 5 nM LHRH agonist as competitor. The commercially available compound WAY207024 was included as a reference compound since it has a known affinity for the GnRH-R. Buserelin was used as a negative control.

SPECT imaging

Rats were anesthetised using isoflurane (Induction 4%, Maintenance 2%, 100% Oxygen). One group of rat were injected iv with [^{123}I]-compound 1 (ID 1.67 MBq ± 0.28 SD). Another group were injected with i.p. (ID 4.12 MBq ± 0.56 SD). A third group of animals was iv injected with Na^{123}I (ID 1.53 MBq ± 0.37 SD).

While constantly kept under anesthesia, the rats were positioned with the brain in the center of the field of view inside a 4 detector configuration Triumph^{TM} II X-SPECT® small animal

PET/SPECT/CT scanner (Trifoil Imaging, Northridge Tri-Modality Imaging, Inc., Chatsworth, CA). Heart rate and breathing was monitored with sensors inside a closed animal cell (Equipment Veterinaire Minerve, Esternay) and the temperature on the heated air flow inside the cell was set to 35°C to prevent hypothermia.

Dynamic SPECT acquisitions for 30 and 60 min with 6-12 image frames, each 5 min long were taken for the animals which were used for 1h and 2h biodistribution studies respectively. The animals subjected to 5 hours accumulation studies were scanned after an average of 4 h and 20min, a static SPECT of 30 min was run. 1.0 mm 5-multipinhole collimator (N5F65A10) and 50 mm radius of rotation (ROR). Images were reconstructed using a 20% energy window and Ordered subset expectation maximization (OSEM) algorithm with 5 iterations and 8 subsets.

Computed tomography (CT) was performed using 80 kVp, 2x2 binning, 512 projections and 1.3x magnification, immediately after SPECT imaging. The raw data were reconstructed using Filtered Back Projection.

Image analysis

Images were analyzed using PMOD (PMOD Technologies Ltd., Zürich). Volumes of interests (VOI) representing the brain-tissue, non-brain-tissue and background regions were delineated based on the anatomical CT images, and transferred to the coregistered dynamic SPECT data. In addition, an average SPECT image over all time frames was calculated for each animal. These images were inspected visually by an experienced biologist.

[123]I-compound-1 Biodistribution

The same animals used for the SPECT imaging were used in the biodistribution study. [123I]-compound-1 and Na123I were injected into anesthetized rats following the same protocol as described in the SPECT imaging studies. Animals were euthanized with an overdose of pentobarbital (ip 100 ml/kg). For each time point 1h post iv injection of [123I]-compound-1, 2h and 5h post ip injection of [123I]-compound-1. Organs were collected, weighed and analysed for radioactivity on an automatic gamma counter (Wizard[2] 2480, Perkin Elmer, USA) Organ distribution was expressed as percentage of injected dose per gram (% ID/g).

Statistical analysis

All of the data are presented as average±SD. Statistical analyses were performed using GraphPad Prism software. Biodistribution and SPECT studies were analysed by paired two-tailed t-test.

RESULTS

Saline and serum stability

Stability test in saline revealed that 46% of the compound remained after 1 hour incubation, decreasing to 10% after 2 hours and to 2% 24 hours post incubation (Table 1). Human and rat serum stability analysis performed by LC-MS showed a 50% decrease of compound 1 after 1 hour (Table 1). After 2 hours incubation, 23% of the compound remained in human serum and approximately 30% of the compound remained in rat serum.

Inhibition assay

A concentration dependent competition study using HEK293T cell lines and LHRH agonist was performed to evaluate the affinity of compound 1. Results showed that compound 1 presented pIC_{50} of 5.29. The Ki was determined by using the cheng-prusoff equation.[14] Compound 1 was found to have a K_i value of 82.0 nM compared to 12.2 nM for the commercially available reference compound WAY207024 (Figure 2). The antagonist affinity of compound 1 dropped approximately one order of magnitude compared to WAY207024 reference.

SPECT imaging

The SPECT images resulted in no visual uptake in the brain region at the doses injected (Figure 4). The Ratios for the VOIs brain vs non-brain and brain vs background were statistically analyzed (Figure 5) and showed no statistical significant difference.

Biodistribution

Organ analyses revealed that most of the activity for $[^{123}I]$-compound-1 was distributed in the stomach 3.6 % ID/g and the thyroid 1.2% ID/g. The uptake in testis and brain was 0.2% ID/g and 0.03% ID/g respectively (Table 2). Similarly, a high $Na^{123}I$ uptake was presented in the thyroid (3.6% ID/g) and stomach (3.4% ID/g). The biodistribution examined 2 hours and 5 hours post ip administration of $[^{123}I]$-compound-1 revealed high uptake in the thyroid 5.8%

ID/g after 2 hours and even higher uptake after 5 hours (13.1% ID/g). By comparison the stomach showed 2.5% ID/g after 2 hours and 2% ID/g after 5 hours. (Table 3).

DISCUSSION

The GnRH-R plays a crucial role in several diseases and it is located within the brain and outside the brain.[1-4] Our aim was to target the GnRH-R with imaging since the GnRH-R expression will give valuable information for diagnosis, treatment and pathophysiology. Initially the discovery of compound 1 was done to evaluate the potential of radiolabelling by the anchimerically assisted Finkelstein approach. We have previously disclosed the radiolabelling of compound 1 by a modified Copper azide –alkyne cycloaddition in 80% analytical RCY and 17% isolated yield (Figure 1).[6] This gave us a straightforward access to a radioiodinated compound. In addition the radiolabelling was done in high yield, in a fast and robust reaction which is in compliance with the requirements for radiolabelling.[15] In addition the affinity to the GnRH-R were evaluated in a competitive binding assay. Compound 1 showed nM affinity (Ki 82nM) to the GnRH-R compared to the reference WAY207024. The stability of α-halogenated compound 1 was a concern due to its nature of reactivity in this position and would therefore not be suitable for physiological conditions. However, literature findings showed SD6 and S70254 with α-halogenated amides labelled with ^{125}I, figure 3.[11-12] Previous reports showed the *in vitro* biological evaluation of α-halogenated amides SD6 and S70254 in cell membrane binding assays, tissue membrane saturation assays and *in vitro* autoradiography of rat and sheep brain and retina. Legros et al explains that these tools are amenable to binding experiments and to autoradiography using sheep and rat tissue and that these specific tools will permit better understanding of the role and implication in physiophatologic processes of the melatonin receptors.[11-12]

The use of these α-halogenated amides with promising results prompted us to pursue the further biological evaluation of compound 1. Serum stability analysis is an initial step in the *in vitro* evaluation.[16] Compound 1 revealed sufficient enough stability for imaging following incubations in saline, rat and human serum. Competitive binding studies in H293T cells presented compound 1 binding affinities for human GNRH-R in the nM range. In total, these indications favored the biodistribution studies of compound-1 in rats and furthermore the *in vivo* evaluation as a GnRH-R SPECT imaging agent.

The SPECT images were evaluated visually for uptake in the brain region. However, we were not able to distinguish any uptake visually for compound 1. We then decided to compare the images from [^{123}I]-compound-1 with Na^{123}I and no visually differences in the SPECT images were seen. The injection were changed to ip injection since we wanted to control our injection technique and since the ip route is much slower in terms of circulation in the blood compared to iv injections and therefore a possible accumulation in brain could be seen.[17] However, no differences between the injection techniques were seen on the SPECT images. We did not change the dose since similar dose were reported in previous preclinical evaluation of ^{123}I- labeled compounds.[18] However, to investigate this further we designed a semi quantitative study to evaluate the uptake. Three VOIs were selected and compared to each other; brain, non-brain region and a background region. The statistically analyses did not show any statistical significant difference.

We evaluated the biodistribution of [^{123}I]-compound-1. The biodistribution of compound 1 is significantly similar to the biodistribution for Na^{123}I. [^{123}I]-compound-1 was mainly distributed in the thyroid and the stomach, indicating possible uptake of free ^{123}I. We observed similar uptake patterns in brain and testis for compound 1 and Na^{123}I, where GnRH-R is known to be expressed, confirming the uptake of free ^{123}I.[4] However, to our knowledge no information of the biodistribution of Na^{123}I are available for male Wistar rats. The biodistribution for free ^{125}I and ^{131}I for male Sprague Dawley rats exists.[19] When we compared the biodistribution for ^{125}I, ^{131}I and ^{123}I they all corresponds to the organs selected.

Despite our predictions of the reactive nature of α-halogenated amides, compound 1 was stable long enough for a sufficient validation of *in vivo* effects. The compound was initially validated in saline, human and rat serum. The biodistribution study in rat compared with Na^{123}I and the SPECT analysis did not show any differences. Compound 1 did not show any uptake in the brain region despite the promising stability and previous literature data. Compound 1 is therefore not suitable as a SPECT radiotracer. Further studies for similar compound with longer chain lengths are planned and our chemically kinetic experiments indicates far more robust compounds.[6]

CONFLICT OF INTEREST
The authors declare no conflict of interest

REFERENCES

1.   Cheung, L. W. T.; Wong, A. S. T., Gonadotropin-releasing hormone: GnRH receptor signaling in extrapituitary tissues. *FEBS Journal* **2008,** *275* (22), 5479-5495.

2.   Maggi, R., Physiology of Gonadotropin-Releasing Hormone (GnRH): Beyond the Control of Reproductive Functions. *MOJ Anat & Physiol* **2016,** *2* (5).

3.   Vadakkadath Meethal, S.; Atwood, C. S., Alzheimer's disease: the impact of age-related changes in reproductive hormones. *Cellular and Molecular Life Sciences CMLS* **2005,** *62* (3), 257-270.

4.   Skinner, D. C.; Albertson, A. J.; Navratil, A.; Smith, A.; Mignot, M.; Talbott, H.; Scanlan-Blake, N., GnRH Effects Outside the Hypothalamo-Pituitary-Reproductive Axis. *Journal of neuroendocrinology* **2009,** *21* (4), 282-292.

5.   Medicine, I. o.; Council, N. R., *Advancing Nuclear Medicine Through Innovation*. The National Academies Press: Washington, DC, 2007; p 173.

6.   Fjellaksel, R.; Dugalic, D.; Demissie, T. B.; Riss, P. J.; Hjelstuen, O.-K.; Sundset, R.; Hansen, J. H., An acylation-Finkelstein approach to radioiodination of bioactives: The role of amide group anchimeric assistance. *Journal of Physical Organic Chemistry* **2018**, e3835-n/a.

7.   Fjellaksel, R.; Boomgaren, M.; Sundset, R.; Haraldsen, I. H.; Hansen, J. H.; Riss, P. J., Small molecule piperazinyl-benzimidazole antagonists of the gonadotropin-releasing hormone (GnRH) receptor. *MedChemComm* **2017,** *8* (10), 1965-1969.

8.   Kämäräinen, E.-L.; Kyllönen, T.; Airaksinen, A.; Lundkvist, C.; Yu, M.; Någren, K.; Sandell, J.; Langer, O.; Vepsäläinen, J.; Hiltunen, J.; Bergström, K.; Lötjönen, S.; Jaakkola, T.; Halldin, C., Preparation of [18F]β-CFT-FP and [11C]β-CFT-FP, selective radioligands for visualisation of the dopamine transporter using positron emission tomography (PET). *Journal of Labelled Compounds and Radiopharmaceuticals* **2000,** *43* (12), 1235-1244.

9.   Block, D.; Coenen, H. H.; Stöcklin, G., The N.C.A. nucleophilic 18F-fluorination of 1,N-disubstituted alkanes as fluoroalkylation agents. *Journal of Labelled Compounds and Radiopharmaceuticals* **1987,** *24* (9), 1029-1042.

10.   Fan, L.; Adams, A. M.; Polisar, J. G.; Ganem, B., Studies on the Chemistry and Reactivity of α-Substituted Ketones in Isonitrile-Based Multicomponent Reactions. *The Journal of organic chemistry* **2008,** *73* (24), 9720-9726.

11.   Legros, C.; Brasseur, C.; Delagrange, P.; Ducrot, P.; Nosjean, O.; Boutin, J. A., Alternative Radioligands for Investigating the Molecular Pharmacology of Melatonin Receptors. *Journal of Pharmacology and Experimental Therapeutics* **2016,** *356* (3), 681.

12.   Legros, C.; Matthey, U.; Grelak, T.; Pedragona-Moreau, S.; Hassler, W.; Yous, S.; Thomas, E.; Suzenet, F.; Folleas, B.; Lefoulon, F.; Berthelot, P.; Caignard, D.-H.; Guillaumet, G.; Delagrange, P.; Brayer, J.-L.; Nosjean, O.; Boutin, A. J., New Radioligands for Describing the Molecular Pharmacology of MT1 and MT2 Melatonin Receptors. *International Journal of Molecular Sciences* **2013,** *14* (5).

13.   Harvey, J. H.; van Rijn, R. M.; Whistler, J. L., A FLIPR Assay for Evaluating Agonists and Antagonists of GPCR Heterodimers. In *Chemical Neurobiology: Methods and Protocols*, Banghart, M. R., Ed. Humana Press: Totowa, NJ, 2013; pp 43-54.

14.   Cheng, Y.-C.; Prusoff, W. H., Relationship between the inhibition constant (KI) and the concentration of inhibitor which causes 50 per cent inhibition (I50) of an enzymatic reaction. *Biochemical Pharmacology* **1973,** *22* (23), 3099-3108.

15.   Cole, E. L.; Stewart, M. N.; Littich, R.; Hoareau, R.; Scott, P. J., Radiosyntheses using fluorine-18: the art and science of late stage fluorination. *Current topics in medicinal chemistry* **2014,** *14* (7), 875-900.

16.   Ghosh, A.; Raju, N.; Tweedle, M.; Kumar, K., In Vitro Mouse and Human Serum Stability of a Heterobivalent Dual-Target Probe That Has Strong Affinity to Gastrin-Releasing Peptide and Neuropeptide Y1 Receptors on Tumor Cells. *Cancer Biotherapy and Radiopharmaceuticals* **2017,** *32* (1), 24-32.

17.   Turner, P. V.; Brabb, T.; Pekow, C.; Vasbinder, M. A., Administration of Substances to Laboratory Animals: Routes of Administration and Factors to Consider. *Journal of the American Association for Laboratory Animal Science : JAALAS* **2011,** *50* (5), 600-613.

18.   Maya, Y.; Okumura, Y.; Kobayashi, R.; Onishi, T.; Shoyama, Y.; Barret, O.; Alagille, D.; Jennings, D.; Marek, K.; Seibyl, J.; Tamagnan, G.; Tanaka, A.; Shirakami, Y., Preclinical properties and human in vivo assessment of (123)I-ABC577 as a novel SPECT agent for imaging amyloid-β. *Brain* **2016,** *139* (1), 193-203.

19.   Spetz, J.; Rudqvist, N.; Forssell-Aronsson, E., Biodistribution and Dosimetry of Free (211)At, (125)I(−) and (131)I(−) in Rats. *Cancer Biotherapy & Radiopharmaceuticals* **2013,** *28* (9), 657-664.

Table legends

Table 1. Stability of compound 1 in human and rat serum.

Results are expressed as % of compound remained in serum after the different incubation time points. Mean±SD (n=3). [a]n=1

Table 2: [^{123}I]-compound-1 and Na^{123}I biodistribution 1h post iv injection.

No significant differences in [^{123}I]-compound-1 organ distribution compared to Na^{123}I were found. Results are expressed as %ID/g ±SD (mean. n=3)

Table 3: [^{123}I]-compound-1 biodistribution 2h and 5h post i.p injection
 Results are expressed as %ID/g ±SD (mean. n=3)

Figure legends

Figure 1: Radiolabeling of compound 1 was performed according to previously published methods in 80% Analytical RCY and 17% isolated yield.[6]

Figure 2: Different α-halogenated molecules for imaging purposes.[11-12]

Figure 3: Competitive binding in competition of 5 nM LHRH agonist. Compound 1 was evaluated in comparison with reference compound WAY207024. Compound 1 have an nM affinity for the GnRH-R and show only a drop of magnitude in affinity compared to WAY207024.

Figure 4: The figure show the areas selected for the VOIs where brain, non-brain and background were selected as VOI. B: Comparison of the selected VOIs measured as intensity which was used to analyze the difference for compound [^{123}I]-compound-1 and Na^{123}I.

Figure 5: Static SPECT images (color) coregistered with CT (black/white) of the rat head. A: Injection of Na^{123}I. B: Intravenous injection of [^{123}I]-compound-1 C: Intraperitoneal injection of [^{123}I]-compound-1.

Tables

Table 1: Stability of compound 1 in human and rat serum

Min	Human serum	Rat serum	Saline[a]
0	100	100	100
10	88±1.6	86±7.3	-
30	74±8.1	82±11.5	-
60	52±1.5	44±5.5	46
120	23±1.6	30±4.8	10
240	3±0.3	8±1.6	-
1320	0	0	-
1440	-	-	1.6

Table 2: ^{123}I-1 and Na^{123}I biodistribution 1h post i.v. injection

Organs	Na^{123}I	±SD	^{123}I-1	±SD
Blood	0.66	0.19	0.54	0.22
Urine	1.07	0.34	0.70	0.57
Bladder	0.45	0.16	0.35	0.14
Heart	0.24	0.08	0.22	0.10
Thyroid	3.59	2.63	1.21	1.48
Thymus	0.19	0.06	0.16	0.07
Saliv. Glands	0.25	0.08	0.22	0.12
Lungs	0.37	0.08	0.33	0.16
Pancreas	0.22	0.10	0.21	0.13
Spleen	0.27	0.08	0.24	0.10
Kidneys	0.37	0.10	0.34	0.19
Large I	0.32	0.08	0.30	0.14
Small I	0.57	0.11	0.93	0.89
Stomach	3.40	1.63	3.62	1.70
Feces	0.23	0.23	0.07	0.04
Brain	0.04	0.01	0.03	0.00
Bone	0.30	0.09	0.33	0.20
Liver	0.25	0.07	0.25	0.08
Muscle	0.14	0.06	0.11	0.05
Skin	1.24	1.18	0.38	0.29
Fat	0.06	0.03	0.09	0.03
Testis	0.25	0.08	0.21	0.11

Table 3: ^{123}**I-1** biodistribution 2h and 5h post i.p injection

Organs	2h post i.p.	±SD	5h post i.p.	±SD
Blood	0.34	0.012	0.19	0.005
Urine	0.14	0.053	0.84	0.524
Bladder	0.32	0.094	0.26	0.087
Heart	0.15	0.026	0.08	0.005
Thyroid	5.79	1.957	13.14	1.809
Thymus	0.12	0.019	0.07	0.009
Saliv. Glands	0.13	0.009	0.08	0.005
Lungs	0.21	0.005	0.12	0.012
Pancreas	0.51	0.257	0.09	0.025
Spleen	0.16	0.022	0.09	0.005
Kidneys	0.18	0.005	0.11	0.005
Large I	0.20	0.054	0.35	0.323
Small I	1.49	0.947	0.20	0.109
Stomach	2.47	0.893	1.64	0.836
Feces	0.05	0.012	0.81	1.117
Brain	0.02	0.000	0.01	0.000
Bone	0.14	0.005	0.08	0.005
Liver	0.15	0.012	0.10	0.008
Muscle	0.06	0.005	0.03	0.005
Skin	0.26	0.042	0.18	0.040
Fat	0.07	0.042	0.14	0.189
Testis	0.13	0.000	0.10	0.005

Figures

Figure 1

Figure 2

1

hGnRHR pIC50 = 5.29
hGnRHR K_i (nM) = 82

WAY207024
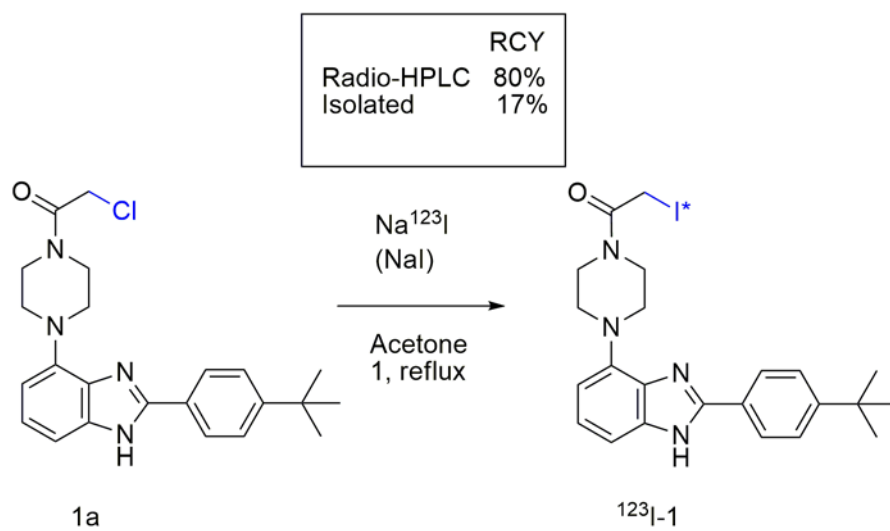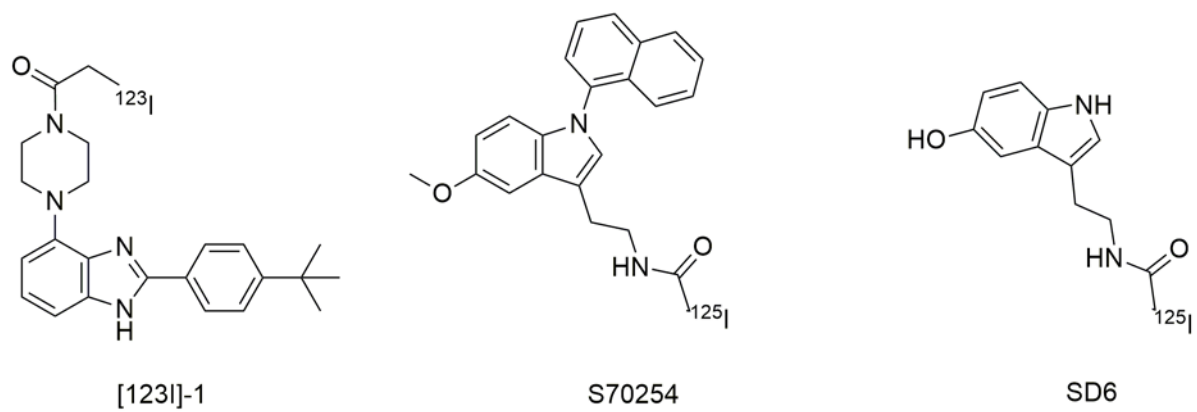
hGnRHR pIC50 = 6.2
hGnRHR K_i (nM) = 12.2
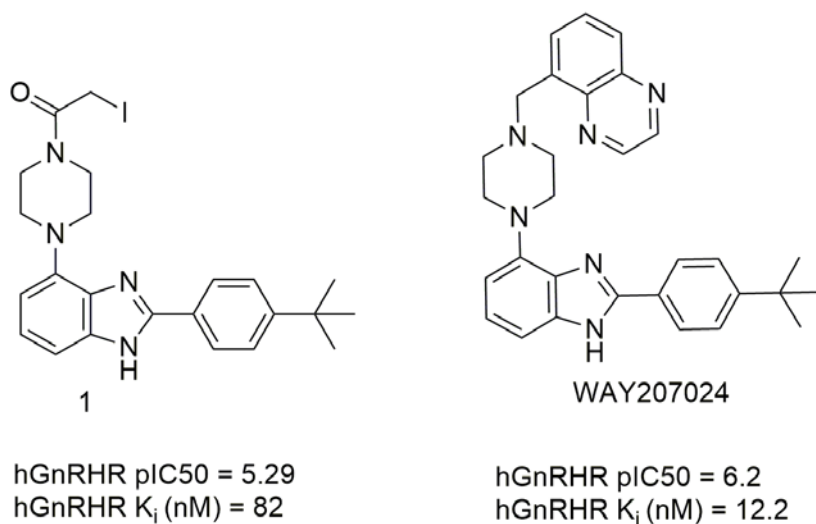
Figure 3
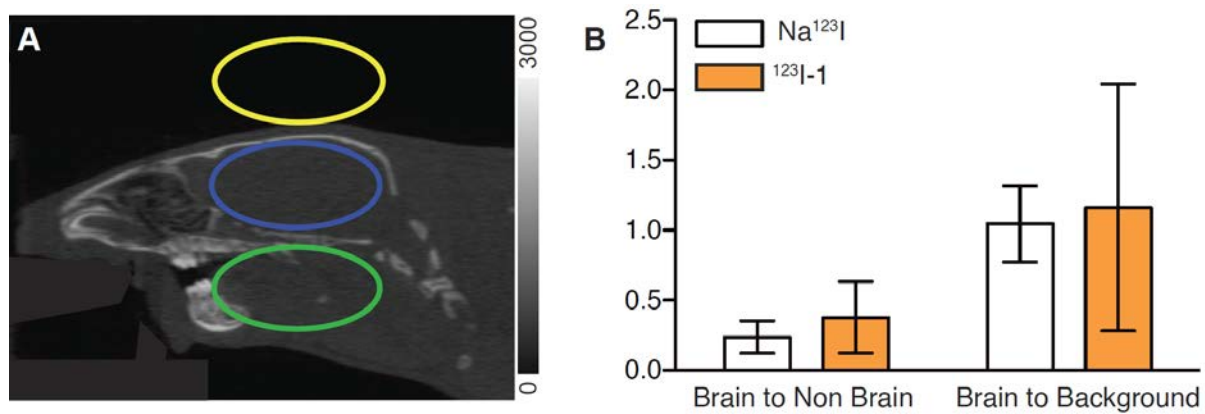

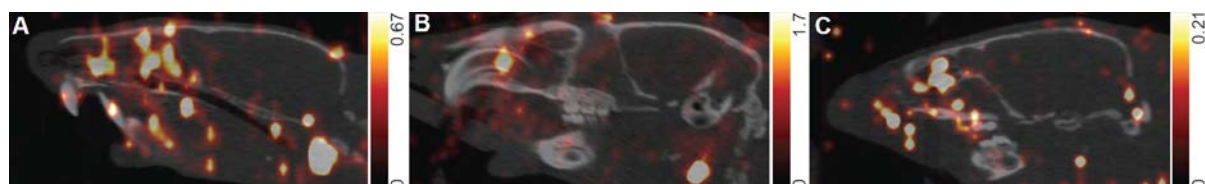**Figure 4**

Figure 5

Errata

Abbrevation listed in alphabetical order

Page 22   Trituration changed to tritiation

Table 7:   Compound 2 changed to compound 3

                 compound 3 changed to compound 4

Figure 19:   Removed 3 and inserted human

Figure 22:   Changed from 1 to 4

References: 15: 317-26 changed to 317-326

                 16: 3314-9 changed to 3314-3319

                 17: 211-6 changed to 211-216

                 23: 451-8 changed to 451-458

                 46: 2148-52 changed to 2148-2152

                 55: 202-8 changed to 202-208

                 56: 4190-5 changed to 4190-4195

                 58: 703-9 changed to 703-709